VOLTAGE-GATED SODIUM CHANNEL $NA_V1.6$ S-PALMITOYLATION REGULATES CHANNEL FUNCTIONS AND NEURONAL EXCITABILITY

Yanling Pan

Submitted to the faculty of the University Graduate School
in partial fulfillment of the requirements
for the degree
Doctor of Philosophy
in the Program of Medical Neuroscience,
Indiana University

April 2020

Accepted by the Graduate Faculty of Indiana University, in partial fulfillment of the requirements for the degree of Doctor of Philosophy.

Doctoral Committee

_____

Jason S. Meyer, Ph.D., Chair

_____

Theodore R, Cummins, Ph.D.

January 16, 2020

_____

Andy Hudmon, Ph.D.

_____

Xiaoming Jin, Ph.D.

_____

Alexander G. Obukhov, Ph.D.

DEDICATION

This work is dedicated to my loving parents.

ACKNOWLEDGEMENT

I would like to express my deepest gratitude to my mentor Dr. Theodore Cummins, for accepting me as part of the *Best Lab Ever*, for guiding me through each stage of my PhD journey, and for providing his generous encouragement and unwavering support even in study interests beyond the scope of my research. The door to Dr. Cummins's office was always open (literally) whenever I had doubts about my research, my writing, or the micromanipulator refused to manipulate. I am profoundly amazed by his tremendous patience, scientific rigor and also his delightful humor. I could not have imagined having a better mentor for my PhD study.

My appreciation also goes to my research committee: Dr. Andy Hudmon, Dr. Jason Meyer, Dr. Xiaoming Jin, and Dr. Alexander Obukhov. Their insightful comments and guidance have made the successful completion of this dissertation possible. I would particularly like to thank Dr. Andy Hudmon. The biochemistry work in this dissertation would not exist without his invaluable input and encouragement.

I would also like to extend my thanks to our collaborators Dr. Nickolay Brustovetsky and Dr. Jason Meyer for the opportunities to apply my technique to stem cell research.

Additionally, I would like to thank all the previous and current members of the Cummins lab that I worked with: Dr. Yucheng Xiao, Dr. Zhiyong Tan, James Jackson, Dr. Reesha Patel, Dr. Cindy Barbosa, Dr. Zifan Pei, Emily Mason, Agnes Zybura, Ashley Frazee, and Patrick Milder. They created an exceptional lab environment and their continued support and companionship has made the grad school experience enjoyable. Especially, I would like to thank Dr. Yucheng Xiao, who has helped and taught me immensely since my research began. His

enormous lab experience and his generosity with advice has saved my day countless times.

I would like to acknowledge the faculty and staff of the Stark Neurosciences Research Institute, the Department of Biology, and the Indiana School of Medicine Biomedical Gateway (IBMG) program: Dr. Gerry Oxford, Dr. Gary Landreth, Dr. Karmen Yoder, Nastassia Belton, Rene Baugh, Diana Kelley, Angela Longfellow, Leslie Santos, Tara Hobson and Brandy Wood.

I appreciate all my fellow graduate students in the Medical Neuroscience program and my friends in science. Special mention goes to Dr. Liangping Li, Dr. Yihui Zhang, Dr. Qian Wang and Dr. Qian Feng. They embody the tenacious girl power in neuroscience and in life.

Special thanks also go to Rong Yuan and Jiaxiang Hu. They led me down the rabbit hole of the coding world and I will always “hold them responsible” for the wonderful adventures that followed. They taught me a whole new way of thinking about the world and inspired me in many different ways. Without them, the last five years would have been much less fun.

Last but not least, I am extremely grateful to my parents and friends for their love and support throughout my years of study, no matter the distance and the time difference. None of this could have happened without them.

Yanling Pan

VOLTAGE-GATED SODIUM CHANNEL $NA_V1.6$ S-PALMITOYLATION REGULATES CHANNEL FUNCTIONS AND NEURONAL EXCITABILITY

The voltage-gated sodium channels (VGSCs) are critical determinants of neuronal excitability. They set the threshold for action potential generation. The VGSC isoform Nav1.6 participates in various physiological processes and contributes to distinct pathological conditions, but how Nav1.6 function is differentially regulated in different cell types and subcellular locations is not clearly understood. Some VGSC isoforms are subject to S-palmitoylation and exhibit altered functional properties in different S-palmitoylation states. This dissertation investigates the role of S-palmitoylation in Nav1.6 regulation and explores the consequences of S-palmitoylation in modulating neuronal excitability in physiological and pathological conditions.

The aims of this dissertation were to 1) provide biochemical and electrophysiological evidence of Nav1.6 regulation by S-palmitoylation and identify specific S-palmitoylation sites in Nav1.6 that are important for excitability modulation, 2) determine the biophysical consequences of epilepsy-associated mutations in Nav1.6 and employ computational models for excitability prediction and 3) test the modulating effects of S-palmitoylation on aberrant Nav1.6 activity incurred by epilepsy mutations.

To address these aims, an acyl-biotin exchange assay was used for S-palmitoylation detection and whole-cell electrophysiology was used for channel characterization and excitability examination. The results demonstrate that 1) Nav1.6 is biochemically modified and functionally regulated by S-palmitoylation in an isoform- and site-specific manner and altered S-palmitoylation status of the channel results in substantial changes of neuronal excitability, 2) epilepsy-

associated Nav1.6 mutations affect different aspects of channel function, but may all converge to gain-of-function alterations with enhanced resurgent currents and increased neuronal excitability and 3) S-palmitoylation can target specific Nav1.6 properties and could possibly be used to rescue abnormal channel function in diseased conditions. Overall, this dissertation reveals S-palmitoylation as a new mechanism for Nav1.6 regulation. This knowledge is critical for understanding the potential role of S-palmitoylation in isoform-specific regulation for VGSCs and providing potential targets for the modulation of excitability disorders.

Jason S. Meyer, Ph.D., Chair

TABLE OF CONTENTS

LIST OF TABLES

LIST OF FIGURES

LIST OF ABBREVIATIONS

2BP	2-Bromo palmitate, or 2-Bromohexadecanoic acid
ABE	acyl-biotin exchange
AIS	axon initial segment
AKAP	A-kinase anchoring protein
AMPA	α-amino-3-hydroxy-5-methyl-4-isoxazolepropionic acid
AP	action potential
APP	amyloid precursor protein
APT	acyl-protein thioesterase
Aβ	beta-amyloid
BACE1	beta-secretase
CNS	central nervous system
CRMP2	collapsin response mediator protein 2
CTD	carboxyl terminal domain
DRG	dorsal root ganglion
EGFP	enhanced green florescent protein
EIEE	early infantile epileptic encephalopathy
ER	endoplasmic reticulum
FHF	fibroblast homologous factor
GABA	gamma-Aminobutyric acid
GAP	GTPase-activating protein
GEFS+	generalized epilepsy with febrile seizures plus
HA	hydroxylamine
HEK	human embryonic kidney cells
hNav1.6	human voltage-gated sodium channel isoform 1.6
iCell GlutaNeuron	human glutamatergic neurons derived from iPSC
iPSC	induced pluripotent stem cell
IRES	internal ribosome entry site
mNav1.6	mouse voltage-gated sodium channel isoform 1.6

N-terminal	amino terminal
Nav1.6	voltage-gated sodium channel isoform 1.6
NEM	N-ethylmaleimide
NMDA	N-methyl-D-aspartate
p38 MAPK	p38 mitogen-activated protein kinase
PA	palmitic acid
PAT	palmitoyl-acyl transferase
PNS	peripheral nervous system
PPT	palmitoyl protein thioesterase
PSD	post-synaptic density
PSD95	post-synaptic density protein 95
PTM	post-translational modification
shRNA	small hairpin RNA
siRNA	small interference RNA
SNP	single-nucleotide polymorphism
TTX	tetrodotoxin
TTXr	tetrodotoxin-resistant
TTXs	tetrodotoxin-sensitive
VGSC	voltage-gated sodium channel
WT	wildtype
zDHHC	zinc-finger and aspartate-histidine-histidine-cysteine motif

I. INTRODUCTION

A. Overview of the thesis project

Signal transduction in the nervous system depends on the ability of neurons to generate and propagate action potentials. As the common neuronal output, action potential generation permits synaptic release for intercellular signal transmission. By backpropagating to the soma and dendrites, action potentials modulate somatodendritic inputs, influencing synaptic plasticity, signal integration and ultimately axonal output. The threshold for action potential generation is set by voltage-gated sodium channels (VGSCs). Thus, they are ideally positioned to regulate neural signal transduction, and their malfunction can cause severe neurological and psychiatric diseases, including epilepsy, pain, motor disorders, autism, cognitive deficits and schizophrenia.

The VGSCs are tightly regulated. The intrinsic properties of these channels are determined by their molecular structure. Their biophysics are modulated by an intricate network of interacting proteins. Additionally, the VGSCs are subject to a wide range of post-translational modifications that can exert profound impact on channel activity. Importantly, these modifications are dynamically regulated by neuronal activity, extracellular signals, as well as intracellular signaling pathways, engaging the channels in various interactive cellular processes. Despite four decades of research, the complexity of VGSC modulation is still being determined. This dissertation explores a novel mechanism of VGSC regulation.

S-palmitoylation has emerged as a new mechanism that regulates protein functions. As a post-translational modification, S-palmitoylation covalently attaches a long-chain fatty acid to proteins and alters their hydrophobicity; consequently, S-palmitoylation regulates intracellular trafficking and membrane association. Notably, S-palmitoylation is the only lipid modification that is

reversible. The cycle of palmitoylation – depalmitoylation empowers S-palmitoylation to regulate protein functions in a dynamic fashion. Indeed, the activity-dependent localization of a great variety of synaptic proteins relies on the rapid cycle of S-palmitoylation on these proteins. However, the functional significance of S-palmitoylation of VGSCs is understudied and underestimated. This dissertation focuses on the investigation of S-palmitoylation of the VGSC isoform Nav1.6.

Nav1.6 has powerful control over neuronal excitability. It is ubiquitously expressed in both the central nervous system and the peripheral nervous system and has high density at the axon initial segment (AIS), where action potentials are initiated. Nav1.6 is unique in its biophysical properties and supports high frequency repetitive firing in many neuronal cell types. Dysfunction of the channel has been associated with severe neurological disorders. This dissertation examines the biological consequences of Nav1.6 S-palmitoylation and the potential to regulate Nav1.6 activity with isoform specificity and modulate neuronal excitability in physiological and diseased conditions.

Overall, this dissertation reveals S-palmitoylation as a crucial mechanism for VGSC regulation with site- and isoform-specificity. This knowledge contributes to the understanding of the complex network of VGSC regulation and identifies a new strategy to modulate VGSC activity and neuronal excitability in diseased conditions.

B. Neuronal excitability and action potential generation

Excitability of a neuron is defined by its ability to generate action potentials. It is determined by the composition, distribution, and properties of ion channels in the plasma membrane. These include Na^+-K^+ pump, Ca^{2+} pump, Na^+-Ca^{2+} exchanger, Na^+-K^+-Cl^- cotransporter, and K^+-Cl^- cotransporter that

regulate the chemical concentration gradients of Na^+, K^+, Ca^{2+}, and Cl^- ions across the plasma membrane, setting the steady state resting membrane potential; a set of voltage-dependent Na^+ and K^+ channels that rapidly disturb the resting ionic balance and generate the action potential; as well as other voltage-gated Ca^{2+} and HCN channel that help shape the amplitude and time course of the action potential (Kandel, Schwartz et al. 2000). Slight alteration of the biophysics of these channels can have profound impact on neuronal excitability.

Action potential generation involves a series sequential events (Fig.1). As the membrane depolarized, voltage-gated sodium channels are activated and rapidly open, producing inward Na^+ current that counteracts the outward K^+ and resting currents and further depolarizing the membrane in a graded manner. This drives the membrane potential towards the threshold voltage for action potential generation. Once the threshold voltage is reached, an action potential is generated, leading to even more Na^+ channels being activated in a regenerative manner. The Na^+ influx pushes the membrane potential towards the reversal potential for Na^+, accounting for the rising phase of the action potential. The action potential starts to decay when voltage-gated sodium channels gradually inactivate, decreasing the inward current. Concurrently, voltage-gated potassium channels open, producing outward K^+ current that counteracts the residual Na^+ current. Then the outward K^+ current starts repolarizing the membrane potential, accounting for the falling phase of the action potential. The non-inactivating K^+ current also contributes to a small hyperpolarizing after-potential before the membrane potential recovers to its resting level.

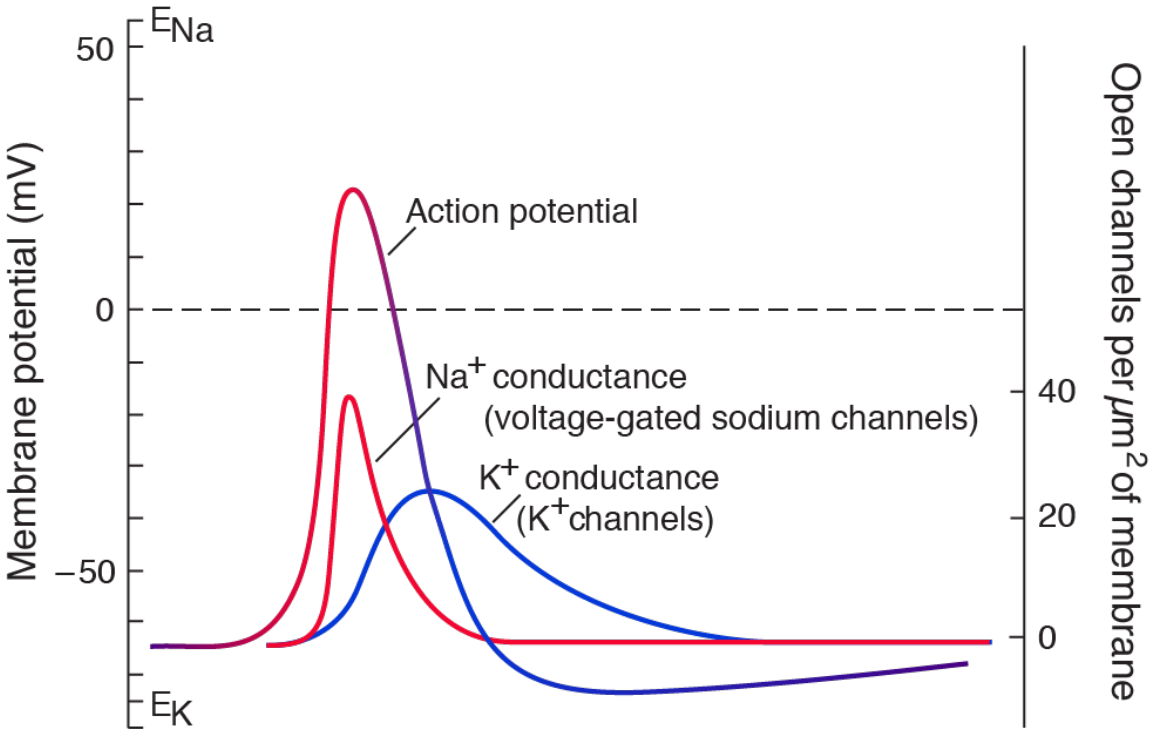

modified from (Kandel, Schwartz et al. 2000)

Figure 1. The sequential opening of voltage-gated Na+ and K+ channels generates the action potential.

C. VGSC structure and functions

1. Structure

The VGSC is a pore-forming multi-pass transmembrane protein comprised of a α subunit and multiple β subunits (Fig.2).

The VGSC α subunit is a single polypeptide chain of about 2000 residues that folds into four homologous but non-identical domains (DI-DIV). Each domain contains six transmembrane segments (S1-S6) (Fig.2). S1-S4 comprise the voltage sensors (Catterall 2010), while S5-S6 combine to form the sodium conducting pore with Asp/Glu/Lys/Ala (DEKA) residues from the four domains constituting the Na^+ selectivity filter. These regions are essential for normal voltage sensing and sodium ion selectivity. The extracellular loops are frequent binding sites for peptidic gating modifier toxins like conotoxins, protoxins and huwentoxins (Pan, Li et al. 2019, Shen, Liu et al. 2019). The intracellular loops and cytosolic N- and C-terminal domains are heavily involved in protein-protein interactions and are subject to extensive post-translational modifications (Pei, Pan et al. 2017).

VGSC β subunits were initially identified as auxiliary components of the VGSC complex that facilitate α subunit functions, but now they are considered multifunctional signaling proteins that also function without the α subunits, for example, for cell adhesion and gene regulation (O'Malley and Isom 2015). Four β subunits, Navβ1-4, have been identified. They are encoded by *SCN1B*, *SCN2B*, *SCN3B*, *SCN4B* respectively. Navβ subunits are single transmembrane proteins with an extracellular N-terminal Ig domain and an intracellular C-terminal domain. β1 and β3 form non-covalent interaction with α subunits with their N- and C-termini (McCormick, Isom et al. 1998, Meadows, Malhotra et al. 2001, Spampanato, Kearney et al. 2004), while β2 and β4 form covalent disulfide

bonds with α subunits via cysteines in their extracellular immunoglobulin domains (Ferriera, Lilly et al. 2003, Gilchrist, Das et al. 2013).

2. Activation

The gating of a VGSC is steeply dependent on the plasma membrane potential. The channel is in resting / closed state at resting membrane potential. Upon membrane depolarization, it activates, allowing sodium influx, and rapidly inactivates, occluding the ion conducting pore. In the inactivated state, the channel is refractory to further depolarization and cannot be activated again before it recovers from inactivation at hyperpolarizing potential (Fig.2C). These transitions between resting, activated and inactivated states are realized by sophisticated conformational changes of the channel in response to membrane potential change.

The voltage-dependent property of VGSCs is conferred by the VSDs along with the S4-S5 linkers. The VSDs are relatively independent to the S5-P-S6 pore domain (PD), except for the interaction of S4-S5 linker with the Pro-X-Pro motif in S6, serving to couple voltage sensing to pore opening and closing (Long, Campbell et al. 2005). Voltage sensing by the VSD is mainly carried out by the movement of S4, which typically contains five positively charged residues (4 arginines and 1 lysine) at every third positions in the transmembrane segment. In response to depolarization of the membrane electric field, S4s move outward with a screw motion, bringing its gating charges nearer to the extracellular face of the membrane (Pathak, Yarov-Yarovoy et al. 2007). Upon completion of the final outward motion, the last gating charge residue (Lys5) in S4 interacts with a Phe occluding residue that prevents further movement of S4 (Tao, Lee et al. 2010), while the first four gating charges (Arg1-Arg4) form transient salt bridges with acidic residues in S1 and S2, stabilizing the S4 position. This converts the channel into an activated-not-open state. A concerted movement of S4, S5, S4-

S5 linker and S6 in all four domains transforms the channel into the open state, completing the channel activation (Jensen, Jogini et al. 2012).

3. Inactivation

During voltage sensing, only the movements of S4s in DI-III are considered to be responsible for channel activation, while the relatively slower movement of DIV S4 is involved in channel inactivation. It has been proposed that the delayed movement of S4 in DIV in response to voltage change accounts for the voltage dependence of VGSC inactivation, explaining the strong voltage-dependence of VGSC inactivation. This fits perfectly with the Hodgkin-Huxley model that predicts three activation gates and one single inactivation gate in a VGSC (Schwiening 2012). It has now been confirmed that the inactivation particle locates in the intracellular linker of DIII-IV with a key motif containing three highly conserved hydrophobic residues (ile/phe/met, IFM) (West, Patton et al. 1992, Eaholtz, Scheuer et al. 1994). Upon occlusion of the channel pore, the IFM inactivation particle is stabilized by binding to specific residues in the S3-S4 linker of DIII and DIV (Lerche, Peter et al. 1997, Smith and Goldin 1997). Interestingly, it has been suggested that the intracellular C-terminal domain (CTD) also participates in stabilizing inactivation and prevents channel reopening (Motoike, Liu et al. 2004, Nguyen and Goldin 2010). Indeed, the CTD has been shown to interact with the IFM inactivation gate via static interaction between charged residues (Shen, Zhou et al. 2017, Johnson, Potet et al. 2018). Removing any of the charges can disrupt the interaction and affect normal inactivation (Lee and Goldin 2008, Nguyen and Goldin 2010, Johnson, Potet et al. 2018). Moreover, multiple epilepsy-associated mutations in the CTD have demonstrated inactivation-related dysfunction, highlighting the functional significance of the IFM-CTD interaction for channel inactivation (Wagnon, Barker et al. 2016).

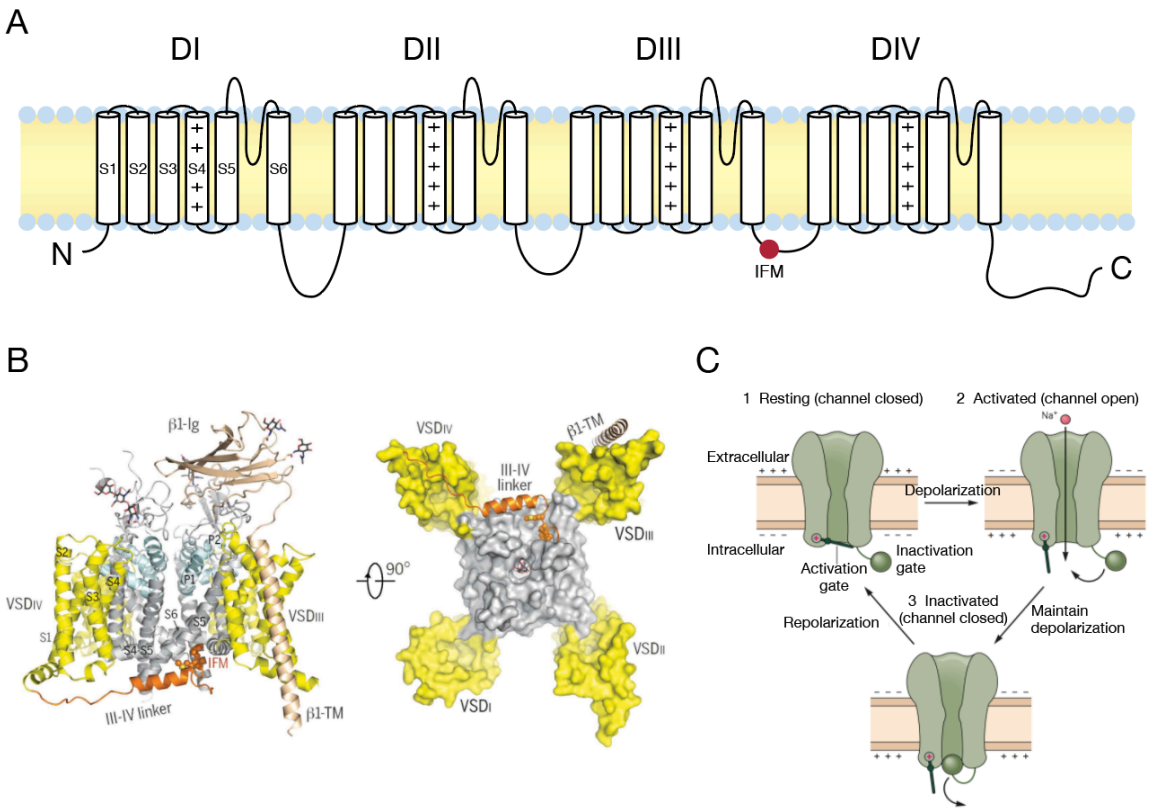

Figure 2. Voltage-gated sodium channel structure and states.

A, Topology of a voltage-gated sodium channel showing the IFM inactivation particle in DIII-DIV linker as a red circle. B, Perpendicular views of a voltage gated sodium channel α subunit complexed with a β1 subunit. Left: Side view in ribbon cartoon. Yellow: VSD; light cyan: selectivity filter and P1, P2 supporting helices; orange: DIII-IV linker with the IFM motif shown as spheres. Right: Bottom view in surface presentation from (Pan, Li et al. 2018). C, Resting, activated, inactivated states of voltage gated sodium channel from (Kandel, Schwartz et al. 2000).

D. Diversity of VGSC isoforms

The VGSC family has 9 isoforms (Nav1.1 - Nav1.9) (Catterall, Goldin et al. 2005). They have distinct pharmacological and biophysical properties. For example, the 9 isoforms are categorized according to their sensitivity to tetrodotoxin (TTX) block: Nav1.5, Nav1.8 and Nav1.9 are TTX-resistant with IC50 values in the μM range, while the other isoforms are TTX-sensitive with IC50 values in the nM range. The VGSC isoforms also have differential cellular and subcellular distribution (Catterall 2012) and are responsible for the electrical signal transduction in a wide range of physiological processes. Very generally, Nav1.1, Nav1.2, Nav1.3 and Nav1.6 are the major isoforms in the central nervous system (CNS), Nav1.4 functions in skeletal muscle, Nav1.5 is the cardiac sodium channel, and Nav1.6, Nav1.7, Nav1.8 and Nav1.9 are the predominant isoforms in the peripheral nervous system (PNS). It is important to note that the expression of the 9 isoforms are not restricted to their primary tissue. As a result, abnormal or dysregulated VGSC activity can lead to varied diseased conditions including epilepsy, pain, autism, cognitive deficit, cardiac arrhythmia, and skeletal muscle disorders. Therefore, VGSCs have long been therapeutically desirable targets in the drug discovery industry. However, the high sequence and structural conservation shared among the Navs have posed a significant challenge to the development of isoform-specific medicines with minimum side effects.

The VSD and PD that convey the critical functions of voltage sensing and sodium conducting are highly conserved among all Nav isoforms. The relatively less conserved extracellular loops are frequent binding sites for peptidic gating modifier toxins like conotoxins, protoxins and huwentoxins (Pan, Li et al. 2019, Shen, Liu et al. 2019). These sites present some degree of isoform specificity, and thus have attracted tremendous pharmacological interest over the past two decades (Catterall 2012, Bagal, Marron et al. 2015). The first and second

intracellular loops and cytosolic N- and C-terminal domains are highly variable regions. Importantly, these intracellular regions are heavily involved in protein-protein interactions and are subject to extensive post-translational modifications (Pei, Pan et al. 2017). Therefore, understanding the important roles of the Nav intracellular regions, their post-translational modifications and their interacting partners can provide new insight into Nav isoform-specific regulation and shed lights on potential strategy to target Nav with improved specificity.

E. The VGSC Nav1.6 isoform

1. Tissue, cell type, subcellular distribution

The VGSC isoform 1.6 (Nav1.6) is encoded by the gene *SCN8A*. Nav1.6 is one of the CNS isoforms of VGSC, along with Nav1.1 (*SCN1A*), Nav1.2 (*SCN2A*) and Nav1.3 (*SCN3A*). It is noteworthy that Nav1.6 is the only VGSC isoform that is ubiquitously expressed in almost all neurons throughout the CNS and the PNS. This is in contrast with the region- and cell type-restricted distribution of other Navs. Developmentally, Nav1.6 replaces Nav1.2 and becomes the major Nav isoform at the axon initial segment (AIS) and the nodes of Ranvier in myelinated excitatory neurons (Boiko, Rasband et al. 2001, Boiko, Van Wart et al. 2003, Van Wart and Matthews 2006), where it plays a dominating role in action potential initiation and propagation (Hu, Tian et al. 2009). Nav1.6 is also found at the AIS of some inhibitory interneurons (Ogiwara, Miyamoto et al. 2007, Lorincz and Nusser 2008, Makinson, Tanaka et al. 2017), although Nav1.1 is considered to be the primary driving force for action potential initiation, and thus for excitability of most inhibitory interneurons. The functional significance of Nav1.6 in inhibitory interneurons is largely unclear. Although some evidence indicates a role for Nav1.6 in establishing synaptic inhibition in the thalamic network (Makinson, Tanaka et al. 2017), conditional expression of the epilepsy-associated R1872W mutation in mouse inhibitory neurons did not induce

seizures but expression in excitatory neurons did (Bunton-Stasyshyn, Wagnon et al. 2019). Nav1.6 is also enriched in the inhibitory cerebellar Purkinje neurons, which are the sole output neurons of the cerebellar cortex and play pivotal roles in motor coordination, motor control and motor learning.

2. Unique functional properties

Nav1.6 is unique in its biophysical properties. It activates at more hyperpolarized voltages than Nav1.1 (Spampanato, Escayg et al. 2001) and Nav1.2 (Rush, Dib-Hajj et al. 2005), allowing a lower threshold for action potential generation. It is also more resistant to use-dependent inactivation during high-frequency (Spampanato, Escayg et al. 2001, Rush, Dib-Hajj et al. 2005, Patel, Barbosa et al. 2016). Importantly, it can conduct higher levels of persistent current (Smith, Smith et al. 1998, Maurice, Tkatch et al. 2001) and resurgent current (Raman, Sprunger et al. 1997, Jarecki, Piekarz et al. 2010). Persistent currents often reflect incomplete inactivation and can contribute to repetitive action potential firing.

Incomplete inactivation can also present as enhanced resurgent currents. Fig.3 shows the current understanding of the mechanism of resurgent current generation. When a VGSC activates and opens, an intracellular open channel blocker can compete with the fast inactivation gate to block sodium flux, mimicking the normal fast inactivation process. However, unlike the fast inactivation gate that remains closed during intermediate membrane repolarization, the open channel blocker can unbind, allowing sodium flux resurge and generating the resurgent current before the channel enter the fast inactivation or closed state. This enables the channel to bypass the fast inactivation state that prevents the channel from re-opening upon further stimulation during the refractory period. Substantial evidence indicates that in many neurons an open channel blocker can lead to increased probability of

action potential firing (Raman and Bean 2001, Khaliq, Gouwens et al. 2003). The Navβ4 subunit has been implicated as one likely open channel blocker contributing to resurgent currents and Nav1.6 has been identified as a predominant generator of resurgent currents in different neurons (Grieco, Malhotra et al. 2005, Bant and Raman 2010, Jarecki, Piekarz et al. 2010, Barbosa, Tan et al. 2015, Patel, Barbosa et al. 2015, Xie, Tan et al. 2016).

The combination of these features makes Nav1.6 a favorable isoform to support high frequency, repetitive firing in a wide range of CNS neurons (Maurice, Tkatch et al. 2001, Khaliq, Gouwens et al. 2003, Do and Bean 2004, Van Wart and Matthews 2006, Enomoto, Han et al. 2007, Mercer, Chan et al. 2007, Royeck, Horstmann et al. 2008, Osorio, Cathala et al. 2010).

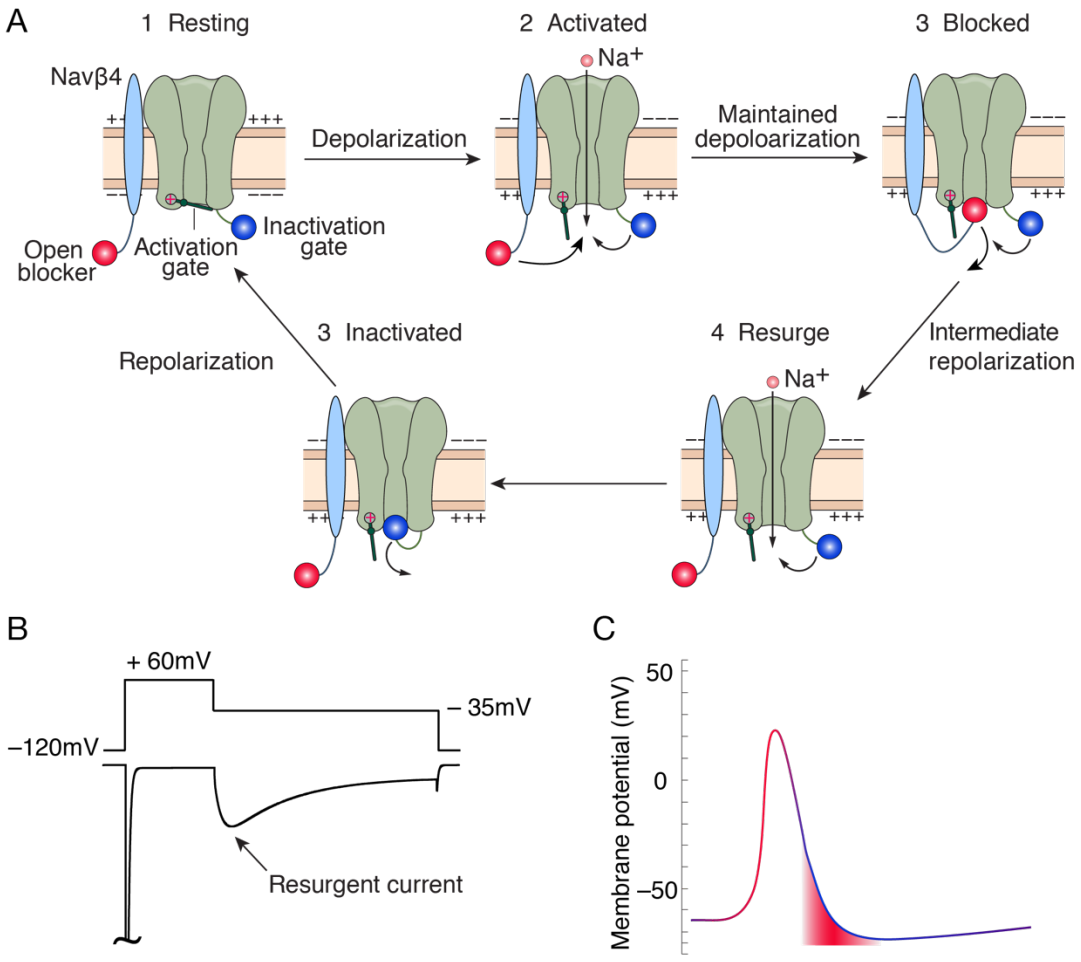

Figure 3 Mechanism of resurgent current generation.

(A) Illustration of the conformational changes of an voltage-gated sodium channel to generate resurgent current, modified from (Kandel, Schwartz et al. 2000). (B) An example of the experimental protocol for resurgent current induction (upper) and the correspondent resurgent current. (C) Depiction of where inward resurgent current would occur during a typical action potential, modified from (Kandel, Schwartz et al. 2000).

F. VGSC disease implications

The Nav family is involved in a wide range physiological processes. Dysregulation of these channels causes numerous human diseases. Gain-of-function (GOF) and loss-of-function (LOF) mutations in the brain isoforms Nav1.1, Nav1.2, Nav1.3 and Nav1.6 are attributed to intellectual disability, developmental disorder, autism spectrum disorder, absence seizure, Alzheimer's disease, varied movement disorders, and different types of early infantile epileptic encephalopathy (EIEE), (Catterall, Kalume et al. 2010, Sanders, Campbell et al. 2018, Smith, Kenny et al. 2018, Symonds and Zuberi 2018, Zaman, Helbig et al. 2018); Nav1.4 is associated with muscular disorders like myotonia and periodic paralysis hyperkalemic (Pan, Li et al. 2018); Nav1.5 is linked to cardiac arrhythmia, underlying long-QT and Brugada syndromes (Gardill, Rivera-Acevedo et al. 2018); mutations in Nav1.7, Nav1.8 and Nav1.9 are mainly involved in neuropathic pain disorders including erythromelalgia and anosmia (Huang, Han et al. 2014).

Functional defects in brain isoforms Nav1.1, Nav1.2, Nav1.3 and Nav1.6 present clinically distinct phenotypes and have highly variable electrophysiological outcomes, due to their differential expression pattern in brain region, neuronal cell type, subcellular compartment and during development.

Nav1.1 is predominantly expressed in inhibitory interneurons, the activity of which provides the inhibitory tone in the neural network. As a result, LOF mutations in Nav1.1 lead to seizure-related disorders with varied severity. Complete LOF mutations, usually resulting from protein truncation, cause severe myoclonic epilepsy of infancy, also known as Dravet's Syndrome; mild LOF mutations are considered genetic predisposition to febrile seizures; other LOF mutations, resulting in intermediate impairment of Nav1.1 function, cause generalized epilepsy with febrile seizures plus (GEFS+) (Catterall, Kalume et al.

2010). Moreover, mouse model with selective *SCN1A* deletion in inhibitory neurons cause seizures and premature mortality (Cheah, Frank et al. 2012, Kalume, Westenbroek et al. 2013, Rubinstein, Han et al. 2015). Therefore, this evidence supports a predominant role of Nav1.1 in the excitability of inhibitory interneurons, and thus loss of Nav1.1 activity decreases the inhibitory tone in the neural network, leading to hyperexcitability found in seizure-related disorders.

Nav1.2 is widely expressed in excitatory neurons in the CNS. The subcellular localization of the channel changes remarkably during development and differs between brain regions. Initially, Nav1.2 is found throughout the axon and exhibit high density at the axon initial segments (AIS) in cortical excitatory neurons. During development, Nav1.2 at the distal AIS is gradually replaced by Nav1.6 and is not usually found at the nodes of Ranvier or other parts of the myelinated axon. The restricted localization of Nav1.2 to the proximal AIS is thought to play an essential role in action potential backpropagation (Hu, Tian et al. 2009). On the other hand, in the cerebellar cortex, Nav1.2 expression persists throughout development and is co-expressed with Nav1.6 in adult unmyelinated axons (Martínez-Hernández, Ballesteros-Merino et al. 2013). Recent findings reveal an unexpected role of Nav1.2 in synaptic modulation well beyond the developing stage and suggest a dendritic distribution of Nav1.2 in the prefrontal cortex (Spratt, Ben-Shalom et al. 2019). With this complicated and developmentally dynamic pattern of distribution, Nav1.2 mutations manifest in distinct neurological disorders.

GOF mutations in Nav1.2 lead to seizure-related disorders, the severity of which depends on the degree of functional potentiation. Severe variants are generally *de novo* mutations and lead to EIEE, while milder variants can be inherited or *de novo* and cause benign (familial) infantile seizures (BISs) that usually resolve by 2 years of age. On the contrary, LOF mutations in Nav1.2 are related to autism spectrum disorder (ASD) and intellectual disability (ID).

Nav1.3 is the least understood Nav isoform in the human brain. It is robustly expressed across human cortical regions during gestation but downregulated postnatally. It is enriched in cortical progenitors and neurons, which was reported to not generate action potentials (Smith, Kenny et al. 2018). Therefore, the precise role of Nav1.3 is still unclear, it is proposed to be important for cortical folding and gyral formation during prenatal development. Both GOF and LOF mutations in Nav1.3 have been associated with seizure related disorders (Estacion, Gasser et al. 2010, Lamar, Vanoye et al. 2017, Zaman, Helbig et al. 2018) and speech and oral motor dysfunction (Smith, Kenny et al. 2018).

Nav1.6 starts its expression relatively late in development, but it has the widest distribution in the CNS throughout the adult life. As a result, Nav1.6 dysfunction has been associated with many severe neurological disorders. Indeed, Nav1.6 is among the top 2% of human proteins that are least tolerant of genetic variation (Wagnon and Meisler 2015), and Nav1.6 null mice exhibit juvenile lethality (Burgess, Kohrman et al. 1995, Meisler, Plummer et al. 2004, Sharkey, Cheng et al. 2009). The first Nav1.6-associated disorder was identified in a patient with cerebellar atrophy, ataxia, and mental retardation (Trudeau, Dalton et al. 2006). In 2012, the first epilepsy-related *SCN8A* mutation has been identified using whole-genome sequencing (Veeramah, O'Brien et al. 2012). To this date, it is generally accepted that GOF mutations in Nav1.6 result in EIEE, while LOF mutations are associated with intellectual disability, developmental delay, and absence seizure. These disorders are usually comorbid with varied degree of movement disorders, which can be explained by the predominant localization of Nav1.6 in cerebellar Purkinje neurons. Interestingly, a recent finding identifies Nav1.6 abnormality in an Alzheimer's disease mouse model (Ciccone, Franco et al. 2019).

G. VGSC regulation and modulation

VGSCs are critical determinants of excitability. Their expression and function are tightly regulated by interacting proteins, toxins, and post-translational modifications.

The Nav α subunit interacts with a myriad of important interacting partners including but not limited to Nav β subunits (Hull and Isom 2018), calmodulin, fibroblast growth factor homologous factors (FHFs) (Wang, Chung et al. 2012, Wang, Chung et al. 2014) and ankyrinG (ankG) (Shirahata, Iwasaki et al. 2006, Gasser, Ho et al. 2012). These protein partners can regulate Nav trafficking, expression pattern and gating in isoform- and cell type-specific manners (Deschênes, Neyroud et al. 2002, Herzog, Liu et al. 2003, Chichili, Xiao et al. 2013, Ben-Johny, Yang et al. 2014, Barbosa, Xiao et al. 2017, Yan, Wang et al. 2017).

The exact outcome of β regulation depends on Navα isoform and cell type. Generally, β1 accelerates activation and inactivation kinetics (Isom, De Jongh et al. 1992). β2 promotes surface expression of Navα subunits (Chen, Bharucha et al. 2002, Chen, Westenbroek et al. 2004). β3 shifts the voltage dependence of activation and increases persistent current (Morgan, Stevens et al. 2000). β4 is considered one of the important components that support the generation of sodium resurgent currents (Raman, Sprunger et al. 1997, Grieco, Malhotra et al. 2005, Jarecki, Piekarz et al. 2010).

H. Post-translational modifications of VGSC

VGSC function is determined by the intrinsic biophysical properties, but it can also be regulated by post-translational modifications. Multiple post-translational modifications that covalently modify VGSCs in neurons and muscle

have been identified. These include, but are not limited to, phosphorylation, ubiquitination, S-palmitoylation, nitrosylation, glycosylation, and SUMOylation. Post-translational modifications of VGSCs can have profound impact on cellular excitability, contributing to normal and abnormal physiology. While some modifications have similar effects on the various VGSC isoforms, others display isoform-specific modulations. In addition, while much has been learned about how individual modifications can impact VGSC function, there is still more to be learned about how different modifications can interact.

Post-translational VGSC modulation appears to be critically important in neurons and cardiac tissue. It is less clear what the physiological role of sodium channel modulation is in skeletal muscle, although it is likely to be involved in disease states such as critical illness myopathy (Teener and Rich 2006). CaMKII phosphorylation of brain VGSCs has been implicated as a major regulator of VGSC persistent currents (Thompson, Hawkins et al. 2017) and is likely to contribute to pathophysiologies such as epilepsy. Cardiac sodium channel modulation is believed to be important in rhythmogenesis (Schubert, Vandongen et al. 1990, Wagner, Maier et al. 2015). As a result, Nav1.5 modulation has been extensively studied, and Nav1.5 is the target of a multitude of post-translational modifications including glycosylation, phosphorylation, methylation, acetylation, redox modifications, S-palmitoylation, and ubiquitination (Ashpole, Herren et al. 2012, Marionneau and Abriel 2015, Pei, Xiao et al. 2016). Because of modern protein analysis technologies such as mass spectrometry, researchers are able to better determine the precise location of post-translational modification sites and consensus sequence among different VGSC subtypes, leading to a better understanding of the mechanistic details of these regulations.

1. Phosphorylation

Phosphorylation is the most extensively studied post-translational modification of VGSCs. The identification of VGSC phosphorylation reveals the involvement of VGSC in dynamic cellular processes and its potential crosstalk with numerous second-messenger pathways (Cantrell and Catterall 2001). Various protein kinases have been identified to modify different isoforms of VGSC. These include protein kinase A and C (PKA and PKC) (Murray, Fahrig et al. 1994, Murray, Hu et al. 1997, Shin and Murray 2001), adenosine monophosphate-activation protein kinase (AMPK) (Light, Wallace et al. 2003), Ca2+/calmodulin-dependent serine/threonine protein kinase (CaMK) (Ashpole, Herren et al. 2012, Thompson, Hawkins et al. 2017), p38 MAP kinase (Wittmack, Rush et al. 2005, Gasser, Cheng et al. 2010, Wu, Cao et al. 2016), phosphatidylinositol 3-kinase (PI3K) (Lu, Jiang et al. 2013), and GSK3β (Scala, Nenov et al. 2018).

These kinases can add a negatively charged phosphate group to select serine, threonine, or tyrosine residues. It is not possible to give a comprehensive review of all the findings relating to this powerful form of VGSC modulation, so here only a few specific areas are covered to provide highlights of what can be learned from the study of VGSC phosphorylation. Many of the phosphorylation sites that have been identified are located in the first intracellular linker loop (DI–DII linker), and a number of these are conserved among different species and subtypes (Marionneau and Abriel 2015). Early estimates indicated that the Navα subunit could be phosphorylated at somewhere between 2 and 20 sites by PKA, PKC, and possibly other protein kinases. Numann et al. (Numann, Catterall et al. 1991) studied the effect of PKC on rat brain Nav1.2 expressed in Chinese hamster ovary cells. They reported that activation of PKC with a membrane-permeant agent, l-oleoyl-2-acetyl-sn-glycerol (OAG), both inhibited the peak current and slowed macroscopic fast inactivation of rat neuronal sodium

channels. West et al. (West, Numann et al. 1991) reported that phosphorylation of serine 1506 in the III–IV linker by PKC was responsible for the slowing of RIIA (Nav1.2) macroscopic inactivation. After this potential PKC site, located in the III–IV linker, was removed by mutating serine 1506 to an alanine, neither the slowing nor the inhibition by OAG was observed. Additional experiments seemingly confirmed that phosphorylation of S1506 was necessary and sufficient for the observed slowing of inactivation. However, while phosphorylation of S1506 was also necessary for the decrease in current, it was not sufficient: phosphorylation of another site, possibly in the I–II linker, also seemed to be needed for the inhibition (Li, West et al. 1993). However, subsequent studies on PKC modulation of neuronal sodium channels in hippocampal neurons did not observe pronounced slowing of inactivation (Chen, Cantrell et al. 2005). This could be due to complex interactions between post-translational modifications and/or accessory subunits. The putative PKC site in the III–IV linker is conserved in most VGSCs. PKC phosphorylation of the corresponding residue in Nav1.5 causes a major negative shift in the voltage dependence of inactivation (Qu, Rogers et al. 1996). Interestingly, this site is also conserved in Nav1.4, but while PKC also induces a negative shift in the voltage dependence of inactivation for Nav1.4, this effect is not dependent on the corresponding serine in the III–IV linker (Bendahhou, Cummins et al. 1995). Data from Xenopus oocyte experiments indicate that both Nav1.7 and Nav1.8 currents are inhibited by PKC activation and that this also shifts the voltage dependence of activation in the depolarizing direction (Vijayaragavan, Boutjdir et al. 2004). By contrast PKA activation enhanced Nav1.8 but inhibited Nav1.7currents in this experimental system. Recently it was shown that Nav1.7 resurgent sodium currents are enhanced by PKC, and this effect is modulated by the state of the corresponding III–IV linker residue in Nav1.7 (Tan, Priest et al. 2014). This illustrates some of the complexities of determining the functional consequences of VGSC phosphorylation and comparing the effects on various isoforms in various tissues.

Mass spectrometry is providing enhanced estimates of VGSC phosphorylation, although obtaining full coverage can be difficult with complex transmembrane proteins like VGSC. In one study of Nav1.2 (Berendt, Park et al. 2010), 66% cover of the cytoplasmic linkers was obtained. Fifteen sites were identified, 1 in the N-terminus, 11 in the I–II linker, and 3 in the C-terminus. Unfortunately, there was insufficient coverage in the III–IV linker to determine if the conserved serine residue discussed above was phosphorylated in the brain tissue. In a follow-up study on Nav1.2 (Baek, Rubinstein et al. 2014), it was found that acute kainate-induced seizures induced a significant reduction in phosphorylation of nine sites in Nav1.2. Not surprisingly, these are primarily sites located in the I–II linker. However, this study also revealed that this downregulation was due, at least in part, to an increase in methylated arginines at three sites. Thus distinct regulation of phosphorylation and methylated arginines in Nav1.2 is likely to contribute to functional changes in Nav1.2, modulation of neuronal excitability, and perhaps seizure activity.

CaMKII is believed to be an important regulator of excitability in neurons and muscle. CaMKII modulation of VGSCs has also been implicated in physiological and pathophysiological control of excitability. Increased CaMKII activity has been implicated in animal models of heart failure as well as in studies of failing human hearts (Hoch, Meyer et al. 1999, Zhang, Maier et al. 2003). In one study of CaMKII and Nav1.5 (Ashpole, Herren et al. 2012), it was found that a negative shift in Nav1.5 steady-state inactivation resulted from CaMKII-dependent phosphorylation of Nav1.5 at two specific phosphor sites. However, a mass spectroscopy analysis of human Nav1.5 purified from HEK293 cells with >80% coverage identified 23 sites that could be phosphorylated by CaMKII in vitro (Herren, Weber et al. 2015). This suggests that Nav1.5 can be extensively modified by phosphorylation. A study of sodium currents in neurons from a SCN2A (Nav1.2) mutant mouse with epilepsy found that CaMKII

phosphorylation of Nav1.2 increases persistent sodium currents and excitability. Maltsev et al. (Maltsev, Reznikov et al. 2008) reported that CaMKII can also increase persistent sodium currents in cardiac myocytes. Burel et al. (Burel, Coyan et al. 2017) identified two distinct CaMKII phosphor sites in the C-terminus of Nav1.5 that contribute in part to increased Nav1.5 persistent currents; however, this modulation involved altered binding of FGF13 to Nav1.5. Interestingly, these two sites were not among the 23 sites identified by Herren et al (Herren, Weber et al. 2015). Although several hundred studies have investigated how a multitude of kinases modulate VGSC isoforms and a substantial amount of insight has been gained, our knowledge of the interplay between different phosphorylation sites and how this impacts interactions with accessory proteins is still incomplete.

2. Arginine methylation

As mentioned above, VGSCs can also be modified at the nitrogen-containing side-chains of arginine and lysine residues by arginine methylation, which is much less known about compared to VGSC phosphorylation. Mass spectrometry identified arginine methylation of Nav1.5 from both human ventricles and a cell line stably expressing Nav1.5 (Beltran-Alvarez, Pagans et al. 2011, Beltran-Alvarez, Tarradas et al. 2014). Further studies revealed that Nav1.5 arginine methylation enhanced surface expression of the channel and thus increased its current density (Beltran-Alvarez, Espejo et al. 2013, Beltran-Alvarez, Tarradas et al. 2014, Beltran-Alvarez, Feixas et al. 2015). It is likely that other Nav isoforms, in addition to Nav1.2 and Nav1.5, are regulated by arginine methylation. Differential expression of protein arginine methyl transferases may play a role in how VGSCs are modulated in different tissue and subcellular compartments.

3. Glycosylation

Glycosylation is another common post-translational modification of ion channels. It attaches glycans to proteins and affects folding, and modulates the thermostability as well as the overall charge of glycoproteins. These sugar groups can be quite complex and extensive, making analysis complicated. Early reports (Waechter, Schmidt et al. 1983) indicated that glycosylation of neuronal VGSCs played a crucial role in biosynthesis, trafficking, and degradation of these channels. N-linked glycosylation attaches glycans to a nitrogen of asparagine or arginine side-chains, while O-linked glycosylation the hydroxyl oxygen of serine, threonine, tyrosine, hydroxyllysine, or hydroxyproline side-chains, or to oxygens on lipids such as ceramide. These attached glycans are often terminated by sialic acids, altering VGSC properties with their negative charges.

Glycosylation impacts functional properties for multiple VGSC isoforms. It is not completely clear what the underlying mechanisms are, but it is thought that the surface charge of sialic acids is involved in the modulation of VGSC by glycosylation. The impact of glycosylation on Nav1.4 voltage dependence of activation and inactivation can be quite large, with both N-linked glycans and O-linked glycans likely playing a role (Ednie, Harper et al. 2015). Glycosylated Nav1.5 only has a 5% mass increase, which is far less than the 25–30% increase observed with some other VGSC isoforms (Cohen and Levitt 1993). Despite the lesser degree of modification, there is still compelling evidence that glycosylation can be an important determinant of Nav1.5 membrane trafficking (Mercier, Clément et al. 2015). Indeed, it has been shown that the reduction of glycosylation in Nav1.5 can slow fast inactivation and increase the rate of recovery from inactivation, shortening the refractory time of the cardiomyocyte and enhancing susceptibility to ventricular arrhythmias (Ednie, Harper et al. 2015). The sensory neuronal channel Nav1.9 is not extensively glycosylated, yet changes in glycosylation can still impact voltage dependence of steady-state

inactivation, and this appears to be developmentally regulated (Tyrrell, Renganathan et al. 2001). In addition to modifying Navα subunits, it is well established that Navβ subunits can also be glycosylated (Johnson, Montpetit et al. 2004, Patel and Brackenbury 2015)(Laedermannetal.2013a). However, the extent to which Navβ glycosylation is involved in control of excitability is not fully understood, and improved strategies for determining how VGSC glycosylation is controlled will undoubtedly provide invaluable insight in the near future.

4. Ubiquitination

Ubiquitination is another well-studied post-translational modification of VGSCs. It is the enzymatic attachment of ubiquitin, a small protein of 76 amino acids, to the modifying protein. Although ubiquitin is a small protein, only about 8.5 kDa, but is a fairly large addition to a protein compared to most post-translational modifications. The addition can alter protein function in several ways. Ubiquitination can target a protein to proteasomes and induce degradation. It can also alter localization of proteins and/or their functional properties. Modifications can involve addition of a single ubiquitin subunit or a chain of ubiquitin molecules. Addition of an ubiquitin molecule involves three proteins with distinct functions. Abriel et al. (Abriel, Kamynina et al. 2000) investigated the functional consequences of a PY (PPXY) motif in the C-terminus region of Nav1.5. This motif can bind Nedd4, an ubiquitin-protein ligase. Mutation of the PY motif in Nav1.5 increased current density. Interestingly, overexpression of Nedd4 could decrease Nav1.5 but not Nav1.4 current, probably because Nav1.4 lacks the PY motif. This indicated that ubiquitination can be closely associated with Nav1.5 internalization. Ubiquitination of Nav1.5 has been demonstrated in both *in vitro* and *in vivo* studies (van Bemmelen, Rougier et al. 2004, Laedermann, Decosterd et al. 2014). Rougier et al. (Rougier, van Bemmelen et al. 2005) noted that most VGSC isoforms contain a PY motif (the exceptions being Nav1.4 and Nav1.9). They found that Nedd4-2 could downregulate Nav1.2,

Nav1.3, and Nav1.5 currents in HEK293 cells with a corresponding reduction in surface expression. Fotia et al. (Fotia, Ekberg et al. 2004) demonstrated that Nedd4-2 could downregulate Nav1.7 and Nav1.8 currents. While many studies have suggested that regulation of ubiquitination of VGSCs could lead to an altered surface expression level of channels (Rougier, Gavillet et al. 2013, Laedermann, Pertin et al. 2014), the detailed mechanism involved in this process and the study of its clinical relevance are still lacking. Interestingly, several studies were able to demonstrate that reduced Nedd4-2 levels led to DRG hyperexcitability, and conditions that increase pain in rodents downregulate Nedd4-2 expression in DRG, indicating that reduced ubiquitination of VGSCs might be involved in the development of neuropathic pain (Cachemaille, Laedermann et al. 2012, Laedermann, Cachemaille et al. 2013). Although Nav1.6 also has a PY motif in its C-terminus, it also appears to have a potential Nedd4 binding site in the I–II linker. In an elegant study, Gasseret al. (Gasser, Cheng et al. 2010) demonstrated that downregulation of Nav1.6 can be enhanced by p38 MAP kinase phosphorylation of the region involved in the I–II linker, indicating that Nedd4-induced ubiquitination and subsequent internalization of Nav1.6 involve at least two distinct Nedd4 binding sites and may be a stress response that limits cell excitability under pathophysiological conditions.

5. SUMOylation

The small ubiquitin-like modifier (SUMO) protein can also be conjugated to proteins, including ion channels. SUMO proteins are roughly 12 kDa in size and, as with ubiquitin, are added to other proteins by enzymes. Plant et al. (Plant, Marks et al. 2016) found that adding SUMO protein to the pipet solution can increase the amplitude of Nav1.2-mediated currents in HEK293 cells. They also showed that SUMO modulated Nav1.2 currents in cerebellar neurons. SUMOylation occurs on lysine residues. Plant et al. reported that mutating K38 in

the N-terminus of Nav1.2 eliminated the effect of SUMO. Thus Nav1.2 seems to be directly regulated by SUMOylation. This increase in current due to SUMOylation occurred rapidly in response to hypoxic conditions and may underlie some of the initial toxicity associated with hypoxia. SUMOylation also shifted the voltage dependence of activation and steady-state inactivation in the negative direction. While a negative shift in activation can increase excitability, a negative shift in inactivation can decrease excitability. SUMOylation has also been implicated in control of excitability in sensory neurons (Dustrude, Moutal et al. 2016). Reduced SUMOylation of collapsin response mediator protein 2 (CRMP2) can alter CRMP2 binding to Nav1.7. As a consequence, Nav1.7 membrane localization and current density is reduced. CRMP2 enhances ubiquitination and endocytosis of Nav1.7. This illustrates the sometimes complex web of post-translational modifications that can influence VGSCs.

I. S-palmitoylation

S-palmitoylation, also referred to as S-acylation, has emerged as an important mechanism that regulates protein functions. S-palmitoylation was first reported in 1979 (Schmidt and Schlesinger 1979), even earlier than the discovery of tyrosine phosphorylation (Ushiro and Cohen 1980), and yet the study of S-palmitoylation lags far behind that of phosphorylation, largely due to the technical difficulties in the detection and analysis of S-palmitoylation, in producing antibodies that target S-palmitoylated proteins, and in purifying the enzymes responsible for the catalysis of the S-palmitoylation reaction. Recent advancement in S-palmitoylation detection has revealed the large scope of protein S-palmitoylation and its importance in regulating essential cellular processes by modifying both peripheral and integral membrane proteins. However, our knowledge of how S-palmitoylation regulates VGSCs is still limited (Shipston 2011).

1. The S-palmitoylation reaction

S-palmitoylation is a post-translational modification that covalently attaches palmitate, a 16-carbon saturated fatty acid, to cysteine thiols of the target protein via thioester bond (Fig.4). Distinguished from most other lipid post-translational modifications (e.g. myristoylation, O-acylation, and prenylation), S-palmitoylation is reversible, due to the labile nature of the thioester bond. The S-palmitoylation reaction is catalyzed by the enzyme family palmitoyl-acyl transferase (PAT); while the reverse process, depalmitoylation, is catalyzed by the enzyme family acyl-protein thioesterase (APT).

The PAT enzyme family is also referred to as zDHHC-PAT, because they share a signature catalytic domain that has a zinc-finger and aspartate-histidine-histidine-cysteine (zDHHC) motif (Dunphy, Schroeder et al. 2000)(Fig.4). The zDHHC-PATs are transmembrane proteins containing 4 or 6 transmembrane segments and N- and C-terminal domains exposed to the cytosol. The zDHHC motif typically locates in the linker between the second and third transmembrane segments. Some of the zDHHC-PATs also contain an ankyrin repeat in the N-terminal domain (Lemonidis, Sanchez-Perez et al. 2015).

The S-palmitoylation reaction is accomplished with a two-step palmitate transfer process. First, the zDHHC-PAT becomes auto-S-palmitoylated at the cysteine in the zDHHC motif, which has been shown to be crucial for the enzymatic activity of several PATs (Roth, Feng et al. 2002, Smotrys, Schoenfish et al. 2005, Valdez-Taubas and Pelham 2005, Yang, Di Vizio et al. 2010). Then, the S-palmitoylated zDHHC-PAT transfers the attached palmitate to the target protein (Mitchell, Mitchell et al. 2010, Jennings and Linder 2012).

The APTs are cytosolic enzymes. They belong to a metabolic serine hydrolase superfamily (Bachovchin, Ji et al. 2010). Interestingly, the APTs are

also substrates for PATs. The S-palmitoylation status of the APTs serve to regulate their localization between the membrane and the cytosol (Yang, Di Vizio et al. 2010, Kong, Peng et al. 2013). Later studies also identified depalmitoylation enzymes palmitoyl protein thioesterases 1 and 2 (PPT1/2) located in the lysosome (Lin and Conibear 2015), as well as 38 serine hydrolases from mouse (also referred to as ABHD proteins) with depalmitoylated activity (Lin and Conibear 2015, Yokoi, Fukata et al. 2016).

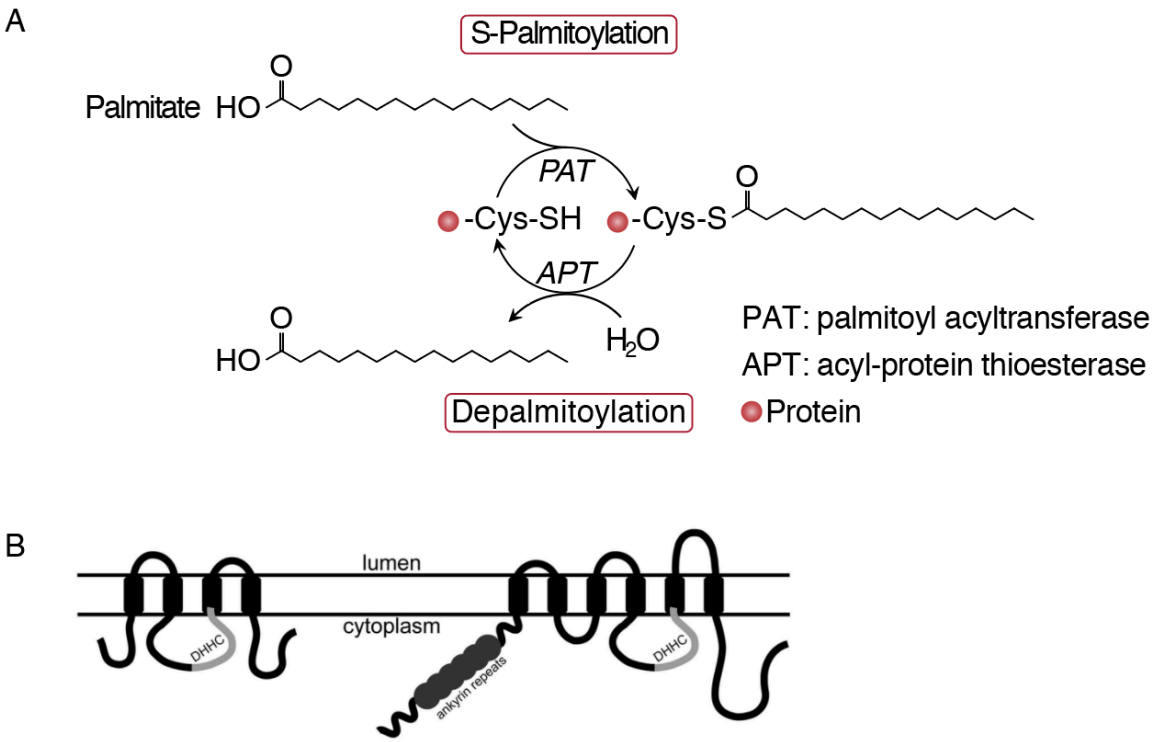

Figure 4. S-palmitoylation reaction and PAT structure.

(A) The S-palmitoylation-depalmitoylation cycle. (B) Topological structure of zDHHC-PATs from (Linder and Jennings 2013).

2. The zDHHC enzyme family and potential enzyme-substrate specificity

The human zDHHC-PATs belong to a large enzyme family. They are encoded by 23 human *zDHHC* genes (*zDHHC1–zDHHC24* with no *zDHHC10*). These zDHHC-PATs display differential cell type and subcellular localization. Table 1 adopted from (Korycka, Łach et al. 2012) summarizes the characteristics of these human zDHHC-PATs. The majority of zDHHC-PATs locate in the endoplasmic reticulum (ER) and the Golgi apparatus, while some are found at the plasma membrane (Ohno, Kihara et al. 2006).

For a long time, S-palmitoylation has been considered stochastic, because a consensus sequence motif has yet to emerge (Rocks, Gerauer et al. 2010). However, it is proposed that the differential tissue, cell type, and subcellular distribution of the zDHHC-PATs creates a spatial, and thus functional segregation among the enzymes, underlying potential enzyme-substrate specificity. Moreover, growing evidence suggests that zDHHC-PATs may recognize their substrates based on protein secondary structure (Plain, Congreve et al. 2017) and / or protein-protein interacting domains (Li, Hu et al. 2010, Thomas, Hayashi et al. 2012, Fredericks, Hoffmann et al. 2014, Brigidi, Santyr et al. 2015, Lemonidis, Sanchez-Perez et al. 2015), instead of relying on a primary amino acid sequence motif. Indeed, experiments have indicated that the zDHHC-PATs display differential but overlapping specificity for substrate proteins (Fukata, Fukata et al. 2004, Roth, Wan et al. 2006, Ponimaskin, Dityateva et al. 2008, Noritake, Fukata et al. 2009, Brigidi, Sun et al. 2014, Lievens, Kuznetsova et al. 2016), supporting the existence of enzyme-substrate specificity for S-palmitoylation (Hou, John Peter et al. 2009, Huang, Sanders et al. 2009, Nadolski and Linder 2009, Thomas, Hayashi et al. 2012, Howie, Reilly et al. 2014, Lemonidis, Sanchez-Perez et al. 2015).

Table 1 Characteristics of the human zDHHC-PAT family

	Accession number	Alternative names	Chromosomal location of gene	Number of spliced variants	Number of SNPs	Size of gene [kb]	Number of exons	Intracellular localization of protein	Tissue-specific distribution
ZDHHC 1	NM_013304.2	ZNF377, C16orf1, HSU90653	16q22.1	15	140	27.11	13	ER	Brain, lung, uterus, placenta
ZDHHC 4	NM_018106.3	ZDHHC4andC7orf26, ZNF374, FLJ10479	7p22.1	25	148	31.33	8	Golgi	Brain, lung, testis, prostate
ZDHHC 5	NM_015457.2	ZNF375, KIAA1748, DKFZp586K0524	11q12.1	9	321	33.44	12	Plasma membrane	Prostate, testis, lung, colon, eye
ZDHHC 6	NM_022494.1	ZNF376, FLJ21952	10q25.2	9	158	17.30	9	ER	Brain, uterus, kidney, lung, colon, thymus, small intestine
ZDHHC 11	NM_024786.2	ZNF399, FLJ13153	5p15.33	10	1176	63.37	16	ER	Testis, placenta, brain, lung, cerebellum
ZDHHC 14	NM_153746.1	NEW1CP, FLJ20984	6q25.3	8	2260	296.68	13	ER	Brain, eye, fetal eyes, prostate, uterus
ZDHHC 15	NM_144969.1	MRX91, FLJ31812, MGC119974, MGC119975, MGC119976	Xq13.3	7	2059	153.08	12	Golgi	Brain, trachea, cerebellum, ear, eye, kidney
ZDHHC 16	NM_198046.1	APH2, MGC2993	10q24.1	18	109	11.63	12	ER	Brain, placenta, lung, uterus, skin
ZDHHC 18	NM_032283.2	DKFZp667O2416, DHHC18	1p36.11	18	243	70.45	6	Golgi	Lung, testis, brain, placenta, carcinoid, kidney, prostate
ZDHHC 19	NM_001039617.1	DHHC19, MGC33345	3q29	8	288	13.99	10	ER	Testis, brain, medulla, placenta
ZDHHC 20	NM_153251.2	FLJ25952, MGC126005	13q12.11	15	872	105.53	17	Plasma membrane	Placenta, uterus, brain, lung, testis
ZDHHC 22	NM_174976.2	C14orf59	14q24.3	2	128	11.47	3	ER/Golgi	Brain, eye, lung
ZDHHC 23	NM_173570.3	NIDD, MGC42530	3q13.31	5	149	15.47	6	ER/Plasma membrane	Testis, brain, colon, kidney
ZDHHC 24	NM_207340.1	–	11q13.2	3	86	25.57	3	ER/Plasma membrane	Brain, pancreas, prostate, stomach

(Korycka, Łach et al. 2012)

3. Functionalities of S-palmitoylation

S-palmitoylation is a multifunctional post-translational modification. The addition of palmitate increases the hydrophobicity of a protein and creates a hydrophobic tethering point to the membrane (Fig.5). This can affect the life cycle of the protein, regulating stability, membrane association, and intracellular trafficking. These functionalities have been extensively demonstrated with multiple peripheral membrane proteins like the small GTPase Ras, the signaling activity of which depends on its dynamic shuttling between the Golgi and the plasma membrane. Ras is S-palmitoylated in the Golgi, after which is routed to the plasma membrane; Ras at the plasma membrane can be depalmitoylated by APT, after which it is dissociated from the plasma membrane and directed back to the Golgi (Cox, Der et al. 2015). Therefore, S-palmitoylation serves as a membrane trap or membrane anchor for peripheral membrane proteins and dictates their membrane attachment in non-polarized cells.

In addition to the plasma membrane, S-palmitoylation also targets proteins to other specialized cellular compartments. The post-synaptic scaffolding protein PSD-95 switches between S-palmitoylated and non-palmitoylated status in an activity dependent manner. Blocking neuronal activity enhances PSD-95 S-palmitoylation and its accumulation at the the post-synaptic density (PSD), while increased synaptic activity accelerates PSD-95 depalmitoylation and dissociates the protein from PSD (Topinka and Bredt 1998, Noritake, Fukata et al. 2009). Interestingly, S-palmitoylation also changes the conformation of PSD-95. Non-palmitoylated PSD-95 is in a compact conformation, which does not interact with AMPA or NMDA receptors. S-palmitoylated PSD-95 transforms into an extended conformation and directly binds with AMPA and NMDA (Jeyifous, Lin et al. 2016). As a result, S-palmitoylation regulates synaptic transmission and plasticity.

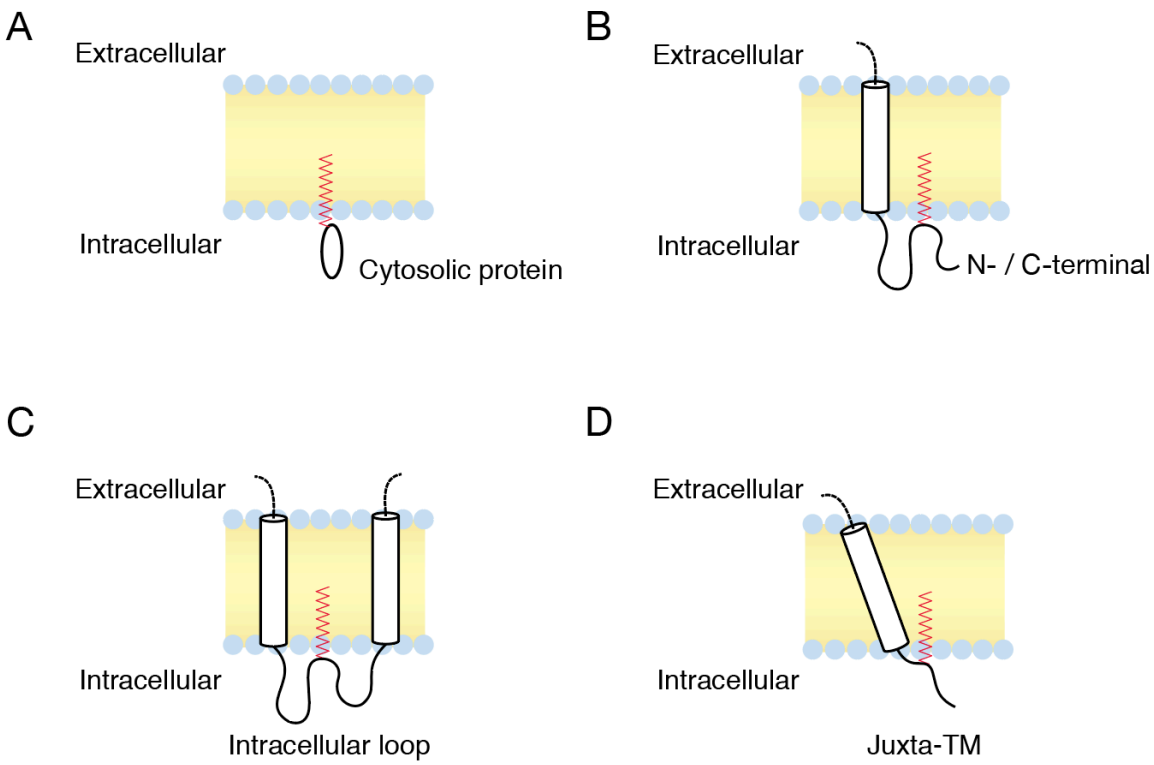

Figure 5. Different location of a hydrophobic tethering point created by S-palmitoylation.

S-palmitoylation also modifies integral membrane proteins, which is important for their correct processing and precise targeting to specific membrane compartments. Numerous neurotransmitter receptors are reported to be regulated by S-palmitoylation. These include but are not limited to AMPA, NMDA and kainate glutamate receptors, GABAA receptor, μ- and δ-opioid receptors, D1-D4 dopamine receptors, CB1 cannabinoid receptor, and 5-$HT_{(1A, 4, 7)}$ serotonin receptors (Naumenko and Ponimaskin 2018). One interesting case is presented by the regulation of AMPA receptor by S-palmitoylation. S-palmitoylation of a cysteine in the TMD2 of AMPA receptor results in Golgi retention, reducing the amount of AMPA receptor at the plasma membrane, while S-palmitoylation of another cysteine in the TMD4 inhibits the interaction between AMPA receptor and membrane-cytoskeleton adaptor protein 4.1N and facilitates AMPA receptor internalization (Hayashi, Rumbaugh et al. 2005, Yang, Xiong et al. 2009). In combination of the regulatory effect of S-palmitoylation on PSD-95, the precise localization of AMPA receptors are regulated by S-palmitoylation at multiple levels. Another intriguing example of integral membrane protein regulation is demonstrated by the dopamine transporter (DAT). The transporting capacity of DAT is reciprocally regulated by PKC-phosphorylation and S-palmitoylation (Moritz, Rastedt et al. 2015). In high phosphorylation / low S-palmitoylation state, DAT transporting capacity is reduced, whereas in low phosphorylation / high S-palmitoylation state, DAT transporting capacity is increased. Such crosstalk between phosphorylation and S-palmitoylation is also found in the BK potassium channel (Tian, Jeffries et al. 2008), in the scaffold protein AKAP79/150 (Woolfrey, O'Leary et al. 2018), and in the neuronal growth-associated protein GAP43 (Gauthier-Kemper, Igaev et al. 2014). Therefore, S-palmitoylation is also involved in complex interplays with other post-translational modification to regulate protein function.

S-palmitoylation also fine-tunes the activity of ion channels by imposing conformational change. Loss of S-palmitoylation in Kv1.1 results in a negative shift of the current-voltage relationship, inactivation at more positive potentials and a reduction of channel conductance (Gubitosi-Klug, Mancuso et al. 2005). It is also reported that S-palmitoylation modulated cardiac excitability by modifying the cardiac sodium channel Nav1.5 (Pei, Xiao et al. 2016), and that manipulating S-palmitoylation status of Nav1.2 altered its voltage dependence and toxin sensitivity (Bosmans, Milescu et al. 2011).

Therefore, S-palmitoylation not only regulates protein shuttling between intracellular compartments by affecting membrane association, but also can have significant impact on protein-protein interaction, protein conformation and ion channel biophysics (Chien, Carr et al. 1996, Hayashi, Rumbaugh et al. 2005, Fukata and Fukata 2010, Bosmans, Milescu et al. 2011, Pei, Xiao et al. 2016, Globa and Bamji 2017, Pei, Pan et al. 2017, Itoh, Yamashita et al. 2018, Naumenko and Ponimaskin 2018, Itoh, Okuno et al. 2019).

Moreover, S-palmitoylation is involved in host-pathogens interactions (Blanc, Blaskovic et al. 2013), membrane curvature modulation (Chlanda, Mekhedov et al. 2017), extrinsic and intrinsic apoptosis pathways (Fröhlich, Dejanovic et al. 2014, Akimzhanov and Boehning 2015), and innate immunity (Chesarino, Hach et al. 2014, Mukai, Konno et al. 2016, McMichael, Zhang et al. 2017).

4. S-palmitoylation disease implications

The most recognized diseased conditions associated with abnormal S-palmitoylation is cancers. For one thing, 78 out of 299 cancer drivers identified by Bailey et al (Bailey, Tokheim et al. 2018) are annotated S-palmitoylated proteins in the SwissPalm database (Blanc, David et al. 2015). For another, altered

zDHHC-PATs have been linked to various cancers (Ko and Dixon 2018). zDHHC11, zDHHC17, and zDHHC20 upregulation is found in several tumor types and thus are identified as potential oncoproteins, while lower zDHHC2 and zDHHC13 expression is found in different cancer types and thus have been considered tumor suppressors. However, conflicting evidence exists for zDHHC5 and zDHHC14, the precise role of which may depend on the specific tissue and/or cancer type.

Another group of S-palmitoylation related disorders are found in the nervous system. zDHHC8 is the most studied zDHHC-PAT that has been implicated in neurological disorders. The *zDHHC8* gene locates in the human chromosome 22q11.2 locus, the microdeletions of which results in cognitive deficits and a high risk of schizophrenia (Chow, Watson et al. 2006, Xu, Roos et al. 2008). Moreover, a single-nucleotide polymorphism (SNP) in *zDHHC8* that leads to a truncated inactive form of the enzyme is related to the development of schizophrenia (Mukai, Liu et al. 2004, Mukai, Dhilla et al. 2008). Huntington's disease is another S-palmitoylation associated neurological disorder. A reduction of S-palmitoylation by zDHHC17 has been observed in the disease causing huntingtin protein (Huang, Yanai et al. 2004, Yanai, Huang et al. 2006). S-palmitoylation is also implicated in Alzheimer's disease. The amyloid precursor protein (APP) is the substrate of zDHHC7 and zDHHC21. It has been shown that S-palmitoylated APP is preferably subject to enzymatic cleavage by β-secretase (encoded by *BACE1*) instead of α-secretase, enhancing the amyloidogenic pathway that produces Aβ (Buxbaum, Liu et al. 1998, Allinson, Parkin et al. 2003, Mizumaru, Saito et al. 2009, Bhattacharyya, Barren et al. 2013). Moreover, β-secretase is also S-palmitoylated at three different sites (Benjannet, Elagoz et al. 2001, Vetrivel, Meckler et al. 2009), but the precise role of S-palmitoyaltion in Aβ production is still in debate (Cordy, Hussain et al. 2003, Sidera, Parsons et al. 2004, Parsons and Austen 2007, Motoki, Kume et al. 2012). There is also evidence of the involvement of zDHHC9 and zDHHC15 in some cases of X-

linked mental retardation (Mansouri, Marklund et al. 2005, Raymond, Tarpey et al. 2007, Tarpey, Smith et al. 2009, Mitchell, Hamel et al. 2014, Hu, Haas et al. 2016). Considering the fact that S-palmitoylation is a common post-translational modification for a large scope of neuronal proteins, S-palmitoylation may have an unrecognized role in many other neurological and psychiatric diseases.

J. Hypothesis and specific aims

Ion channel regulation provides important insights into channel biophysics in physiological condition as well as strategies for channel modulation in pathological conditions. Nav1.6 plays a central role in determining neuronal excitability throughout the nervous system. It has been an attractive target for excitability modulation. However, the extremely high structural conservation between sodium channel isoforms and their overlapping tissue and cell type distribution hinder the development of isoform specific targeting compounds. Moreover, due to the ubiquitous distribution of Nav1.6, targeting strategies with tissue and cell type specificity is highly desirable. So far, no known regulatory mechanism offers a satisfactory solution. Therefore, a new regulatory mechanism that provides isoform and cell type specificity is in high demand.

1. S-palmitoylation regulation of Nav1.6

S-palmitoylation is a lipid post-translational modification that dynamically regulates protein functions. Importantly, the two large S-palmitoylation enzyme families with the distinctive but overlapping distribution may serve as drugable targets with potential specificity. S-palmitoylation of VGSCs was first revealed in Nav1.2 from the rat brain (Schmidt and Catterall 1987). Since then, only two studies attempted to unravel the functionality of S-palmitoylation on VGSCs, and yet they demonstrate that S-palmitoylation regulates Nav1.2 and Nav1.5 with isoform specificity (Bosmans, Milescu et al. 2011, Pei, Xiao et al. 2016). CSS-

palm, a S-palmitoylation site prediction software, has predicted multiple S-palmitoylation sites in Nav1.6. Moreover, a proteomic analysis of neuronal proteins from the mouse forebrain has indicated Nav1.6 and other brain isoforms of VGSC as likely S-palmitoylated proteins (Collins, Woodley et al. 2017). I hypothesized that Nav1.6 is post-translationally modified by S-palmitoylation. Therefore the first aim of this dissertation is to provide direct biochemical evidence of Nav1.6 S-palmitoylation (Aim 1.1).

Nav1.6 function is tightly controlled by an intricate network of regulatory mechanisms. The results from Aim 1.1 provide direct evidence of Nav1.6 S-palmitoylation *in vivo* and *in vitro*. Therefore, I hypothesized that S-palmitoylation serves important regulatory function for Nav1.6. Although S-palmitoylation is a common modification for a wide range of neuronal proteins and is shown to be heavily involved in shuttling proteins between intracellular compartments, the functionality of S-palmitoylation on Nav1.6 can be very different due to its complex structure as a large single polypeptide chain, multi-domain transmembrane protein. It has been shown that the S-palmitoylation status of proteins can be altered by pharmacological treatments. Aim 1.2 of this dissertation is to reveal the functionalities of the S-palmitoylation on Nav1.6 by comparing the electrophysiological properties of the channel in different S-palmitoylation status.

The findings in Aim 1.2 reveals two major functional outcomes of manipulating S-palmitoylation status of Nav1.6. Thus Aim 1.3 of this dissertation is to identify the specific S-palmitoylation site(s) in Nav1.6 that are responsible for the functional regulation. Moreover, the identified S-palmitoylation sites will be biochemically verified with ABE assay. Additionally, the important S-palmitoylation sites in Nav1.6 will be mapped and compared to the other two known S-palmitoylated VGSCs to reveal potential isoform specific regulation (Aim 1.4).

Aim 1.1 and 1.2 provide evidence of functional modulation of Nav1.6 by S-palmitoylation in a non-neuronal heterologous system. It is important to demonstrate that such functional significance persist in neuronal environment, where the Nav1.6 channel functions in physiological condition. Thus, Aim 1.5 is to examine how Nav1.6 S-palmitoylation affect channel activity and neuronal excitability in DRG neurons and iCell GlutaNeuron (a highly pure population of human glutamatergic neurons derived from iPSCs).

2. Functional consequence of epilepsy-associated mutations in Nav1.6

Nav1.6 mutation is a known cause for early infantile epileptic encephalopathy. Although previous studies have revealed gain-of-function alteration in the vast majority of characterized mutant Nav1.6 channels, a clear genotype-phenotype connection has not been established. Moreover, the functional consequence of these mutations are highly variable and no commonality has been identified. Additionally, previous studies of functional characterization used a rodent Nav1.6 construct, which may not be functionally identical to the human Nav1.6 channel and thus not ideal for disease characterization and pharmacology testing. I hypothesized that a systematic characterization of various epilepsy mutations using the human Nav1.6 (hNav1.6) construct provides more accurate estimation of functional alteration in human diseased conditions. Aim 2.1 of this dissertation is to functionally characterize four epilepsy-associated mutations located in distinct parts of Nav1.6 and elucidate potential commonalities among Nav1.6 epilepsy mutations. Findings in this aim may also provide a better understanding of the molecular components in Nav1.6. Also, the functional alterations revealed in the hNav1.6 are compared to those obtained in the rodent channel to recognize important distinctions.

The results from Aim 2.1 present distinct alterations of Nav1.6 properties by different mutations. However, it is largely unclear how these alterations affect neuronal excitability and how amino acid mutations in different parts of the channel converge as a single clinical outcome as network over-excitation that underlies seizure activity. Moreover, the vast number of epilepsy mutations in Nav1.6 makes it impractical to extend functional assays to all identified mutations. Therefore, I hypothesized that computational modeling and simulation is a useful tool to help predict the integrated consequence of single amino acid mutation in an ion channel. Thus, Aim 2.2 of this dissertation is to model Nav1.6 sodium current based on the experimental results in Aim 2.1 and perform simulations in modeled neurons to predict the excitability outcomes of the epilepsy mutations.

3. S-palmitoylation modulation of Nav1.6 epilepsy mutations

Aim 1 provides evidence that loss of S-palmitoylation at specific residues in Nav1.6 has major impact on neuronal excitability. The loss of S-palmitoylation due to a C981F mutation in the cardiac sodium channel Nav1.5 causes significant functional alteration in the channel and may be responsible for cardiac arrhythmia in human patients (Pei, Xiao et al. 2016). I hypothesized that mutations that result in either gain or loss of a S-palmitoylation site in Nav1.6 can be pathogenic and lead to abnormal channel activity. An arginine to cysteine mutation (R662C) in Nav1.6 was identified in an epilepsy patient (Carvill, Heavin et al. 2013), but no functional characterization has been reported. Importantly, a cysteine at this position in Nav1.6 was predicted to be a S-palmitoylation site in CSS-Palm. Aim 3.1 of this dissertation is to characterize the R662C mutant Nav1.6 channel and test whether it has increased sensitivity to S-palmitoylation manipulation that can imply an introduction of a S-palmitoylation site.

Aim 1 also demonstrates that S-palmitoylation modulates specific aspects of Nav1.6 function. Therefore, I hypothesized that I can exploit S-palmitoylation to target specific channel abnormalities caused by disease mutations. Aim 3.2 of this dissertation is to test whether S-palmitoylation manipulation can normalize specific aspect of mutant Nav1.6 function.

The findings in this dissertation reveal S-palmitoylation as a new regulatory mechanism for Nav1.6. Importantly, it identifies both isoform specific and conserved modification sites in VGSCs that differentially regulate distinct properties of the channel. Moreover, this dissertation presents a potential commonality among the gain-of-function mutations in Nav1.6 that cause epileptic encephalopathy and provides proof-of-concept evidence that Nav1.6 S-palmitoylation can be a drugable target to modulate excitability disorders with or without the Nav1.6 abnormality. The implication of these findings on VGSC regulation and future directions of this work are further discussed in Chapter VI.

II. MATERIALS AND METHODS

A. cDNA constructs

1. Mouse Nav1.6 channel constructs

This construct, referred to as mNav1.6r, was used in experiments presented in Chapter III and Chapter V for the characterization of Nav1.6 S-palmitoylation. The pcDNA3-Nav1.6r encoding for the mouse Nav1.6 was modified from a pcDNA3-Nav1.6r-EGFP construct (Gasser, Ho et al. 2012). The Nav1.6 channel has been rendered tetrodotoxin-resistant (TTXr) by the Y371S substitution, enabling the isolation of currents from the transfected Nav1.6 channels in whole-cell patch clamp recordings. The amino acid sequence of the c-terminal EGFP was deleted by introducing a stop codon at the end of the Nav1.6 channel sequence, in order to eliminate the potentially confounding influence of the c-terminal EGFP on channel properties and to achieve higher level of channel expression in our heterologous system.

Mutations C1169,1170A (mNav1.6r-CCAA), C1978A (mNav1.6r-C1978A), C1169,1170,1978A (mNav1.6r-CCCAAA) and (mNav1.6r-R660C) were introduced into the construct using QuikChange® II XL site-directed mutagenesis kit from Agilent Technologies according to the manufacturer's instructions. Mutant channel constructs were fully sequenced (ACGT, Inc.) to confirm the presence of the correct mutation and the absence of additional mutations.

2. Human Nav1.6 channel constructs

This construct was used in experiments presented in Chapter IV and Chapter V for the characterization of Nav1.6-associated epilepsy mutations. The codon optimized human cDNA construct for wild-type (WT) Nav1.6, encoding for the amino acid sequence corresponding to the accession number NP_055006.1

in the NCBI database, was designed in-house (Patel, Barbosa et al. 2016) and synthesized by GenScript (Piscataway, NJ). A Y371S amino acid substitution was introduced into the construct, rendering the channel resistant to TTX block.

Mutations R850Q, T767I, R1617Q and R1872Q were introduced into the WT construct using QuikChange® II XL site-directed mutagenesis kit from Agilent Technologies according to the manufacturer's instructions. Mutant channel constructs were fully sequenced (ACGT, Inc.) to confirm the presence of the correct mutation and the absence of additional mutations.

3. Human Nav1.2 channel constructs

This construct was used in experiments presented in Chapter III for the characterization of Nav1.2 S-palmitoylation. The codon optimized human cDNA construct for Nav1.2 was designed in-house and synthesized by GenScript (Piscataway, NJ). The amino acid sequence for the construct was correspondent to the accession number NG_008143.1 in the NCBI database. The Nav1.2 channel was rendered resistant to TTX-R by a F385S substitution.

The mutation K2005C (Nav1.2r- K2005C) was introduced into the construct using QuikChange® II XL site-directed mutagenesis kit from Agilent Technologies according to the manufacturer's instructions. Mutant channel constructs were fully sequenced (ACGT, Inc.) to confirm the presence of the correct mutation and the absence of additional mutations.

4. Fusion CD4-Nav1.6-Loop2 and CD4-Nav1.6-CTD constructs

These construct were used in experiments presented in Chapter III for the acyl-biotin exchange experiments. The fusion proteins CD4-Nav1.6-Loop2 and CD4-Nav1.6-CTD were designed in-house and synthesized by GenScript

(Piscataway, NJ). The extracellular and transmembrane segments of CD4 (amino acid 1-418) were fused with Nav1.6-Loop2 (amino acid 976-1193) or Nav1.6-CTD (amino acid 1768-1978).

Cysteine to alanine mutations correspondent to amino acid residues 1163, 1169,1170 and 1978 in Nav1.6 were introduced into the wild-type cDNA constructs using QuickChange II XL site-directed mutagenesis kit from Agilent Technologies according to the manufacture's instructions. Mutant constructs were fully sequenced (ACGT, Inc.) to confirm correct mutation and absence of additional mutations.

B. Cell cultures and transfections

1. Culture of ND7/23 cells and HEK cells

The neuronal cell line ND7/23 was used for transient expression of WT and mutant mNav1.6, hNav1.6 and hNav1.2 channels in electrophysiological experiments. The HEK293 cell line was used for stable expression of the WT hNav1.6 channel and transient expression of WT and mutant CD4 fusion proteins in acyl-biotin experiments. Both cell lines were maintained in Dulbecco's Modified Eagle Medium (Life Technologies, Grand ISLAND, NY, USA) supplemented with 10% fetal bovine serum (Atlanta Biologicals, Laurenceville, GA, USA) and 1% penicillin/streptomycin (Invitrogen #15140-122, Grand Island, NY, USA) and kept at 37°C incubator with 5% CO2.

2. Lipofectamine® transfection of ND7/23 cells and HEK cells

Transient transfection of ND7/23 cells and HEK cells was performed using Invitrogen Lipofectamine® 2000 Transfection Reagent according to the manufacturer's instructions.

For transfection of channel proteins in ND7/23 cells, lipid-DNA mixture in Opti-MEM medium with 5µg channel construct and 0.5µg enhanced green fluorescent protein (EGFP) construct was added to cells for 4h, after which transfected cells were split onto 35mm dish with fresh medium. Transfected cells were incubated at 30ºC overnight to increase channel surface expression. whole-cell voltage-clamp recordings were performed 24-32h after transfection. Transfected cells were identified by EGFP expression under a fluorescent microscope.

For transfection of CD4-Nav1.6 fusion protein in HEK cells, lipid-DNA mixture in Opti-MEM medium with 5µg cDNA construct was added to cells for 2.5h, after which the medium was removed and replaced by fresh medium. Acyl-biotin exchange was performed 24-32h after transfection.

3. Primary culture of DRG neurons

Rat DRG neurons were dissociated and cultured as described (Cummins et al., 2000). In adherence with animal procedures approved by the Indiana University School of Medicine and the School of Science Institutional Animal Care and Use Committees, young adult male Sprague Dawley rats, were euthanized by carbon dioxide overexposure followed by decapitation. All DRGs were harvested and subsequently incubated in collagenase D (1 mg/ml) and protease (1 mg/ml) for 70min. The DRGs were then spun down and washed with Dulbecco's Modified Eagle Medium supplemented with 10% fetal bovine serum and 1% penicillin/streptomycin, following which the DRGs were resuspended for trituration. 60µl of the triturated cells were seeded on each coverslip coated with poly-D-lysine and laminin and incubated for 1h in a 37°C / 5% CO2 incubator before supplementing with 500µl DMEM with 10% FBS and 1%

penicillin/streptomycin and kept in a 37°C / 5% CO2 incubator for 48h before transient transfection.

4. Biolistic transfection of DRG neurons

Transient transfection in DRG neurons was performed using the Helios Gene Gun (Bio-Rad Laboratories) according to the manufacture's instructions as previously described (Herzog, Cummins et al. 2003, Dib-Hajj, Choi et al. 2009, Jarecki, Piekarz et al. 2010)(Herzog et al., 2003; Dib-Hajj et al., 2009; Jarecki et al., 2010). Cells were co-transfected with 10 µg Nav1.6r cDNA and 5 µg Nav1.8 (small hairpin RNA) shRNA (Mikami and Yang 2005, Barbosa, Tan et al. 2015) with an internal ribosome entry site–EGFP (IRES-EGFP). Previous data has shown that the Nav1.8 shRNA reduces endogenous Nav1.8 current in DRG neurons by 98% (Jarecki et al., 2010). Patch clamp recordings were performed 48h after transfection. For current-clamp recordings, the medium was supplemented with 50 ng/ml mouse nerve growth factor (mNGF) (Sigma).

5. Culture of iCell® GlutaNeurons

iCell® GlutaNeurons were purchased from Cellular Dynamics International, Inc. and cultured according to the manufacture's instructions. The iCell® GlutaNeurons Were thawed and plated on coverslips coated with Poly-L-Ornithine (Sigma-Aldrich) and Corning® Matrigel® Basement Membrane Matrix and maintained in BrainPhy™ Neuronal Medium (STEMCELL Technologies Inc.) supplemented with iCell Neurons Medium Supplement (Cellular Dynamics International), iCell Nervous System Supplement (Cellular Dynamics International), N-2 Supplement (Sigma-Aldrich) and 1% penicillin/streptomycin (Invitrogen). The culture was maintained with 50% medium exchange every other day before transient transfection at 10 days post-plating.

6. ViaFectTM transfection of iCell® GlutaNeurons

Transient transfection of the iCell® GlutaNeurons was perform on day 10 post-plating using the ViaFectTM Transfection Reagent according to the manufacture's instructions. 6µl of viaFect reagent was added to the cDNA mixture of 2µg hNav1.6 construct and 0.1 µg EGFP construct in BrainPhy™ Neuronal Medium and incubated for 20min before adding to the cells. Patch clamp recordings were performed 48h after transfection.

7. Establishment of a Nav1.6 stable cell line

5µg hNav1.6 cDNA construct was transfected in the HEK cell line using Invitrogen Lipofectamine® 2000 Transfection Reagent according to the manufacturer's instructions. The cells were incubated with the transfection complex for 3h before being split on 10cm dish in fresh medium. G418 was added to the culture medium for selection. The culture was maintained with medium exchange every other day. After colonies were formed, isolated colonies were picked, dissociated and seeded on 10mm coverslips for functionality selection. At least three cells from each colony were randomly chosen for electrophysiological characterization. The colonies with all tested cells expressing Nav1.6 current at least 1nA in amplitude were selected for further expansion. The established cell lines were maintained in standard culture medium supplemented with G418.

8. S-palmitoylation treatments

2-Bromo palmitate (2BP, 2-Bromohexadecanoic acid, Sigma-Aldrich) was used to block S-palmitoylation and palmitic acid (PA, Sigma-Aldrich) was used to enhance S-palmitoylation. Although one single study (Pedro, Vilcaes et al. 2013) showed that 2BP may inhibit acyl-protein thioesterase activity at 150 µM, such

inhibition is not detected at 50 μM or 25 μM (the concentration used in our study). Both drugs were dissolved in DMSO in 1000X working concentration. They were diluted in warm medium and added to transfected cells at 25μM and 10μM concentrations respectively for overnight incubation.

C. Acyl-biotin exchange assay

1. Chemicals

β-Mercaptoethanol, Fisher, BP176
Chloroform, Acros Organics, AC158210010
EZ-Link™ HPDP-Biotin, Thermo Scientific, 21341
Hydroxylamine solution, Sigma-Aldrich, 467804
Methanol, Fisher Scientific, A412-4
N-ethylmaleimide (NEM), Pierce, cat. no. PI 23030
Pierce™ NeutrAvidin™ Agarose, Thermo Fisher, 29200
Protease Inhibitor Cocktail Set V, Animal-Free, Calbiochem, 535141
Triton™ X-100 Surfact-Amps™ Detergent Solution, Thermo Fisher, 28314
UltraPure™ SDS Solution, 10%, Thermo Fisher, 15553027

2. Antibodies

Mouse anti-beta-actin antibody, clone 4C2, Millipore, MABT825
Mouse anti-sodium channel, pan antibody, Sigma-Aldrich, S8809
Rabbit anti-CD4 antibody, Abcam, 133616
Rabbit anti-SCN8A sodium channel antibody, Millipore, AB5580
Goat anti-Mouse IgG H&L (IRDye® 800CW), Abcam, ab216772
Goat anti-Rabbit IgG H&L (IRDye® 800CW), Abcam, ab216773

3. Protocol

ABE assay was performed as previously described with minor modifications (Pei, Xiao et al. 2016). HEK 293 cells stably expressing Nav1.6 or transiently transfected with CD4-Loop2, CD4-CTD or their mutant variants were lysed and treated with N-ethylmaleimide (NEM) overnight to block free cysteines at 4ºC with end-to-end rotation. Next day, NEM was removed by chloroform-methanol precipitation and dissolved in 4% SDS buffer. The soluble protein was then divided into two equal parts and treated with either NH_2OH (0.7 M hydroxylamine, 1 mM biotin, 0.2% Triton X-100 and 1 x protease inhibitor) or tris buffered solution (200 mM tris, 1 mM biotin, 0.2% Triton X-100 and 1 x protease inhibitor). The reaction was carried out in dark for 1h. Chemicals were removed by chloroform-methanol precipitation. Protein was resolubilized in 2% SDS buffer and subsequently diluted with lysis buffer to achieve 0.1% SDS concentration for streptavidin-agarose beads capture. BCA protein assay was performed to ensure equal amount of proteins from different groups were subjected to the streptavidin-agarose beads capture. After 1 h incubation at room temperature, beads were washed four times with lysis buffer containing 1% Triton X-100 and 0.1% SDS. Protein was eluted in LDS sample buffer (Invitrogen) with 2% β-mercaptoethanol and heated at 65ºC for 5 min before probing with western blotting.

D. Whole-cell patch clamp recordings

1. Solutions

For voltage-clamp recordings, the intracellular solution contained (in mM): 140 CsF, 10 NaCl, 1.1 EGTA, and 10 HEPES, adjusted to a pH of 7.30 with CsOH. For recordings in ND7/23 cells, the extracellular solution contained (in mM): 140 NaCl, 20 TEA-Cl, 3 KCl, 1 $MgCl_2$, 1 $CaCl_2$ and 10 HEPES, adjusted to

a pH of 7.30 with NaOH. For recordings in DRG neurons, the extracellular solution contained (in mM): 140 NaCl, 20 TEA-Cl, 3 KCl, 1 $MgCl_2$, 1 $CaCl_2$, 0.1 $CdCl_2$ and 10 HEPES, adjusted to a pH of 7.30 with NaOH. 500nM TTX was added to the extracellular solution to block endogenous sodium currents and isolate TTX-resistant current generated by transfected channels. Osmolarity of all solutions was adjusted to 300 mOsm.

For current-clamp recordings, the intracellular solution contained (in mM): 140 KCl, 5 $MgCl_2$, 5 EGTA, 2.5 $CaCl_2$ and 10 HEPES, adjusted to a pH of 7.30 with KOH. The extracellular solution contained (in mM): 140 NaCl, 5 KCl, 2 $CaCl_2$, 1 MgCl and 10 HEPES, adjusted to a pH of 7.30 with NaOH. Osmolarity of solutions was adjusted to 300 mOsm.

2. Protocols

All recordings were obtained at room temperature (~22ºC) using a HEKA EPC-10 amplifier and the PatchMaster program (v2x73.2, HEKA Electronic). For voltage-clamp recordings, Electrodes were fabricated from 1.7mm capillary glass and fire-polished to a resistance of 0.8–1.0 MΩ using a Sutter P-1000 Micropipette puller (Sutter Instrument Company). The series of recording protocols was started 3 min after break-in for each cell, which controlled for time-dependent shifts in channel properties. For resurgent current recording, the protocol was started 5 min after break-in to allow sufficient time for Navβ4 peptide diffusion. Cells were not considered for analysis if the initial seal resistance was < 1 GΩ or if they had a series resistance > 3 MΩ. Voltage errors were minimized using 80% series resistance compensation and passive leak currents were cancelled by subtraction. To induce resurgent currents in ND7/23 cells, 200μM Navβ4 peptide (KKLITFILKKTREK-OH) (Biopeptide Co), a peptide that corresponds to part of the C-terminal tail of the full-length Navβ4 subunit, was included in the intracellular solution. For current-clamp recordings,

electrodes were fabricated from 1.2mm capillary glass to achieve a resistance of 4.0 – 6.0 MΩ. The series of recording protocols was started 2 min after break-in for each cell.

2.4.1 Activation protocol.

Transient sodium current (I_{NaT}) was measured during a 50ms depolarizing step (–80mV to +45mV; 5mV increment) from a holding potential of –120mV (Fig.11D upper). The current density was calculated by dividing the measured I_{NaT} by the capacitance of the cell. Persistent sodium current (I_{NaP}) was measured at the last 1ms during the depolarizing steps and presented as a percentage normalized to the maximal I_{NaT} of each cell. Sodium current conductance (G_{Na}) was converted from I_{NaT} using the equation

$$G_{Na} = I_{NaT} / (V - V_{rev}),$$

where V_{rev} is the reversal potential of Na^+ obtained in FitMaster (v2x73.5, HEKA Electronic) for each cell. Activation curves were generated by plotting normalized G_{Na} against depolarizing potentials and fitting it with the Boltzmann function in the form of

$$G_{Na} / G_{max} = 1 / (1 + \exp[(V_{50,act} - V) / k_{act}]),$$

where G_{max} is the maximal G_{Na}, $V_{50,act}$ is the potential at which activation is half-maximal, V is the depolarizing potential, and k_{act} is the slope factor. Rate of decay (τ_{NaT}) for I_{NaT} was obtained in FitMaster by fitting the current traces 1ms into the depolarizing steps with a single exponential function.

2.4.2 Steady-state inactivation.

Availability of sodium channels was measured by the peak sodium current during a 20ms test pulse at 0mV following a 500ms prepulse (–140mV to +10mV; 10mV increment) that allows channels to enter equilibrium states (Fig.11D lower). Steady-state inactivation curves were generated by plotting normalized

sodium current against prepulse potentials and fitting it with the Boltzmann function in the form of

$$I / I_{max} = 1 / (1 + \exp[(V_{50,inact} - V) / k_{inact}]),$$

where I_{max} is the maximal sodium current obtained in this protocol, $V_{50,inact}$ is the potential at which half of the sodium channels are available for activation, V is the prepulse potential, and k_{inact} is the slope factor.

2.4.3 Recovery from inactivation.

A 20ms depolarization prepulse at 0mV was applied to allow channel activation and subsequent inactivation, which was followed by a repolarizing step to –80mV for durations ranging from 0ms to 50ms with 2ms increment. The non-inactivated sodium currents were measured during a subsequent 20ms test pulse at 0mV and normalized to the maximum current obtained in this protocol. The normalized non-inactivated sodium current was plotted against the duration of repolarizing step and fitted with a single exponential function.

2.4.4 Resurgent current.

Resurgent currents (I_{NaR}) were recorded with 200μM Navβ4 peptide in the intracellular solution and elicited by a protocol (Fig.18J top) with a step depolarization from –120 mV to +60 mV for 20 ms to open channels, allowing them to undergo open-channel block and subsequently repolarizing to a series of potentials (+25mV to –80mV; 5mV decrement) for 50 ms to allow the blocker to unbind, generating the resurgent current. I_{NaR} was presented as a percentage normalized to the maximal I_{NaT} obtained from the activation protocol and plotted against the repolarization potentials. Rate of decay (τ_{rsg}) for resurgent current was obtained in FitMaster by fitting the decay phase of the resurgent current traces, starting at 3ms (or 6.5ms for R1617Q due to its extremely slow resurgent

current kinetics) in the repolarizing steps of the resurgent current protocol with a single exponential function.

E. Computational modeling and simulations

1. Modelling Nav1.6 current

Computational modeling of sodium currents and simulation of action potential firing were conducted in NEURON v7.5 (Hines and Carnevale 1997). The sodium current model was based on a Markov state model described in detail previously (Khaliq, Gouwens et al. 2003) with minor modifications to partially segregate the coupling of voltage dependence of activation and inactivation (Fig.22). To model WT Nav1.6 current, the kinetic parameters remained identical to the original model, except for O_{on}, the rate constant for the $O \rightarrow I_6$ transition (I_{NaT} decay), was modified from 0.75 to 1.132 to match the experimental result. Mutant Nav1.6 currents were modeled as changes relative to this baseline. Quantitative analysis and curve fitting were performed to reconcile experimental and modelled data. ε, the rate constant for O→OB was not altered for experiments with open channel block (resurgent current) implemented, while it was set to 0 otherwise. All modified parameters were reported in Table 2.

2. Simulation of action potential firing

Simulations of neuronal activity were performed in a single compartment model of a Purkinje neuron (Khaliq, Gouwens et al. 2003) and a multi-compartment model of a cortical pyramidal neuron (Ben-Shalom, Keeshen et al. 2017). To simulate action potential firing of the Purkinje neuron, sodium conductance in the original model (Khaliq, Gouwens et al. 2003) was replaced by the modeled Nav1.6 current. For the simulation in the cortical pyramidal neuron model (Ben-Shalom, Keeshen et al. 2017), the sodium conductance that

represents Nav1.6 current was replaced by the modeled Nav1.6 current. To simulate heterozygous mutant conditions in both models, 50% of the modelled WT Nav1.6 conductance was replaced by the modelled mutant Nav1.6 conductance. Neuronal morphology, channel distributions and kinetics of other channels remained the same as the original models.

F. Data analysis

GraphPad Prism (v 6.00, GraphPad Software) was used for statistical analysis and curve fitting. The ROUT method in GraphPad Prism was used to identify outliers, which were then excluded from plotting and analysis. D'Agostino & Pearson omnibus normality test was used to confirm normal distribution of the data. Nonlinear least-squares minimization method was used for curve fitting. All data are presented as mean ± standard error of mean (SEM) of the indicated number of cells (n). Electrophysiological data for the WT group was collected along with each mutant group to eliminate potential differences in cell batch and in transfection efficiency. I found some significant difference of I_{NaT} current density, but not any other channel properties, between the various WT groups from different batches. Therefore, for comparisons of I_{NaT} current density, data from different WT batches was not pooled for comparison to mutants, and thus was presented with different number of cells (n). For comparisons of I_{NaT} current density, I_{NaP} percentage, I_{NaR} percentage, rate of decay for I_{NaT}, and rate of decay for I_{NaR}, two-way ANOVA with Sidak's multiple comparisons test was performed between WT and mutants. For comparisons of $V_{50,act}$, k_{act}, $V_{50,inact}$, k_{inact}, and recovery rate, student's *t-test* was performed on the parameters extrapolated from curve fitting.

III. NAV1.6 S-PALMITOYLATION REGULATES CHANNEL ACTIVITY AND NEURONAL EXCITABILITY

A. Overview

Some Nav isoforms are modified by S-palmitoylation. The cardiac sodium channel Nav1.5 was shown to be biochemically modified and functionally regulated by S-palmitoylation (Pei, Xiao et al. 2016). Additionally, the functional properties and toxin sensitivity of Nav1.2 are altered by manipulating the S-palmitoylation status of the channel with pharmacological treatment (Bosmans, Milescu et al. 2011). However, it is unclear whether other Nav isoforms are differentially regulated by S-palmitoylation. This chapter presents experiments addressing the questions whether Nav1.6 is modified by S-palmitoylation and how Nav1.6 S-palmitoylation modulates channel activity.

B. Nav1.6 is post-translationally modified by S-palmitoylation.

1. Detection of Nav1.6 S-palmitoylation in mouse cerebellum.

The acyl-biotin exchange assay was performed with proteins extracted from the mouse cerebellum due to its enriched expression of Nav1.6. Fig.6 shows that native Nav1.6 in the mouse brain is S-palmitoylated. This is signified by the stark contrast of the intensity of Nav1.6 signal between the groups with and without hydroxylamine (HA) treatment, which selectively severs the labile thioester bond of S-palmitoylation and exposes the originally S-palmitoylated thiols for biotinylation and subsequent strep-avidin capture.

2. Detection of Nav1.6 S-palmitoylation in Nav1.6 stable cell line.

To further confirm the generalization of Nav1.6 S-palmitoylation, the channel was heterologously transfected in the HEK cell line. As shown in Fig.6B,

transient transfection (trans.) achieved very low level of total Nav1.6 expression compared to that selected for stable expression (stabl.) in HEK cells, probably due to the low transfection efficiency of the channel. The selectivity of the pan-Nav antibody I used was confirmed by the lack of signal in HEK cells without transfection. With the Nav1.6 stable cell line, the ABE assay shows that heterologously expressed Nav1.6 was also S-palmitoylated, indicated by the contrast of signal intensity of pan-Nav probed proteins between +HA and –HA groups (Fig.6C).

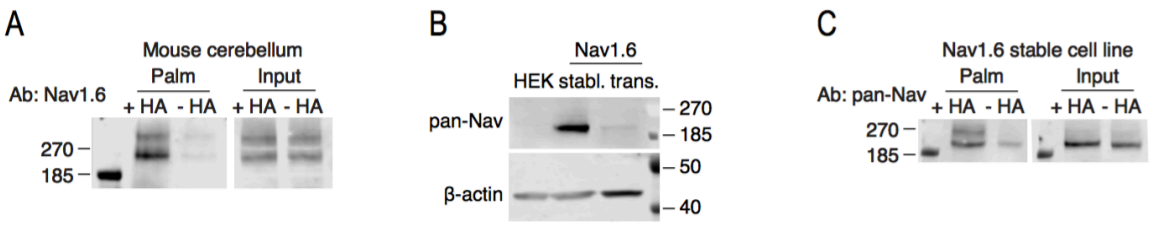

Figure 6. Nav1.6 is biochemically modified by S-palmitoylation.
(A) Acyl-biotin exchange assay on mouse cerebellum probed with Nav1.6 antibody. (B) Nav1.6 probed with pan-Nav antibody in HEK cells with no transfection (left), with Nav1.6 stably transfected (middle) and with Nav1.6 transiently transfected (right). (C) Acyl-biotin exchange assay on HEK cell line stably expressing Nav1.6 probed with pan-Nav antibody.

C. Nav1.6 activity is regulated by S-palmitoylation.

1. S-palmitoylation regulates Nav1.6 current amplitude.

To understand the potential significance of Nav1.6 S-palmitoylation for channel function, whole-cell voltage clamp recordings was performed on ND7/23 cells transiently transfected with Nav1.6. The S-palmitoylation status of the channel was manipulated by overnight treatment of the transfected cells with either 10μM palmitate acid (PA), the substrate for S-palmitoylation, to enhance S-palmitoylation, or 25μM 2-bromo-palmitate (2BP), a metabolically stable analog of palmitate acid, to block S-palmitoylation. These concentrations were determined by previous experiments in our lab that showed optimal enhancement and blockage of S-palmitoylation in our heterologous expression system (Pei, Xiao et al. 2016).

The representative traces of Nav1.6 currents from each treatment group are shown in Fig.7A. The measured peak sodium currents were normalized by the capacitance of each cell, which reflects the area of plasma membrane. As shown in Fig.7B, blocking S-palmitoylation with 2BP reduced Nav1.6 current by 2.5 fold (2BP: - 32.02 ± 6.65 pA/pF vs. DMSO: - 80.16 ± 8.30 pA/pF), while enhancing S-palmitoylation with PA increased Nav1.6 current by 1.8 fold (- 142.4 ± 17.27 pA/pF). Notably, the current density in the PA group is more than four-fold larger than that of the 2BP group. To eliminate the possibility that these bidirectional effects were mediated by different mechanisms, transfected cells were simultaneously treated with 25 μM 2BP and 10 μM PA. The current density of the co-treated cells (- 31.12 ± 7.43 pA/pF) was similar to that of the 2BP group, suggesting that the bidirectional current density effects produced by individual 2BP and PA treatments were very likely mediated by S-palmitoylation. These data also demonstrated that 2BP effectively blocked S-palmitoylation in our

expression system, although excessive S-palmitoylation substrate were provided to bias the palmitoylation – depalmitoylation equilibrium.

2. S-palmitoylation regulates Nav1.6 voltage dependence.

In addition to regulating Nav1.6 current amplitude, S-palmitoylation also modulates voltage dependence of the channel. Fig.7C shows that blocking S-palmitoylation with 2BP resulted in an 8mV hyperpolarizing shift of steady-state inactivation (2BP: V1/2 = - 72.34 ± 0.28 mV vs. DMSO: V1/2 = - 64.46 ± 0.21 mV), similar to the modulations seen in Nav1.2 (Bosmans, 2011) and Nav1.5 (Pei, 2016). Also, there is a slight, though statistically significant, hyperpolarizing shift of voltage dependence of activation (Fig.7D 2BP: V1/2 = - 22.48 ± 0.84 mV vs. DMSO: V1/2 = - 19.7 ± 0.18 mV). On the other hand, enhancing S-palmitoylation with PA did not alter Nav1.6 voltage dependence of activation or steady-state inactivation (Fig.7CD).

3. S-palmitoylation has no prominent effect on Nav1.6 recovery from inactivation or Nav1.6 resurgent current.

Blocking S-palmitoylation revealed a slight slowing effect on the channel recovery from inactivation, while enhancing S-palmitoylation with PA showed no effect (Fig.7E, 2BP: τ = 13.18 ± 1.28 ms, DMSO: τ = 9.84 ± 0.76 ms, PA: τ = 10.54 ± 0.45 ms). Additionally, altering Nav1.6 S-palmitoylation status did not change the percentage of Nav1.6 resurgent current induced by the β4 peptide in the intracellular solution (Fig.7H).

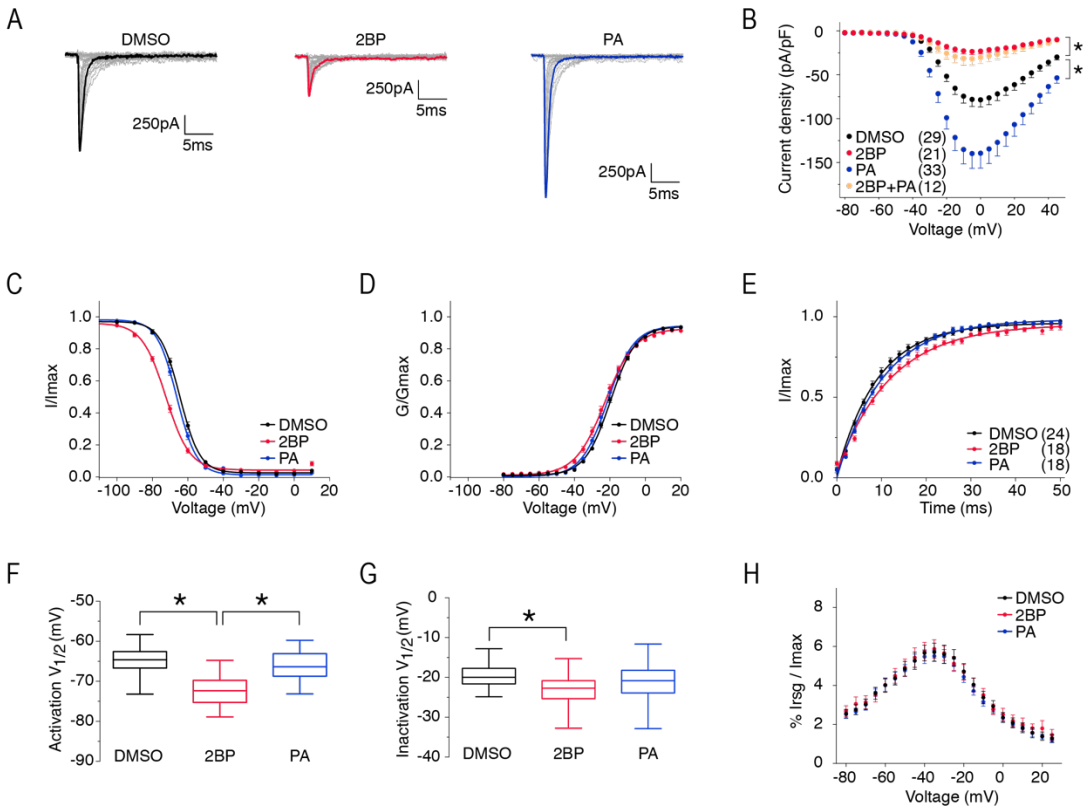

Figure 7. S-palmitoylation regulates Nav1.6 functional properties

(A) Representative current traces from each treatment group elicited with the activation protocol. Maximum current traces are highlighted with black, red and blue respectively. (B) Current density-voltage plot. * $P < 0.05$ compared to WT in two-way ANOVA. (C) Voltage dependence of activation and (D) Steady-state inactivation curves fitted with Boltzmann functions. (E) Recovery from inactivation with recovery time duration from 0 to 50ms. (F,G) Quantification of the mid-point voltage ($V_{1/2}$) of steady-state inactivation and activation extrapolated from (C,D), respectively. (H) Percentage of resurgent current normalized to maximum peak sodium current obtained from the activation protocol with 200μM Navβ4 peptide in the intracellular solution. Data presented as mean ± SEM. Values are reported in Table 2.

D. Identification of S-palmitoylation sites in Nav1.6

1. S-palmitoylation site prediction using CSS-Palm

So far, there is no consensus sequence motif for S-palmitoylation. The identification of potential sites relies on prediction tools like CSS-Palm (Xue, Liu et al. 2011) that provides site prediction based on a limited pool of known S-palmitoylation proteins using a clustering and scoring strategy (CSS) algorithm.

In the Nav1.6 amino acid sequence, 14 residues are predicted to be S-palmitoylation sites with medium stringent threshold (Fig.8A). Six of them are exposed to the cytoplasm (Fig.8B), which are more likely to be accessible by palmitoyl acyltransferases and thioesterases, and thus have higher probability to be modified by S-palmitoylation and to undergo the dynamic palmitoylation – deplamitoylation cycle for dynamic regulation of Nav1.6 functions. Among them, three residues, C1169, C1170 and C1978, are of particular of interest. The two adjacent cysteines in the second intracellular loop (Loop2) are highly conserved among all isoforms of voltage-gated sodium channel (Fig.8C). And yet, they confer distinct functional modulations: in Nav1.2, depalmitoylation of the first of the two cysteines was shown to hyperpolarize voltage-dependence of inactivation (Bosmans, Milescu et al. 2011); a similar modulation was seen in Nav1.5, however, it was not conveyed by the homologous cysteine, but by a Nav1.5-exclusive residue (C981) in Loop2 instead (Pei, Xiao et al. 2016). This indicates potential isoform-specific functionality of S-palmitoylation. Because an 8mV hyperpolarization of voltage-dependence of inactivation was observed in Nav1.6 upon S-palmitoylation blockage (Fig.7C), it would be interesting to test whether the two conserved cysteines were involved in the regulation and how it might differ from Nav1.2 and Nav1.5.

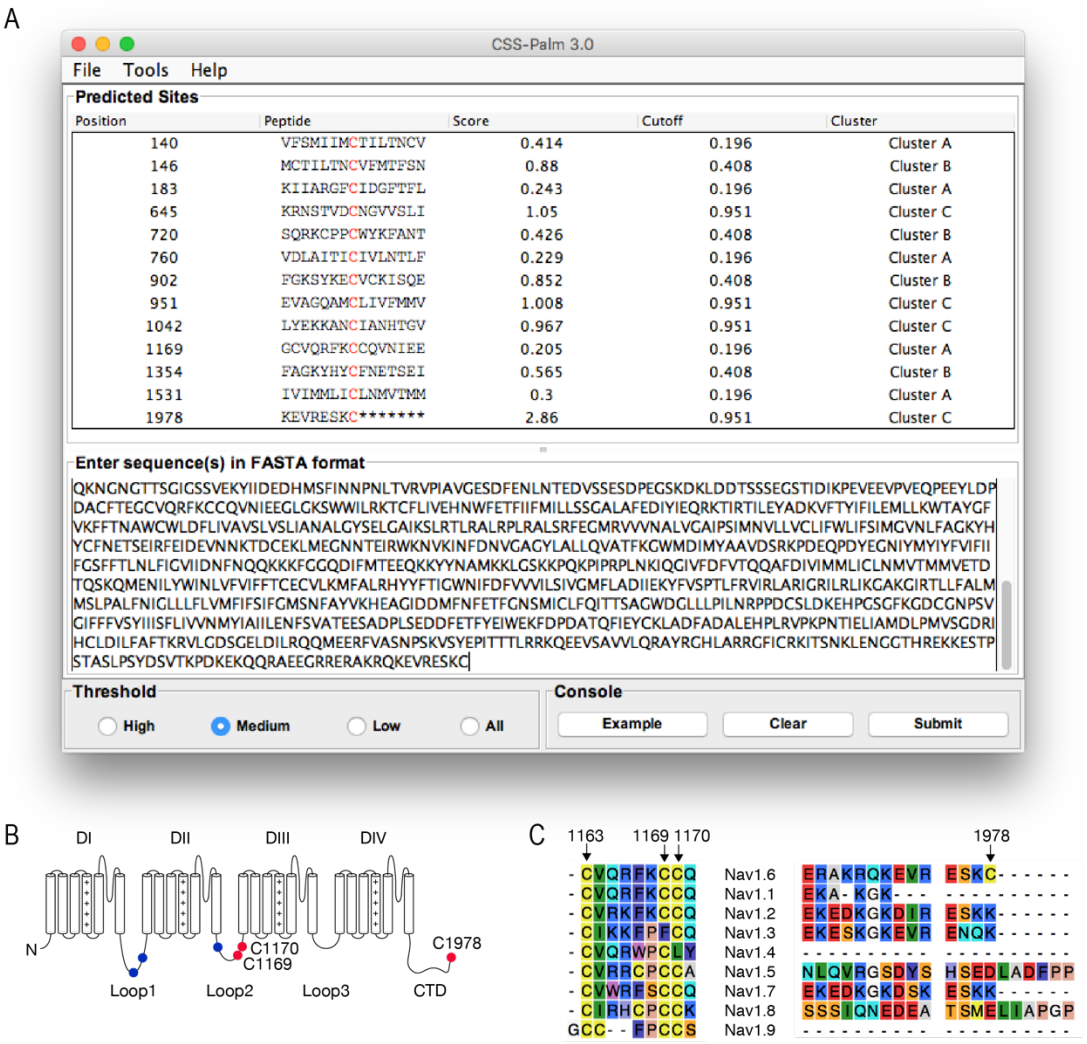

Figure 8. S-palmitoylation site prediction in Nav1.6.

(A) CSS-Palm interface showing 14 predicted S-palmitoylation sites in Nav1.6 with medium stringent threshold. (B) Predicted S-palmitoylation sites mapped to the sodium channel topology. Sites of interest C1169, C1170, C1978 are highlighted in red. (C) Two segments of sequence alignment of the 9 VGSC isoforms showing Nav1.6-C1169, C1170, C1978 in their immediate sequence environment.

Another site of interest, C1978, locates at the very end of the C-terminal domain in Nav1.6 (Fig.8B). This site is unique to Nav1.6 and not found in any other sodium channel isoform (Fig.8C). In addition, the C-terminus cysteine is evolutionally conserved in Nav1.6 among most species with a few exceptions in lower vertebrates (Fig.9). Therefore, this residue may carry functional significance that is exclusive to the Nav1.6 isoform. Moreover, C-terminus S-palmitoylation has been shown to regulate protein surface expression (Hayashi, Rumbaugh et al. 2005, Roth, Wan et al. 2006, Jindal, Folco et al. 2008, Ebersole, Petko et al. 2015), which might explain the bi-directional modulation of Nav1.6 current amplitude induced by S-palmitoylation manipulation.

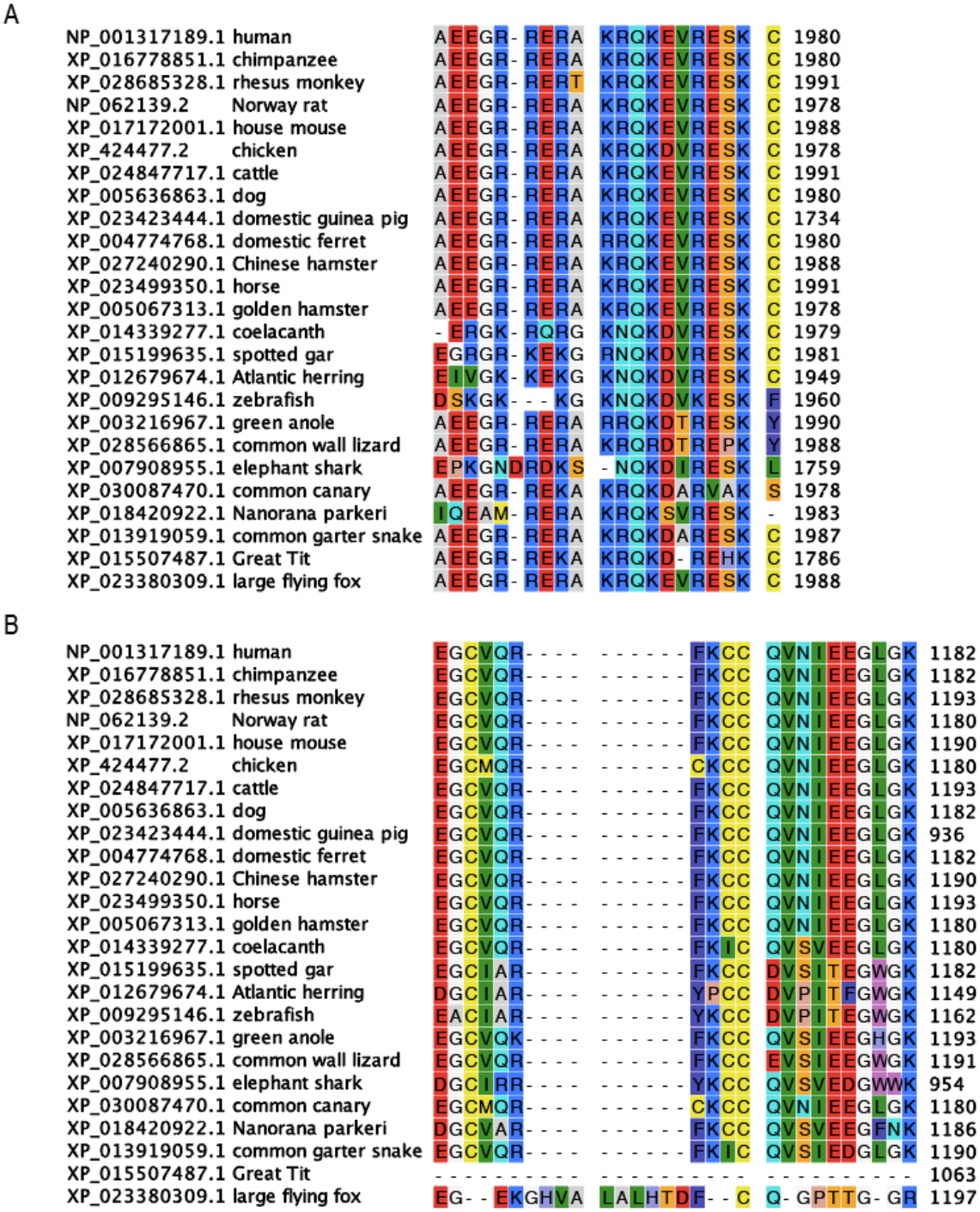

Figure 9. Evolutionary conservation of cysteines in VGSC.

(A) C-terminal domain and (B) Loop2 in Nav1.6.

2. C1169, C1170 and C1978 are major S-palmitoylation sites in Nav1.6

To biochemically confirm S-palmitoylation occurs at C1169 and C1170, I designed a CD4-Nav1.6-Loop2 fusion protein for ABE assay due to low expression level of Nav1.6 in our heterologous expression system (Fig.10A). This construct was transiently transfected in the HEK cell line. I validated that the CD4 antibody is specific for detecting the transfected fusion protein (Fig.10B) and the signal intensity is linear with protein loading, and thus can be used for quantification in the experiments (Fig.10C).

The ABE assay showed that the CD4-Loop2 fusion protein was S-palmitoylated and the S-palmitoylation signal was enhanced by PA treatment and reduced by 2BP treatment (Fig.10D). To eliminate S-palmitoylation at the cysteines corresponding to C1169 and C1170 in Nav1.6, both cysteines were mutated to non-palmitoylatable alanines (Loop2-CCAA). Fig.10DF shows that the S-palmitoylation signal of Loop2-CCAA was greatly reduced compared to Loop2-WT, suggesting that C1169 and C1170 were major S-palmitoylation sites in Loop2. However, S-palmitoylation was not completely abolished in Loop2-CCAA. This may indicate additional S-palmitoylation site(s) in the protein. In addition to C1169 and C1170, there are four other cysteines in Loop2 (1042, 1058, 1163 and 1189). Intriguingly, C1163, a cysteine near the double cysteines 1169 and 1170 (Fig.10C), became a predicted S-palmitoylation site in CSS-Palm in both Nav1.6-CCAA and Loop2-CCAA, while it was not a predicted site in the WT proteins. This indicated the possibility to unmask and favor S-palmitoylation at non-canonical residues upon the removal of primary S-palmitoylation sites in a protein. Indeed, the ABE assay showed that Loop2-C1163A displayed similar S-palmitoylation signal as Loop2-WT, affirming that C1163 was not a major S-palmitoylation site in WT CD4-Nav1.6-Loop2, although it might become one when neighboring S-palmitoylation sites were removed (Loop2-CCAA). Further, mutating the three cysteines (1163, 1169, 1170) eliminated the S-palmitoylation

signal from CD4-Loop2, which suggested the remaining three cysteines (C1042, C1158, C1189) were not S-palmitoylation site in Loop2. Fig.10EG shows that CD4-CTD was also S-palmitoylated and the C-terminus cysteine was the major S-palmitoylation site in the CTD. As a negative control to show the level of S-palmitoylation signal in the experiments in the absent of S-palmitoylatable site, all cysteines in CD4-Loop2 were removed by deleting the sequence segment with 5 cysteines clustered (1058-1193) and mutating the last cysteine (C1042A) making a CD4-Loop2-ΔC construct (Fig.10HI).

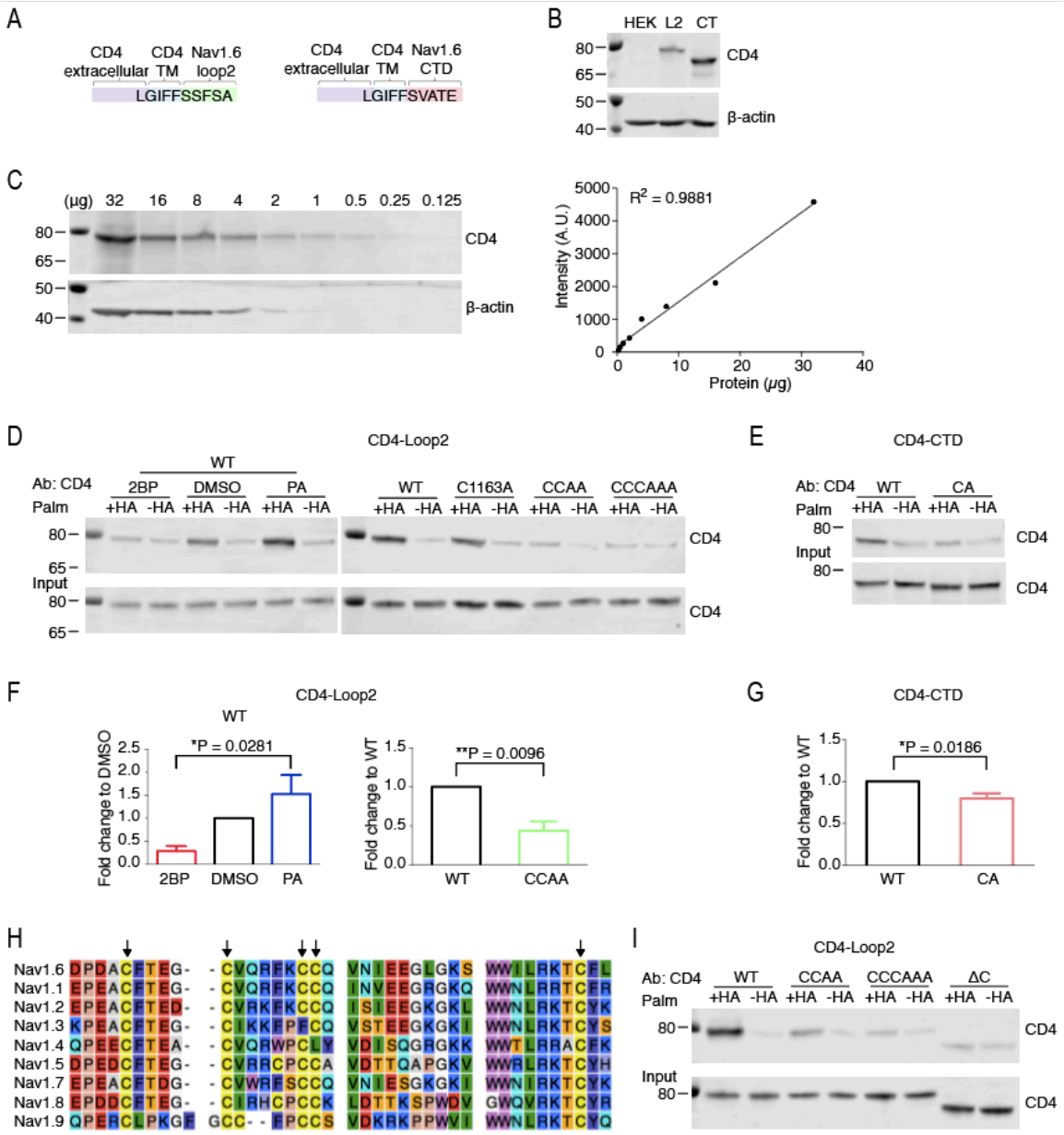

Figure 10. Acyl-biotin exchange assays (ABE) of CD4-Nav1.6 fusion proteins. (A) Schematic illustrations of the CD4-Nav1.6-loop2 and CD4-Nav1.6-CTD fusion proteins showing the linker region between CD4 and Nav1.6-loop2/CTD (last five amino acids of the CD4 transmembrane segment and the first five amino acids of the Nav1.6-loop2/CTD). (B,C) Detection of CD4-Nav1.6 fusion proteins transiently expressed in HEK cells with CD4 antibody. (D,E,I) ABE assays on WT and mutant fusion protein-transfected HEK cells. (F,G) Quantification of S-palmitoylation signals in ABE. P value for 2BP, DMSO and PA treatments in

CD4-Loop2 was obtained from one-way ANOVA with Tukey multiple comparison test (n = 3 in each group), P values for WT vs. mutants were obtained from t-test (n = 3 for CD4-Loop2, n = 4 for CD4-CTD). (H) A segment of Nav sequence alignment showing the cluster of 5 cysteines in Loop2.

3. S-palmitoylation at C1169, C1170 regulates voltage-dependence of Nav1.6

Since C1169 and C1170 are major S-palmitoylation sites in Loop2 of Nav1.6, next I set out to test the function of this modification. S-palmitoylation at C1169 and C1170 was eliminated by mutating both to non-palmitoylatable alanines (Nav1.6-CCAA). Fig.11A shows the representative traces of TTX-resistant Nav1.6-CCAA current from each treatment group. Compared to Nav1.6-WT, Nav1.6-CCAA displays a 11mV hyperpolarizing shift in voltage dependence of steady-state inactivation (V1/2 = - 75.5 ± 0.39 mV) (Fig.11C). This replicates, if not exaggerates, the voltage dependence modulation seen in Nav1.6-WT with S-palmitoylation blockage, suggesting that S-palmitoylation at C1169 and C1170 are critical for voltage dependence regulation of Nav1.6. However, the Nav1.6-CCAA channel does not completely lose its sensitivity to 2BP treatment and still displays a minor (5mV) but statistically significant hyperpolarizing shift in steady-state inactivation (V1/2 = - 80.48 ± 0.30 mV) (Fig.11D). This may be due to slight modulation conveyed by the unmasked S-palmitoylation site (C1163) when C1169 and C1170 were removed (Fig.10). Further experiments with all these three cysteines replaced are needed to test this hypothesis.

Consistent with the WT channel, enhancing S-palmitoylation with PA treatment does not alter the voltage dependence of activation, steady-state inactivation (Fig.11D), or recovery from inactivation (Fig.11E), while blocking S-palmitoylation with 2BP treatment results in slower recovery from inactivation (2BP: τ = 12.69 ± 0.69ms; DMSO: τ = 10.7 ± 0.384 ms). Interestingly, Nav1.6-CCAA exhibits the same bidirectional current density response to 2BP and PA treatments as the WT channel (Fig.11B), indicating that C1169 and C1170 do not regulate current amplitude of the channel.

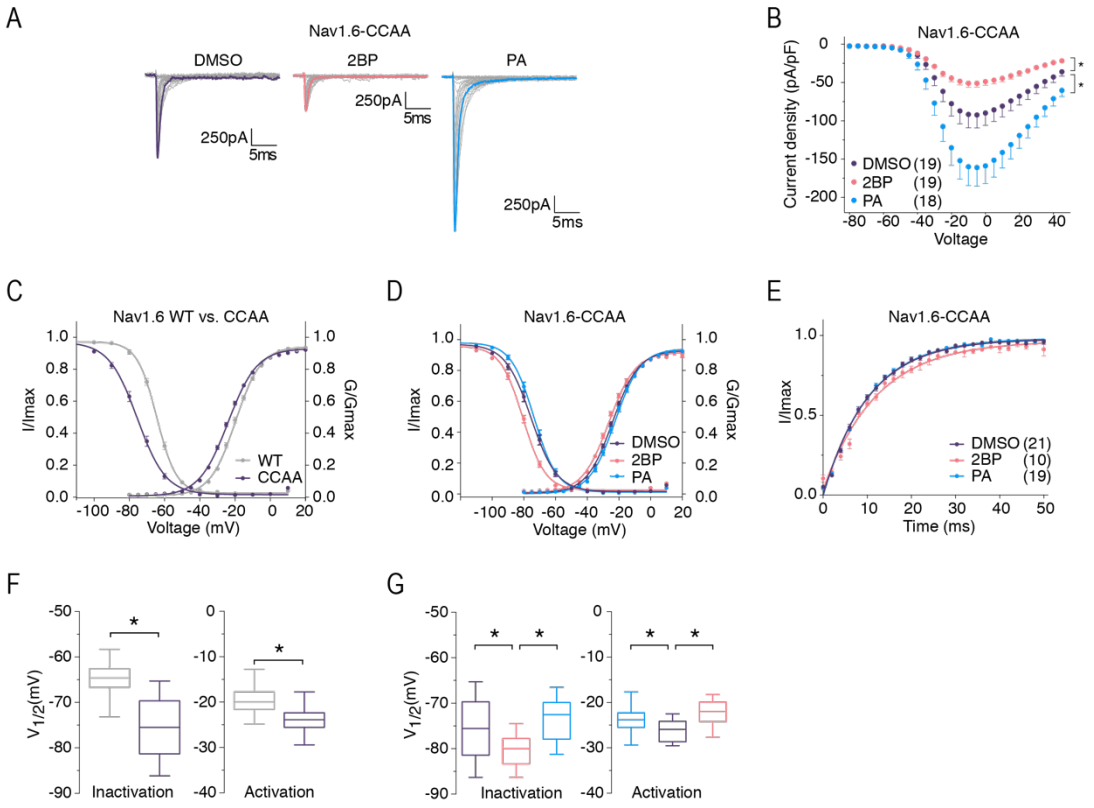

Figure 11. S-palmitoylation of C1169, C1170 regulates Nav1.6 voltage-dependence of inactivation, but not Nav1.6 current amplitude.

(A) Representative current traces elicited from Nav1.6-CCAA with different treatments. (B) Current density-voltage plot. * $P < 0.05$ compared to WT in two-way ANOVA. Data presented as mean ± SEM. Values are reported in Table. (C)(D) Steady-state inactivation and activation curves of Nav1.6-WT and Nav1.6-CCAA fitted with Boltzmann functions. (E) Recovery from inactivation with recovery time duration from 0 to 50ms. (F,G) Quantification of the mid-point voltage ($V_{1/2}$) of steady-state inactivation and activation extrapolated from (C,D), respectively.

4. S-palmitoylation at C1978 regulates current amplitude of Nav1.6

Since S-palmitoylation at C1169 and C1170 is only involved in regulating Nav1.6 voltage dependence, I set out to identify the S-palmitoylation site responsible for the regulation of Nav1.6 current amplitude. C1978 is a probable candidate. For one thing, it is a major S-palmitoylation site in the CTD (Fig.10EG). For another, it is the last residue of Nav1.6, locating at the very end of the cytoplasmic CTD; and S-palmitoylation at C-terminus of ion channels have been shown to regulate protein trafficking and their surface expression (Hayashi, Rumbaugh et al. 2005, Jindal, Folco et al. 2008, Hayashi, Thomas et al. 2009). More importantly, C1978 is of tremendous interest, because it is exclusive to and evolutionally conserved in Nav1.6. Therefore, I hypothesized that Nav1.6-C1978 S-palmitoylation regulates Nav1.6 surface expression, and thus produced the opposite current density effects upon 2BP and PA treatments (Fig.7B).

To test the above hypothesis, I eliminated S-palmitoylation at C1978 in Nav1.6 by mutating it into a non-palmitoylatable alanine and examined the functional properties of this mutant channel. Fig.12A shows the representative traces of TTX-resistant Nav1.6-C1978A current from each treatment group. I found that enhancing S-palmitoylation with PA no longer increased Nav1.6 current (PA: - 118.3 ± 16.14 pA/pF, vs. DMSO: 110.9 ± 13.75 pA/pF) (Fig.12B). However, blocking S-palmitoylation with 2BP still slightly decreased Nav1.6-C1978A current (- 71.4 ± 12.76 pA/pF), although the reduction did not reach statistic significance ($P = 0.0544$ in two-way ANOVA) (Fig.12B). I speculated that this decrease of Nav1.6-C1978A current by 2BP treatment may be accountable for by secondary S-palmitoylation site(s), similar to the additional hyperpolarization of steady state inactivation in Nav1.6-CCAA upon 2BP treatment. Alternatively, the S-palmitoylation of a Nav1.6 interacting protein can be involved in the additional regulation of the current amplitude. Importantly, Nav1.6-C1978A demonstrated the same voltage dependence response to 2BP

and PA treatments as Nav1.6-WT (Fig.12CD), suggesting that S-palmitoylation at C1978 did not regulate voltage dependence of the channel.

It is note worthy that there was no functional interaction or competition between S-palmitoylation at C1169, C1170 and that at C1978, because the triple cysteine mutant (Nav1.6-CCCAAA) with all these three cysteines mutated to alanines, replicated the voltage-dependent response of Nav1.6-CCAA and the current density response of Nav1.6-C1978A (Fig.12HIJ). Together, the data demonstrates that S-palmitoylation at different residues of Nav1.6 differentially regulate distinct channel functions.

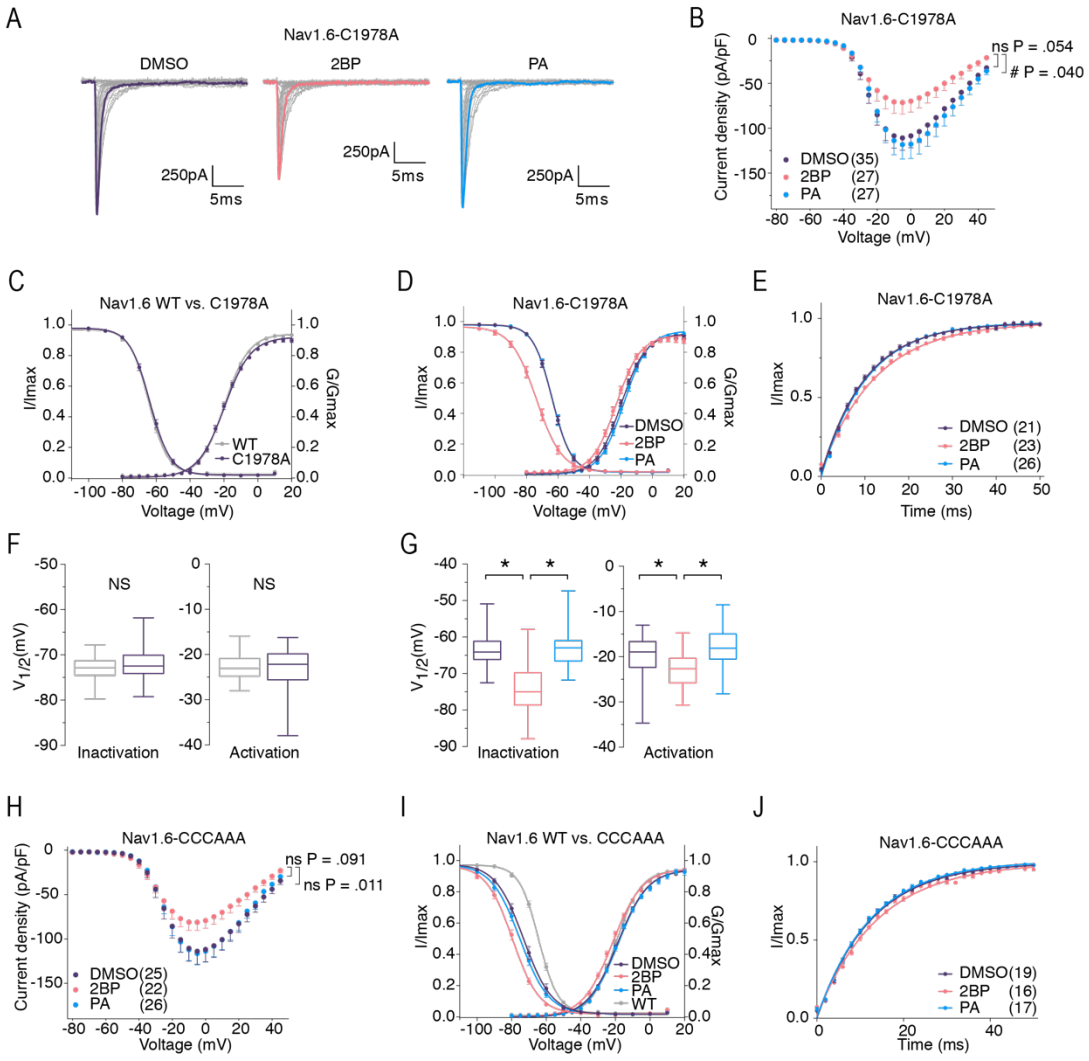

Figure 12. C1978A eliminates Nav1.6 current enhancement by PA without altering voltage-dependence response to S-palmitoylation manipulation.
(A) Representative current traces of Nav1.6-C1978A. (B,H) Current density-voltage plots. # $P < 0.05$ compared to 2BP in two-way ANOVA. (C,D,I) Steady-state inactivation and activation curves of Nav1.6-C1978A and Nav1.6-CCCAAA fitted with Boltzmann functions. (E,J) Recovery from inactivation of Nav1.6-C1978A and Nav1.6-CCCAAA with recovery time duration from 0 to 50ms. (F,G) Quantification of the mid-point voltage ($V_{1/2}$) of steady-state inactivation and activation extrapolated from (C,D), respectively. Data presented as mean ± SEM. Values are reported in Table 2.

E. S-palmitoylation regulations for VGSCs are isoform-dependent

1. Nav1.2 current is not increased by S-palmitoylation

Since C1978 is exclusive to Nav1.6, I asked whether other Nav isoforms lacked similar current amplitude regulation by S-palmitoylation. To address this question, I evaluated how S-palmitoylation affected the functional properties of Nav1.2. The Nav1.2 isoform has high degree of sequence homology and a similar expression pattern in the central nervous system as Nav1.6. It has a lysine (K2005) at the Nav1.6-C1978 homologous site. Fig.13A shows the representative traces of Nav1.2-WT currents. I found that enhancing S-palmitoylation with PA treatment did not increase Nav1.2 current density (PA: - 641.2± 92.95 pA/pF vs. DMSO: - 648.7 ± 69.50 pA/pF) (Fig.13B), although blocking S-palmitoylation with 2BP decreased Nav1.2 current (- 397.3 ± 47.31 pA/pF) (Fig.13B). This resembled the pattern of current density response to 2BP and PA treatments observed in the Nav1.6-C1978A channel. This suggested that a voltage gated sodium channel lacking S-palmitoylation at the C-terminus was unlikely to be subjected to current amplitude enhancement by S-palmitoylation.

On the other hand, the voltage dependence of steady-state inactivation of Nav1.2 was altered by its S-palmitoylation states (Fig.13C): blocking S-palmitoylation with 2BP caused a 4mV hyperpolarizing shift (2BP: V1/2 = - 61.95 ± 0.21 mV vs. DMSO: V1/2 = - 57.79 ± 0.18 mV), while S-palmitoylation resulted in a 4mV depolarizing shift (V1/2 = - 54.01 ± 0.10 mV) (Fig.13C), similar to previous result from oocyte (Bosman, 2011).

With this data, I demonstrated that Nav1.2 failed to display sensitivity to current enhancement by S-palmitoylation, but preserved the voltage dependence modulation conveyed by the conserved double cysteines in loop2.

2. An engineered cysteine renders Nav1.2 current sensitive to S-palmitoylation enhancement

To further explore the role of S-palmitoylation at the C-terminus of a voltage-gated sodium channel other than Nav1.6, I introduced an exogenous cysteine to Nav1.2 at its C-terminus (K2005), which is a predicted S-palmitoylation site in CSS-Palm. Fig.13A shows the representative traces of TTX-resistant Nav1.2-K2005C currents. I observed that Nav1.2-K2005C displayed the bidirectional current density modulation produced by 2BP and PA treatments (Fig.13E) just as Nav1.6-WT (Fig.13C), suggesting that S-palmitoylation at the exogenous cysteine in Nav1.2 altered the Nav1.2 current density response to S-palmitoylation treatments. This indicates that the functional importance of S-palmitoylation at this position may apply to multiple voltage gated sodium channel isoforms. However, the bidirectional modulation of Nav1.2 current was not as dramatic as that observed in Nav1.6. This might be due to the lower S-palmitoylation efficiency at this particular site in Nav1.2 possibly due to difference in sequence environment, protein conformation and / or interacting partners associated with the channel.

Unexpectedly, the pattern of voltage dependence response of Nav1.2-K2005C was more similar to WT Nav1.6, rather than WT Nav1.2 (Fig.13F): enhancing S-palmitoylation with PA did not depolarize the voltage dependence of steady-state inactivation in Nav1.2-K2005C (PA: V1/2 = - 55.57 ± 0.22 mV vs. DMSO: V1/2 = - 57.20 ± 0.19 mV), while blocking S-palmitoylation with 2BP caused a hyperpolarizing shift in the voltage dependence of steady-state inactivation (V1/2 = - 62.91± 0.26 mV). The loss of PA response to voltage dependence modulation could be caused by the introduction of an extra S-palmitoylation. This is in stark contrast to Nav1.6, where the S-palmitoylation status of the two sites seem to be unrelated, further supporting the notion that S-

palmitoylation modifies Navs functions in an isoform-dependent manner. Moreover, the data also suggested that whether 2BP and PA individual treatment can lead to appreciable effect also depend on the saturation level of S-palmitoylation at specific sites: if saturated, possibly as in the case of C1169 and C1170 in Nav1.6, providing more substrate for S-palmitoylation would not show appreciable effect on channel properties; while if a S-palmitoylation site is non-saturated, likely as the case of the double cysteine in Nav1.2 and C1978 in Nav1.6, manipulating the S-palmitoylation status of the channels with 2BP and PA treatments result in bidirectional effects.

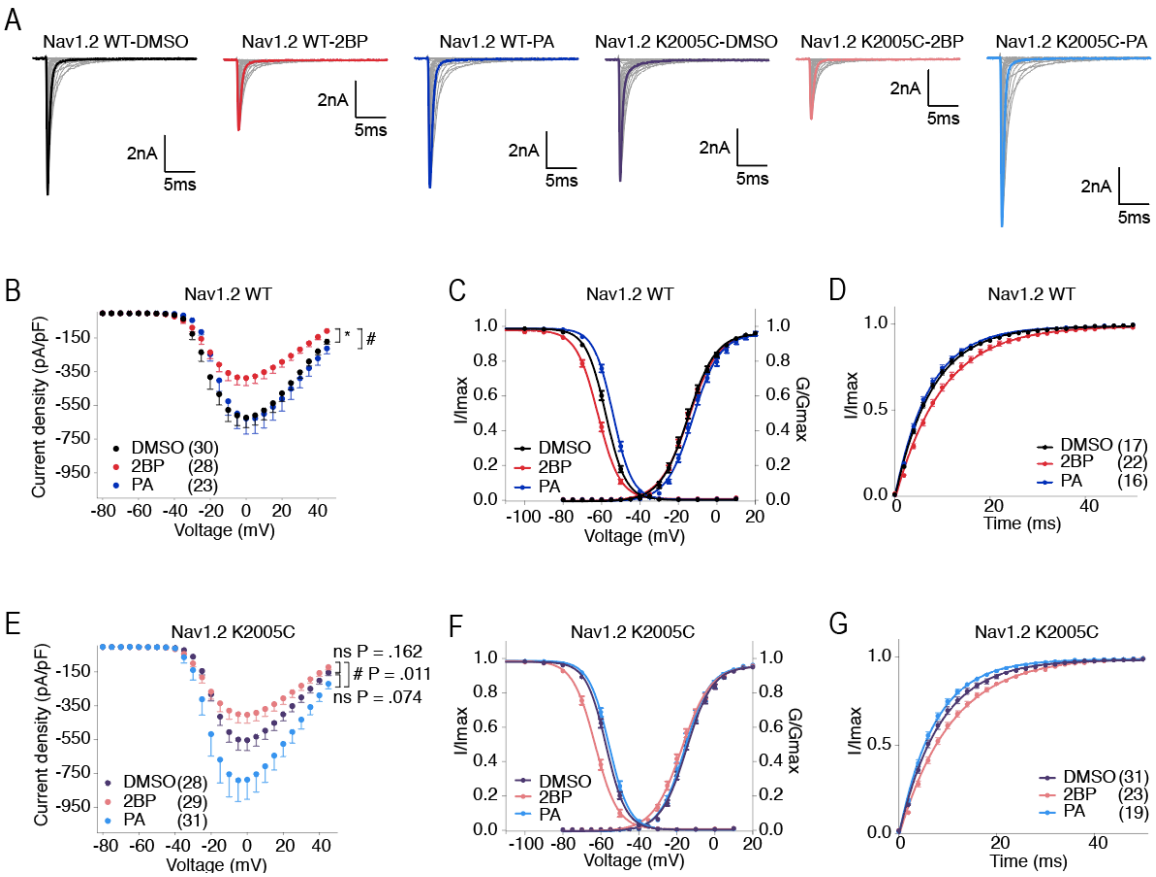

Figure 13. An exogenous cysteine renders Nav1.2 current amplitude enhanced by S-palmitoylation.

Voltage-clamp recordings from ND7/23 cells transiently transfected with TTXr-Nav1.2-WT and Nav1.2-K2005C. Transfected cells were treated with DMSO as solvent control, 2-Br-palmitate (2BP) to block S-palmitoylation and palmitate acid (PA) to enhance S-palmitoylation 24h before recording. (A) Representative current traces from different treatment groups elicited by activation protocol. (B)(E) Current density-voltage plots. * $P < 0.05$ compared to WT, # $P < 0.05$ compared to 2BP in two-way ANOVA. (C)(F) Steady-state inactivation and activation curves fitted with a Boltzmann function. (D)(G) Recovery from inactivation with recovery time duration from 0 to 50ms. Data presented as mean ± SEM. Values are reported in Table 2.

Table 2 Biophysical properties of WT and mutant Nav1.6 and Nav1.2 channel

						Inactivation				Activation						
			Max I density	n		Vhalf		K		n	Vhalf		K		n	Recovery(tau)		n
Nav1.6	WT	DMSO	-80.16 ± 8.30	29		-64.46 ± 0.21		5.32 ± 0.138		30	-19.7 ± 0.18		7.045 ± 0.13		28	9.842 ± 0.76		24
		2BP	-32.02 ± 6.65	22	****	-72.34 ± 0.28	****	6.51 ± 0.243	****	28	-22.48 ± 0.84	*	7.802 ± 0.16	**	22	13.18 ± 1.28	*	18
		PA	-142.4 ± 17.27	33	**####	-66.12 ± 0.18		5.162 ± 0.08		33	-21.32 ± 0.2		6.92 ± 0.203	###	33	10.54 ± 0.45		18
		2BP+PA	-32.12 ± 7.43	12	**													
	CCAA	DMSO	-94.17 ± 17.23	19		-75.5 ± 0.386	^	7.205 ± 0.19	^	26	-22.59 ± 0.93	^^	7.93 ± 0.37	^	18	10.7 ± 0.384		21
		2BP	-52.09 ± 5.11	19	*	-80.48 ± 0.30	**	6.824 ± 0.22		22	-25.88 ± 0.83	*	8.10 ± 0.22		17	12.69 ± 0.69	*	10
		PA	-163.3 ± 24.30	18	*####	-73.57 ± 0.32		6.767 ± 0.19		21	-22.48 ± 0.98	#	7.85 ± 0.18		17	10.45 ± 0.31	##	19
	C1978A	DMSO	-113.2 ± 13.68	35		-63.79 ± 0.23		5.446 ± 0.08		34	-19.81 ± 0.76		7.228 ± 0.12		35	10.32 ± 0.31		21
		2BP	-74.20 ± 12.70	27	P=.054	-73.59 ± 1.39	****	7.107 ± 0.14	****	22	-21.66 ± 0.99		7.76 ± 0.57		17	12.82 ± 0.57	**	26
		PA	-120.5 ± 16.18	27	#	-63.62 ± 0.29	####	5.369 ± 0.11	####	27	-17.95 ± 0.82	##	7.203 ± 0.14		28	10.48 ± 0.55	##	23
	CCCAAA	DMSO	-115.8 ± 15.01	25		-72.91 ± 0.44	^	7.143 ± 0.18	^	21	-18.75 ± 0.2		8.58 ± 0.165	^	23	12.68 ± 0.54		19
		2BP	-83.50 ± 9.69	22	P=.011	-79.56 ± 0.35	***	7.196 ± 0.18		21	-21.61 ± 0.2		8.491 ± 0.10		16	14.36 ± 0.68		15
		PA	-117.5 ± 12.84	26	P=.091	-75.05 ± 0.37		7.779 ± 0.29		22	-18.05 ± 0.5		9.671 ± 1.18		19	12.73 ± 0.55		17
	DRG	WT	-2006 ± 294.9	20		-78.30 ± 1.27		5.936 ± 0.197		20	-34.57 ± 2.16		7.113 ± 0.625		18	11.35 ± 1.17		20
		CCCAAA	-1026 ± 124.7	29	**	-85.17 ± 2.24	*	9.952 ± 0.659	****	25	-31.63 ± 1.37		8.721 ± 0.403	*	27	9.355 ± 0.56		26
Nav1.2	WT	DMSO	-648.7 ± 69.50	30		-57.79 ± 0.18		4.868 ± 0.06		26	-15.01 ± 0.2		6.743 ± 0.24	*	26	7.968 ± 0.38		22
		2BP	-397.3 ± 47.31	28	*	-61.95 ± 0.21	****	5.474 ± 0.15	***	24	-14.59 ± 0.1		7.479 ± 0.16		27	10.41 ± 0.80	**	21
		PA	-641.2 ± 92.95	23	#	-54.01 ± 0.10	****###	4.705 ± 0.10	####	21	-12.43 ± 0.2	*	6.704 ± 0.23	#	21	7.437 ± 0.39	##	20
	K2005C	DMSO	-562.1 ± 62.34	28		-57.20 ± 0.18		4.88 ± 0.088		30	-14.82 ± 0.2		6.608 ± 0.21		27	8.702 ± 0.53		22
		2BP	-416.5 ± 52.65	29	P=.162	-62.91 ± 0.25	****	5.33 ± 0.078	***	29	-17.29 ± 0.2		7.212 ± 0.17	^^	25	11 ± 0.579	**	26
		PA	-837.1± 134.8	31	P=.074,#	-55.57 ± 0.21		4.849 ± 0.08		27	-16.13 ± 0.2		6.028 ± 0.30		27	7.384 ± 0.34	####	23

****P<0.0001, ***P<0.001, **P<0.01, *P<0.05 compared to DMSO of the same DNA

^P<0.0001 compared to WT

compared to 2BP

F. Impact of Nav1.6 S-palmitoylation on DRG neuron activity.

I present that S-palmitoylation of Nav1.6 regulates channel activity in a non-neuronal model system. Due to the important role of Nav1.6 in neuronal excitation, I predict that modulating Nav1.6 S-palmitoylation would exert great impact on neuronal excitability.

1. Loss of S-palmitoylation at C1169, C1170 and C1978 in Nav1.6 reduces channel activity in DRG neurons.

First, I investigated how loss of S-palmitoylation at C1169, C1170 and C1978 affect Nav1.6 activity in DRG neurons. To do this, S-palmitoylation sites at C1169, C1170, and C1978 were eliminated by mutating the three cysteines to alanines (CCCAAA), and then I compared the functional effects of the WT and CCCAAA TTX-resistant Nav1.6 by transient expression of these channels in DRG neurons with the endogenous Nav1.8 knocked down. I found that DRG neurons expressing Nav1.6-CCCAAA conduct smaller TTX-resistant sodium resistant sodium current (Fig.14AB) and have a hyperpolarized shift of steady state inactivation compared to the WT neurons (Fig.14C). This suggests that S-palmitoylation of Nav1.6 also affect channel activity in neuronal environment.

2. Loss of S-palmitoylation at C1169, C1170 and C1978 in Nav1.6 reduces Nav1.6-meidated excitability in DRG neuron.

To explore the excitability outcomes of eliminating critical S-palmitoylation sites in Nav1.6, current-clamp recordings were performed on DRG neurons transfected with WT or CCCAAA TTX-resistant Nav1.6. Endogenous Nav1.8, the major TTX-resistant isoform of VGSC in DRG neurons, were knocked down to isolate Nav1.6-mediated excitability. In the recordings, currents were injected to each neuron to bias the resting membrane potentials to -80mV for better

comparison. I observe both a higher current threshold (Fig.14F, CCCAAA: 459.5 ± 59.82 pA vs. WT: 250.0 ± 46.17 pA) and a higher voltage threshold (Fig.14G, CCCAAA: -6.906 ± 3.471 mV vs. WT: -26.44 ± 4.364 mV) for evoked action potential in CCCAAA neurons with 500ms stimulations. The maximum number of action potentials fired during the 500ms stimulation are not different (Fig.14H). This is because in my experiments the vast majority of the DRG neurons fire only one action potential when the endogenous Nav1.8 channels are knocked down. Moreover, I found that less Nav1.6-CCCAAA cells are able to fire action potential upon a 1ms stimulation up to 1nA (Fig.14I, CCCAAA: 11/22 vs. WT: 2/21 cells, P = 0.0039 in Chi-square test). Collectively, these data suggest that loss of S-palmitoylation at C1169, C1170 and C1978 reduces Nav1.6 activity and dampened Nav1.6-mediated excitability in DRG neurons. This is not due to any discrepancy of intrinsic properties between WT and CCCAAA transfected neurons, as no difference was observed with their resting membrane potential, input resistance, and cell capacitance (Fig.14J).

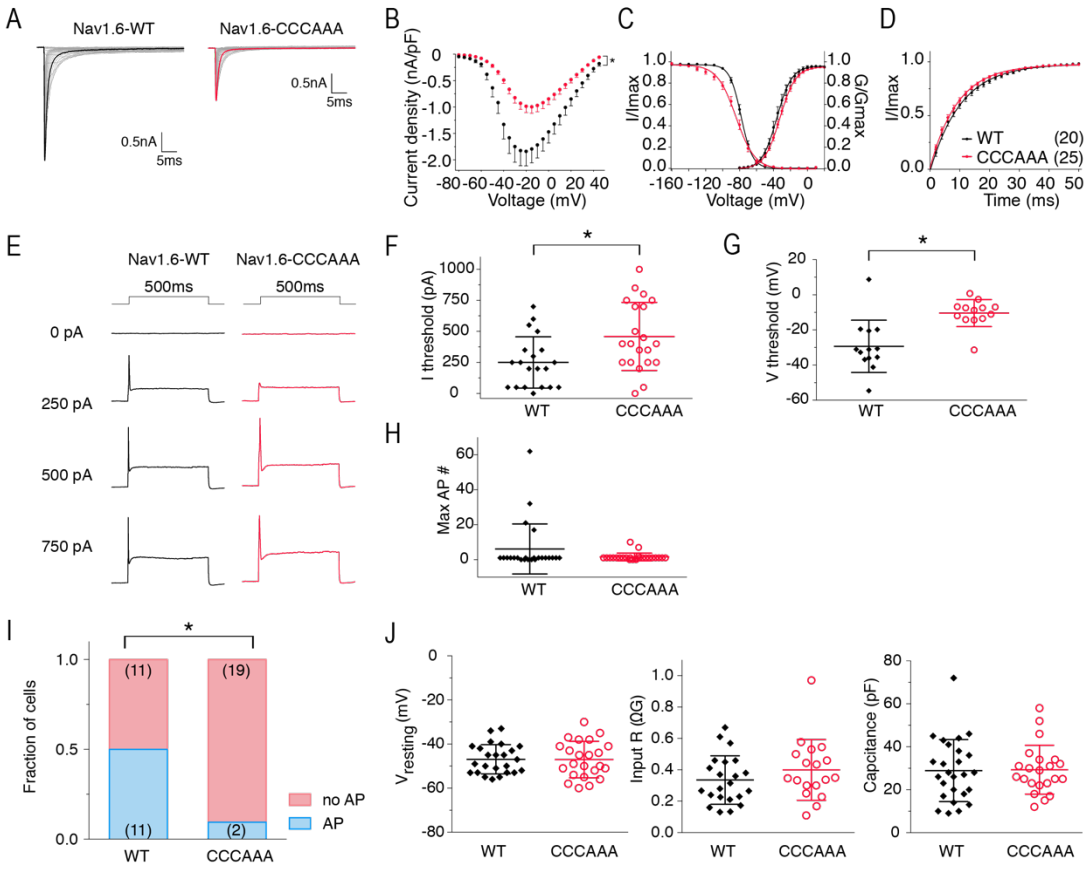

Figure 14. Loss of S-palmitoylation at C1169, C1170 and C1978 reduced Nav1.6 current, channel availability and dampened Nav1.6-mediated excitability in DRG neuron.

(A) Representative TTXr current traces elicited from Nav1.6-WT and Nav1.6-CCCAAA transfected DRG neurons with endogenous Nav1.8 knocked down. (B) Current density-voltage plot. * $P < 0.05$ in two-way ANOVA. (C) Steady-state inactivation and activation curves fitted with Boltzmann functions. (D) Recovery from inactivation with recovery time duration from 0 to 50ms. (E) Representative traces of stimulated action potentials from WT- and CCCAAA-Nav1.6 DRG neurons with endogenous Nav1.8 knocked down. (F,G) Current and voltage threshold for evoked action potential during 500ms stimulation. * $P < 0.05$ in t-test. (H) Maximum number of evoked action potentials during 500ms stimulations from 0pA to 1000pA in 50pA increments. (I) Fraction of cells fired versus did not

fire action potential upon 1ms stimulations from 0pA to 1000pA in 50pA increments. * $P < 0.05$ in Chi-square test. (J) Resting membrane potential, input resistance and cell capacitance of WT- and CCCAAA-Nav1.6 DRG neurons.

G. Impact of Nav1.6 S-palmitoylation on iCell GlutaNeuron activity.

Although Nav1.6 is ubiquitously expressed in the nervous system, it plays a more dominating role in glutamatergic neurons in the central nervous system. Nav1.6 is strategically positioned to exert powerful control over the flow of electric signals within glutamatergic neurons with its concentrated distribution in the axon initial segment and nodes of Ranvier. It is desirable to test how S-palmitoylation of Nav1.6 influenced the excitability of glutamatergic neurons. Here, a highly pure population of human glutamatergic neurons derived from iPSCs (iCell GlutaNeuron, Cellular Dynamics International) were used to reveal the excitability impact of S-palmitoylation deficient Nav1.6.

1. S-palmitoylation alters Nav1.6-mediate excitability of iCell GlutaNeurons.

The iCell GlutaNeurons do not express endogenous TTX-resistant sodium channels. Therefore, to study Nav1.6-mediated excitability in iCell GlutaNeurons, TTX-resistant Nav1.6 was transiently transfected into the cells and current clamp recordings were performed with TTX in bath solution to isolate the impact of transfected Nav1.6 channels. The S-palmitoylation status of Nav1.6 was manipulated by 2BP and PA treatments just as experiments in Nav1.6 transfected ND7/23 cells.

It is worth mentioning that the resting membrane potential of the iCell GlutaNeurons are around – 28.5 mV with or without Nav1.6 transfection (Fig.15A), suggesting that these neurons are immature and may not reflect firing behaviors of mature glutamatergic neurons.

Negative currents were injected to bias the resting membrane potential to mimic mature neurons with more negative resting membrane potential and to eliminate variation between cells. To examine the ability of the Nav1.6

transfected iCell GlutaNeurons to fire action potentials, I applied a 1 ms short stimulus in 50 pA increment steps from 0 pA to 1 nA. The neurons were categorized as excitable and unexcitable according to their ability to fire action potential in response to the stimuli. Fig14D shows that from a holding potential of – 60 mV, the number of excitable cells are smaller in the 2BP treated group compared to DMSO control and PA treatment groups (P = 0.0205 vs. DMSO; P = 0.0013 vs. PA, Chi-square test). The difference between DMSO control and PA treated group was not statistically significant (P = 0.6807, Chi-square test). For the excitable cells, current threshold for action potential generation was measured to reveal their responsiveness to stimuli (Fig14E). As shown in Fig14E, a trend of increased current threshold was observed in the 2BP treatment group, but it was not statistically significant due to the small number of excitable cells in this group (P = 0.056 vs DMSO; P = 0.083 one-way ANOVA with Tukey multiple comparison test). All of above differences were eliminated when cells were biased to the more negative resting membrane potential of -80mV (Fig.15DE). This is aligned with increased availability of Nav1.6 at more negative potentials (left shift of voltage dependence of inactivation).

To test the ability of Nav1.6 transfected iCell GlutaNeurons to fire multiple action potentials, the cells were stimulated with a prolonged (200ms) stimulus in 2 pA increment steps from 0 pA to 200 pA. The cells were categorized according to their ability to fire multiple action potentials, one action potential, or none action potential (Fig.15F). Also, the maximum number of action potentials fired was counted during the stimuli. From holding potentials of both – 60mV and – 80 mV, PA treated cells tended to fire more action potentials, while 2BP treated cells tended to fire less action potentials (Fig.15GHIJK), but none of these trends were statistically significant due to the pronounced variability in repetitive firing. Therefore, I could not draw definitive conclusions on how S-palmitoylation of Nav1.6 modulate excitability of iCell GlutaNeurons from this data set.

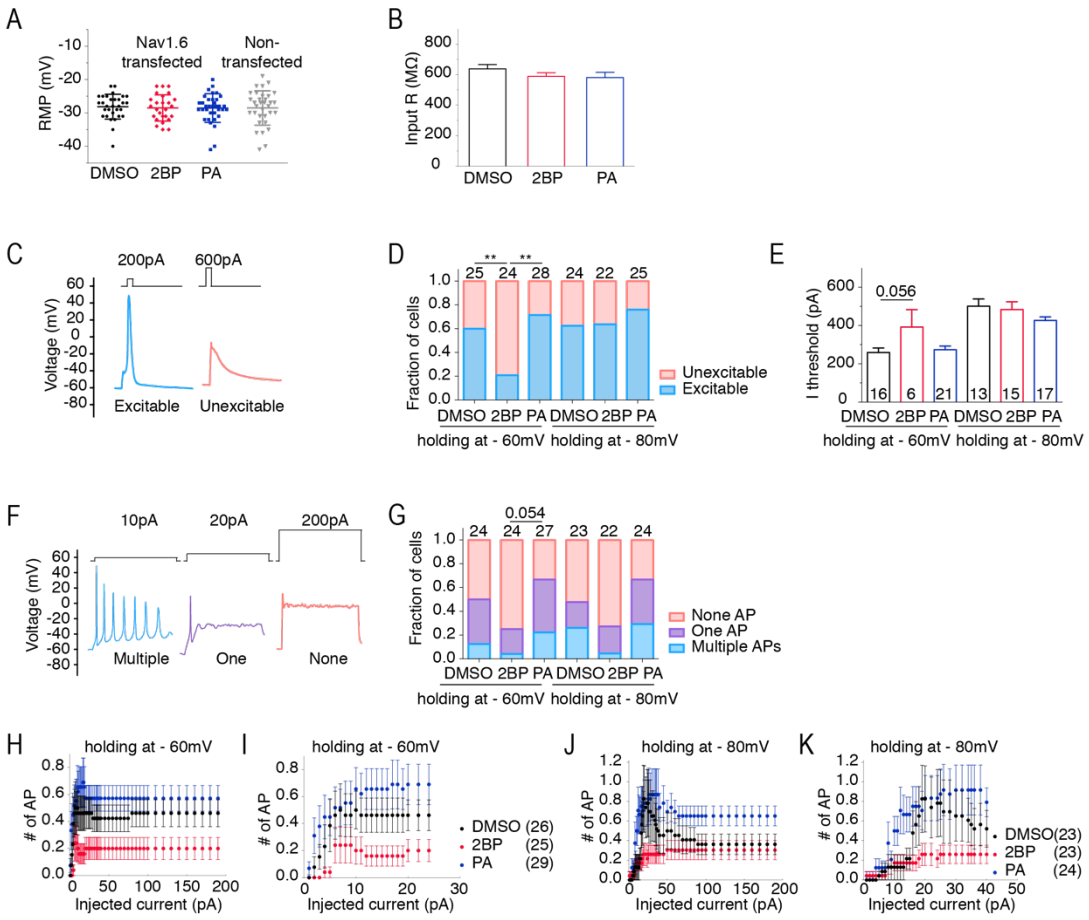

Figure 15. Nav1.6-mediate excitability of iCell GlutaNeurons is altered by S-palmitoylation.

(A) Resting membrane potential (RMP) of iCell GlutaNeurons with and without TTXr-hNav1.6 transfection and treated with DMSO, 2BP and PA. (B) Input resistance of transfected iCell GlutaNeurons in different treatment group. (CF) Example traces of categorized activity evoked by a 1ms stimulus and 200ms stimulus. (D,G) Fraction of categorized cells with membrane potential held at -60mV and -80mV in different treatment groups. ** $P < 0.01$, two-way ANOVA. (E) Current threshold measured by a 1ms stimulus from 0 pA to 1 nA in 50 pA steps with membrane potential held at -60mV and -80mV. (H-K) Number of action potentials elicited by a 500ms stimulus of increasing intensity from a holding potential of -60mV or -80mV.

2. S-palmitoylation regulates Nav1.6 activity in iCell GlutaNeurons.

Since the manipulation of S-palmitoylation in iCell GlutaNeurons failed to show prominent effect on Nav1.6-mediated excitability, I do not have very high confidence about the conclusion drawn from the current clamp data of iCell GlutaNeurons. Voltage-clamp recordings were performed to test whether this resulted from the lack of appropriate S-palmitoylation machinery for Nav1.6 modification in this expression system or from the low expression level of Nav1.6 in these immature neurons. Compared to Nav1.6 transfected ND7/23 cells, I observed that the Nav1.6 transfected in iCell GlutaNeurons present the same voltage dependence modulation by 2BP and PA treatments (Fig.16B). This explains the excitability difference between cells held at -60mV vs. -80mV. Also, recovery from inactivation of the channel is slowed by 2BP treatment. However, the pattern of current density response was different: enhancing S-palmitoylation does not boost Nav1.6 current, although blocking S-palmitoylation still decreases Nav1.6 current. These data suggest that the S-palmitoylation machinery should be intact in these neurons, or at least for the modification of the adjacent S-palmitoylation sites in loop 2. The lack of current enhancement with PA treatment suggests that the C-terminus S-palmitoylation site is saturated in iCell GlutaNeurons. It is also possible that the immature iCell GlutaNeurons lack the S-palmitoylation PATs specifically for the S-palmitoylation of the C-terminus cysteine in Nav1.6, resulting in small Nav1.6 current and limited neuronal excitability. This might account for the subtle increase of excitability observed in the iCell GlutaNeurons with PA treatment. Moreover, it is likely that the limited Nav1.6 expression in the neuron placed a ceiling on current enhancement and thus the limited increase of excitability observed upon PA enhancement.

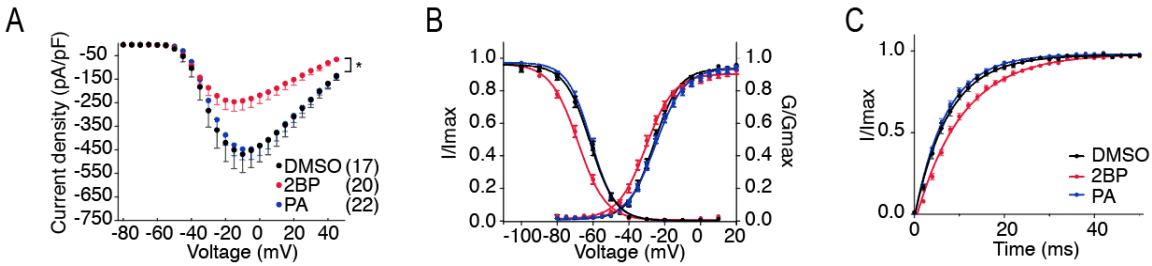

Figure 16. S-Palmitoylation regulates Nav1.6 current in iCell GlutaNeurons. Voltage-clamp recordings from iCell GlutaNeurons transiently transfected with TTXr-Nav1. Transfected cells were treated with DMSO as solvent control, 2-Br-palmitate (2BP) to block palmitoylation and palmitate acid (PA) to enhance palmitoylation 24h before recording. (A) Current density-voltage plot. * $P < 0.001$ WT vs. 2BP and 2BP vs. PA; two-way ANOVA. (B) Steady-state inactivation and activation curves fit with a Boltzmann function. (C) Recovery from inactivation with recovery time duration from 0 to 50ms. Data presented as mean ± SEM.

H. Discussion

I show here that Nav1.6 is modified by S-palmitoylation. 3 major S-palmitoylation sites are identified: two adjacent cysteines in the second intracellular loop (loop 2), C1169 and C1170, and the C-terminus C1978. The two cysteines in loop 2 are highly conserved among Nav isoforms, but their functional significance can vary: in Nav1.6 and Nav1.2, S-palmitoylation at the conserved cysteines modulates channel steady-state inactivation; in Nav1.5, similar modulation is mediated by S-palmitoylation at a non-conserved residue (C981) without involving the conserved cysteine pair. This suggests that the function of a S-palmitoylation site in a voltage-gated sodium channel depends on the specific isoform. It is also possible that S-palmitoylation may not ubiquitously occur at conserved sites in all Nav isoforms.

I also demonstrate that S-palmitoylation regulates distinct Nav1.6 functions by modifying different cysteine residues in the channel. Without affecting steady-state inactivation, the S-palmitoylation status of C1978 substantially modulates the current amplitude of Nav1.6. This uncovers the possibility to fine tune specific channel properties by modulating S-palmitoylation at respective residues. The underlying mechanism of current amplitude regulation might be that S-palmitoylation at Nav1.6-C1978 promotes the surface expression of the channel. However, I were not able to directly test this hypothesis due to the extremely low expression level of Nav1.6 in our heterologous system.

Intriguingly, the C-terminus cysteine is unique to Nav1.6 and absent from all other Nav isoforms. More importantly, this residue is invariant in Nav1.6 among most mammalian and vertebrate species with few exceptions in lower vertebrates. From an evolutionary perspective, this conservation indicates that C1978 is a more recent adaptation for Navs and probably confers critical

regulation that is specific to Nav1.6 and to its special physiological role. Indeed, I observed current enhancement by S-palmitoylation only in the presence of the C-terminus cysteine in Nav1.6. Nav1.2, lacking the homologous S-palmitoylation site, only obtained such modulation when an exogenous was cysteine introduced (K2005C). It is noteworthy that the beginning 2/3 of the CTD is quite conserved among all human Nav isoforms, while the remaining 1/3 that follows the calmodulin binding IQ motif is highly variable. Thus, it is reasonable to speculate that the last 1/3 of the CTD, which includes the unique S-palmitoylation site in Nav1.6, serves isoform-dependent functions for Nav channels. Interestingly, the steady-state inactivation of Nav1.2-K2005C assumed a more similar pattern as Nav1.6-WT, rather than Nav1.2-WT, in response to S-palmitoylation manipulation. This may suggest that the introduction of an exogenous S-palmitoylation site affects the saturation level of S-palmitoylation at the double cysteines that are responsible for the regulation of steady-state inactivation. It is also possible that S-palmitoylation at the C-terminus influences voltage dependence of inactivation in Nav1.2, which does not apply to Nav1.6. This presents another probable evidence for isoform-dependent functionality of S-palmitoylation.

It is important to point out that the dynamic range of current amplitude modulation in Nav1.2-K2005C is far smaller than that in Nav1.6, likely due to lower S-palmitoylation efficiency at an exogenous S-palmitoylation site. There is growing evidence that there is enzyme-substrate specificity for S-palmitoylation (Hou, John Peter et al. 2009, Huang, Sanders et al. 2009, Nadolski and Linder 2009, Thomas, Hayashi et al. 2012, Howie, Reilly et al. 2014, Lemonidis, Sanchez-Perez et al. 2015). Palmitoy-acyl transferases (PATs), the enzymes that catalyze the S-palmitoylation reaction, may recognize their substrates based on protein secondary structure (Plain, Congreve et al. 2017) and / or protein-protein interacting domains (Li, Hu et al. 2010, Thomas, Hayashi et al. 2012, Fredericks, Hoffmann et al. 2014, Brigidi, Santyr et al. 2015, Lemonidis, Sanchez-Perez et al.

2015), although these PATs were once deemed stochastic because a consensus sequence motif has yet to emerge (Rocks, Gerauer et al. 2010). The existence of PAT-substrate specificity is further supported by my observation of sub-optimal effect of current enhancement by S-palmitoylation on an exogenous site in Nav1.2-K2005C as well as the possible lack of S-palmitoylation at the conserved double cysteines in Nav1.5 (Pei, Xiao et al. 2016).

So far, 23 human PATs have been identified. It has been shown that these PATs differ in tissue, cell type, and subcellular distribution (Fukata, Fukata et al. 2004, Fernández-Hernando, Fukata et al. 2006, Mill, Lee et al. 2009, Gorleku, Barns et al. 2011, Greaves, Carmichael et al. 2011, Brigidi, Santyr et al. 2015), creating a spatial, and thus functional segregation among these enzymes. Additionally, PAT distributions are subjected to dynamic regulation (Globa and Bamji 2017), adding another layer of complexity for the regulation of S-palmitoylation. Although more work is needed to clarify the mechanisms of S-palmitoylation and its regulation, the intricacy of PAT specificity and the variety of S-palmitoylation functionalities substantiate its potential of being exploited to target Navs with isoform specificity.

Our discovery of Nav1.6 modification by S-palmitoylation provides a novel strategy to modulate neuronal excitability, considering the crucial role of Nav1.6 in action potential initiation and propagation in both CNS and PNS. I demonstrated, as a proof of concept, that altering S-palmitoylation of Nav1.6 exerts great impact on the excitability of DRG neurons. Nav1.6 has long been an attractive target for excitability modulation due to its unique properties that support high frequency, repetitive firing in a wide range of neurons in CNS and PNS (Maurice, Tkatch et al. 2001, Khaliq, Gouwens et al. 2003, Do and Bean 2004, Van Wart and Matthews 2006, Enomoto, Han et al. 2007, Mercer, Chan et al. 2007, Royeck, Horstmann et al. 2008). Moreover, Nav1.6 is distinguished by its ability to generate high level of persistent current (Smith, Smith et al. 1998,

Maurice, Tkatch et al. 2001) and resurgent current (Raman, Sprunger et al. 1997, Jarecki, Piekarz et al. 2010), which are often perturbed, usually augmented, in channelopathies. Over 200 disease mutations have been identified in Nav1.6, implicating its direct involvement in the etiology of diverse neurological diseases including epilepsy, mental retardation, and movement disorders. Although none of them directly removes or introduces a Nav1.6 S-palmitoylation site, disease mutations that are seemingly distant from a S-palmitoylation site, may influence S-palmitoylation by altering the post-translational code (Pankow, Bamberger et al. 2019), changing the secondary structure or disrupting protein-protein interaction. Additionally, there are complex interplays between different post-translational interactions (Tian, Jeffries et al. 2008, Ho, Selvakumar et al. 2011, Shipston 2014, Pei, Pan et al. 2017, Summers, Milbrandt et al. 2018, Woolfrey, O'Leary et al. 2018). Thus, mutations that interfere with, for example, phosphorylation or its related signaling pathways can also affect S-palmitoylation and indirectly alter channel maturation, trafficking and functional properties. Conversely, altering S-palmitoylation status of specific sites offers an opportunity to attenuate abnormal Nav1.6 activity imposed by disease mutations. Collectively, I present S-palmitoylation as a novel mechanism for isoform specific regulation for voltage-gated sodium channels and provide a new therapeutic strategy to modulate excitability disorders.

IV. DISTINCT FUNCTIONAL ALTERATIONS IN NAV1.6 EPILEPSY MUTANT CHANNELS

A. Overview

Early infantile epileptic encephalopathy (EIEE) is a heterogeneous group of disorders characterized by early onset epileptic seizures and developmental delays. The majority of EIEE patients are resistant to seizure control treatments. Important causes for EIEEs include mutations in voltage-gated sodium channel (Nav) genes *SCN1A*, *SCN2A*, *SCN3A* and *SCN8A*. Among them, *SCN8A* is a relatively novel EIEE gene with the first case reported in 2012 (Veeramah, O'Brien et al. 2012). The number of *SCN8A* mutations and clinical cases have been growing rapidly with the advances of whole genome / exome sequencing as well as the inclusion of *SCN8A* in the diagnostic panels for infantile epileptic encephalopathy (Meisler, Helman et al. 2016). These patients have seizure onset within 18 months of life (5 months on average), after which development delay or regression is typical. Moderate to severe intellectual disability is common and motor deficits are found in 50% of affected individuals. 10% of the published cases reported sudden unexpected death in epilepsy (SUDEP) (Meisler, Helman et al. 2016).

SCN8A encodes the protein voltage-gated sodium channel Nav1.6. More than 150 epilepsy-related mutations have been identified in *SCN8A* (Meisler, Helman et al. 2016). Most of these are *de novo* missense mutations. To date, only about 20 mutations have been functionally characterized. 15 of them are gain-of-function, highlighting Nav1.6 as a potent contributor to neural excitation. Indeed, *SCN8A* expression was increased in chemical and electrical induced seizure models (Blumenfeld, Lampert et al. 2009, Hargus, Nigam et al. 2013, Sun, Wagnon et al. 2013), while reducing *SCN8A* activity conferred seizure protection (Martin, Tang et al. 2007, Makinson, Tanaka et al. 2014, Wong, Makinson et al. 2018). Importantly, *SCN8A* loss-of-function mutations were able

to rescue the seizure phenotypes of *SCN1A* epilepsy models, presumably by tuning down excitation in the inhibition-defected network (Martin, Tang et al. 2007, Hawkins, Martin et al. 2011). Moreover, the *SCN8A*-N1768D knockin mouse, carrying the gain-of-function epilepsy mutation, recapitulated the main features in the human disease (Wagnon, Korn et al. 2014).

The molecular mechanisms and phenotypic outcomes of *SCN8A* epilepsy mutations are highly heterogeneous, in part due to the various location of these mutations in the channel. The highly conserved regions, S1-S4 voltage sensors and S5-S6 ion conducting pore in each of the four domains in the voltage-gated sodium channel, are critical for normal channel functions, and thus are the frequent targets of disease mutations.

The aim of this chapter is to present the characterization of a novel *SCN8A* epilepsy mutation R850Q, systematically compare it to three other *SCN8A* epilepsy mutations (T767I, R1617Q, R1872Q) (Fig.17) and to identify potential commonalities among different *SCN8A* epilepsy mutations in the human Nav1.6 (hNav1.6) channel. Additionally, computational modelling and simulation are used to predict excitability outcomes of these mutations in neurons.

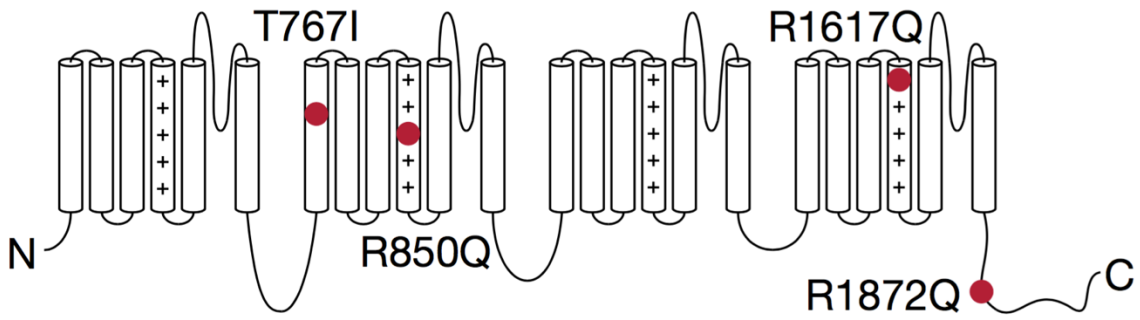

Figure 17. Topology of voltage-gated sodium channel with *SCN8A* epilepsy mutations.

B. Characterizations of epilepsy-related mutant Nav1.6.

1. R850Q hyperpolarizes voltage dependence of activation, increases persistent current and resurgent current, and slows the decay of resurgent current.

R850 is the third charged residue in DII S4 of Nav1.6 (Fig.17). Substitution of this Arg with an uncharged Gln is predicted to impair channel activation and can potentially generate gating pore current. Fig.18A shows the representative traces of transient current from hNav1.6 WT and R850Q. The peak current density (Fig.18B) and rate of decay for the transient current (Fig.18C) were not significantly changed by the R850Q mutation. However, R850Q exhibited altered channel activation as predicted, with a midpoint voltage 4.5mV more negative than the WT channel (V_{50} = -25.61 ± 0.67 mV in R850Q vs V_{50} = -21.07 ± 0.79 mV in WT, $P < 0.0001$) (Fig.18D). This shift indicated premature opening of the mutant channel, while the voltage-dependence of steady-state inactivation remained unchanged (Fig.18E). Collectively, this resulted in larger window currents in the mutant channel as demonstrated in Fig.18F. Fig.18G shows the normalized current traces of WT and R850Q, revealing an increased percentage of persistent current from the mutant channel (1.33 ± 0.06 % in R850Q vs. 0.52 ± 0.03 % in WT, $P < 0.0001$) (Fig.18H). Compared to WT, R850Q did not have a significant change in its rate of recovery from inactivation (Fig.18I). However, the resurgent current amplitude of R850Q increased (7.40 ± 0.53 % in R850Q vs. 5.50 ± 0.23 % in WT, $P < 0.0001$) (Fig.18JK), and the decay of the resurgent current was slower compared to the WT channel (at -35mV repolarization step, 11.35 ± 0.44 ms in R850Q vs. 7.25 ± 0.09 ms in WT, $P < 0.0001$) (Fig.18L).

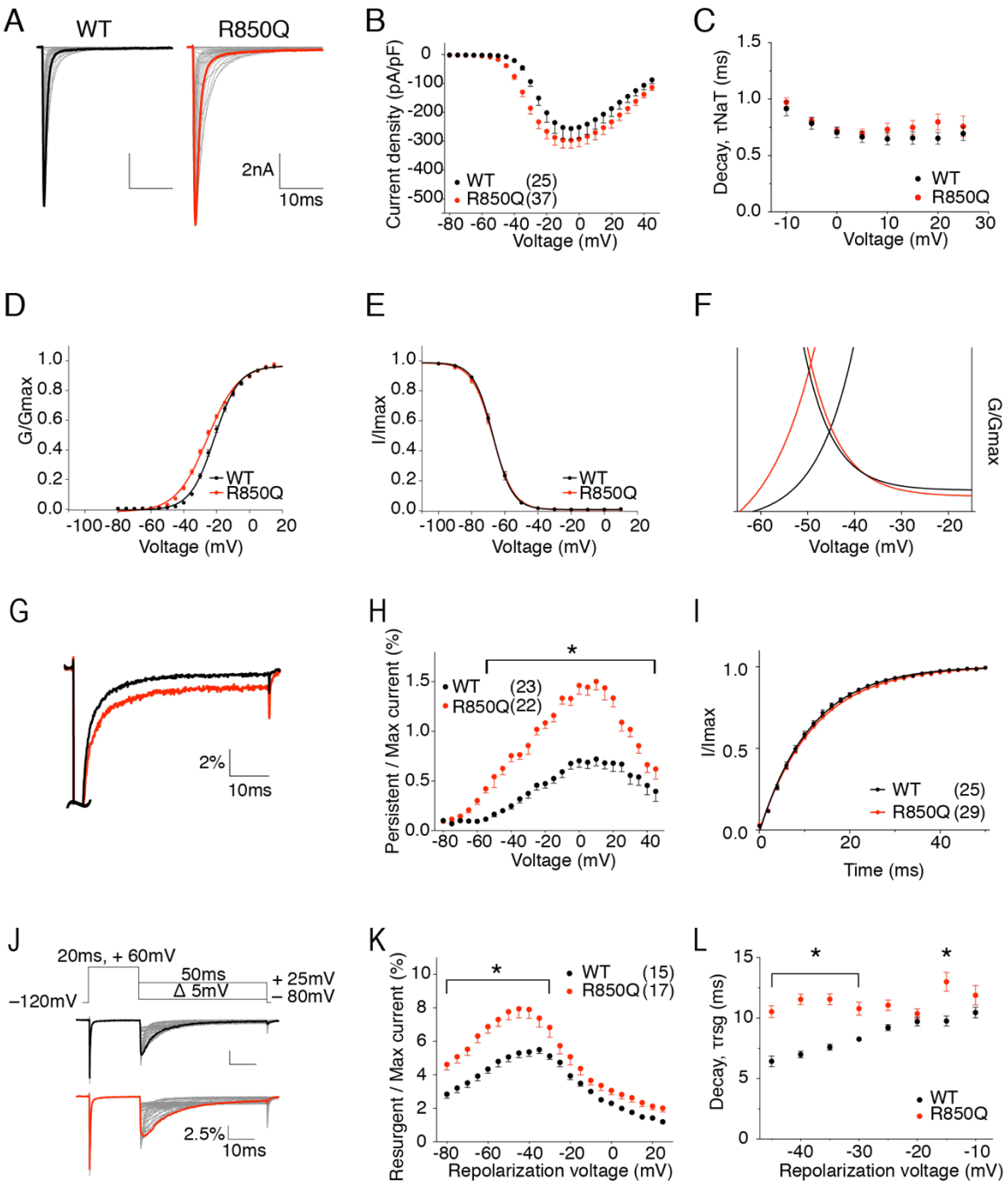

Figure 18. R850Q displayed altered voltage-dependence of activation, increased persistent current, increased resurgent current, and altered resurgent current kinetics.

(A) representative current trace families from hNav1.6 WT (left) and R850Q (right) channels elicited by an activation protocol. Maximum current traces are highlighted with bolded black and red respectively. (B) Current density-voltage

plot of hNav1.6 WT and R850Q. (C) Rate of decay for transient sodium current (τ_{NaT}) at each depolarization voltages. (DE) Activation and steady-state inactivation curves fitted with Boltzmann functions. (F) Window currents shown by Boltzmann fitted curves enlarged from (DE) combined. (G) Representative traces showing persistent current from WT (black) and R850Q (red) channels. Traces shown are elicited at 0mV and are presented as the percentage amplitude normalized to the maximal transient current during the 50ms activation protocol. (H) Per cent persistent current-voltage plot with persistent current measured during the last 1ms of the 50ms activation protocol. $P < 0.01$ from -55mV to 45mV in two-way ANOVA with Sidak multiple comparison test. (I) Recovery from inactivation with recovery duration from 0 to 50ms. (J) Resurgent current protocol and representative traces showing resurgent current from WT (upper) and R850Q (lower) channels. (K) Per cent resurgent current plotted against repolarization voltages. $P < 0.01$ from -80mV to -30mV in two-way ANOVA with Sidak multiple comparison test. (L) Rate of decay for resurgent current (τ_{rsg}) at each repolarization voltages. $P < 0.0001$ from -45mV to -35mV and at -15mV in two-way ANOVA with Sidak multiple comparison test. All values and statistical significance are reported in Table 3.

2. T767I hyperpolarizes voltage dependence of activation, increases persistent current and resurgent current, and slows the decay of resurgent current.

T767 is located in the first transmembrane segment of DII (Fig.17). The mutation from Thr to Ile has been shown to disrupt channel activation in mouse Nav1.6 (Estacion, O'Brien et al. 2014). Representative current traces of hNav1.6 WT and T767I are shown in Fig.19A. The current density (Fig.19B) and rate of decay for transient current (Fig.19C) of T767I in hNav1.6 were not significantly different from the WT channel. In agreement with previous literature, T767I displayed a 10mV hyperpolarizing shift in the voltage-dependence of activation (V_{50} = -31.68 ± 0.81 mV vs V_{50} = -21.07 ± 0.79 mV in WT, $P < 0.0001$) (Fig.19D), indicative of premature channel opening, while it did not alter the steady-state inactivation (Fig.19E). As a result, larger window currents were observed (Fig.19F). The normalized current traces of WT and T767I shown in Fig.19G demonstrates an increased percentage of persistent current in the mutant channel (1.21 ± 0.06 % in T767I vs. 0.52 ± 0.03 % in WT, $P = 0.0012$) (Fig.19H). Compared to WT, T767I had no significant change in the rate of recovery from inactivation (Fig.19I). Fig.19J shows the representative traces of resurgent current generated by WT and T767I. Similar to R850Q, T767I showed significant increase in resurgent current amplitude (7.91 ± 0.42 % in T767I vs. 5.50 ± 0.23 % in WT, $P < 0.0001$) (Fig.19K), and the resurgent currents displayed slower decay kinetics (at -35mV repolarization step, 11.24 ± 0.29 ms in T767I vs. 7.25 ± 0.09 ms in WT, $P < 0.0001$) (Fig.19L).

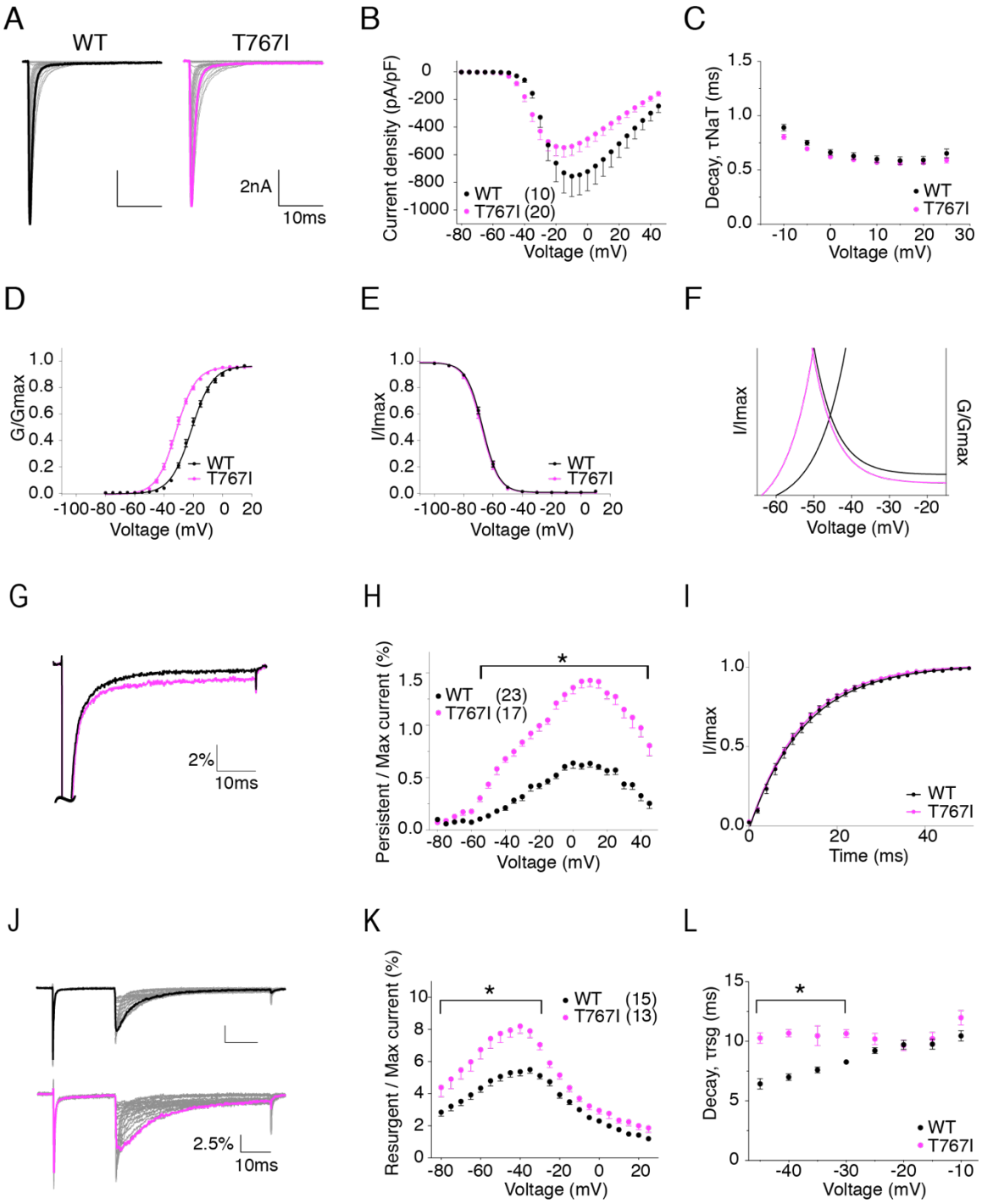

Figure 19. T767I displayed depolarized voltage-dependence of activation, increased persistent current, increased resurgent current, and altered resurgent current kinetics.

(A) representative current trace families from hNav1.6 WT (left) and T767I (right) channels elicited by an activation protocol. Maximum current traces are highlighted with bolded black and pink respectively. (B) Current density-voltage plot of hNav1.6 WT and T767I. (C) Rate of decay for transient sodium current (τ_{NaT}) at each depolarization voltages. (DE) activation and steady-state inactivation curves fitted with Boltzmann functions. (F) window currents shown by Boltzmann fitted curves enlarged from (DE) combined. (G) representative traces showing persistent current from WT (black) and T767I (pink) channels. Traces shown are elicited at 0mV and presented as the percentage amplitude normalized to the maximum peak current during the 50ms activation protocol. (H) per cent persistent current-voltage plot with persistent current measured during the last 1ms of the 50ms activation protocol. $P < 0.0001$ from -50mV to 45mV in two-way ANOVA with Sidak multiple comparison test. (I) recovery from inactivation with recovery duration from 0 to 50ms. (J) representative traces showing resurgent current from WT (top) and T767I (bottom) channels. (K) per cent resurgent current plotted against repolarization voltage. $P < 0.05$ from -80mV to -30mV in two-way ANOVA with Sidak multiple comparison test. (L) Rate of decay for resurgent current (τ_{rsg}) at each repolarization voltages. $P < 0.0001$ from -45mV to -35mV in two-way ANOVA with Sidak multiple comparison test. All values and statistical significance are reported in Table 3.

3. R1617Q slows the decay of transient current, increases persistent current and resurgent current, accelerates recovery from inactivation, and alters voltage dependence of inactivation.

R1617 is the first positively charged arginine in DIV S4 (Fig.17). Loss of the positive charge is predicted to and has been shown to affect channel inactivation in mouse Nav1.6 (Wagnon, Barker et al. 2016). Representative current traces of hNav1.6 WT and R1617Q are shown in Fig.20A. The transient current of R1617Q was not significantly different from WT in current density (Fig.20B) (Table 3). However, it decayed tremendously slower with a time constant about 3.5 times larger than that of the WT channel ($\tau = 3.49 \pm 0.15$ in R1617Q vs. $\tau = 0.89 \pm 0.03$ in WT, $P < 0.0001$) (Fig.20C). Voltage-dependence of activation of R1617Q remained unchanged (Fig.20D), while steady-state inactivation had a shallower slope ($k = 10.07 \pm 0.67$) compared to WT ($k = 5.30 \pm 0.38$) ($P < 0.0001$), but was unaltered in midpoint voltage (Fig.20E), in contrast to the 9 mV depolarizing shift seen by Wagnon et al. with the mouse orthologue. Fig.20F shows the larger window currents of R1617Q due to the change of inactivation time constant. The normalized current traces of WT and R1617Q in Fig.20G demonstrates an increase of persistent current in the mutant channel ($2.68 \pm 0.20\%$ in R1617Q vs. $0.52 \pm 0.03\%$ in WT, $P < 0.0001$) (Fig.20H). Compared to WT, R1617Q had faster recovery from inactivation with a time constant of 5.33 ± 0.20 ms compared to 13.2 ± 0.72 ms in WT ($P < 0.0001$) (Fig.20I). Fig.20J shows the representative resurgent current traces from WT and R1617Q, demonstrating larger resurgent current amplitude generated by R1617Q ($14.13 \pm 0.72\%$ in R1617Q vs. $5.50 \pm 0.23\%$ in WT, $P < 0.0001$) (Fig.20K). In addition, the R1617Q resurgent current also displayed slower decay kinetics (at -10mV repolarization step, 25.87 ± 1.26 ms in R1617Q vs. 10.46 ± 0.43 ms in WT, $P < 0.0001$) (Fig.20L).

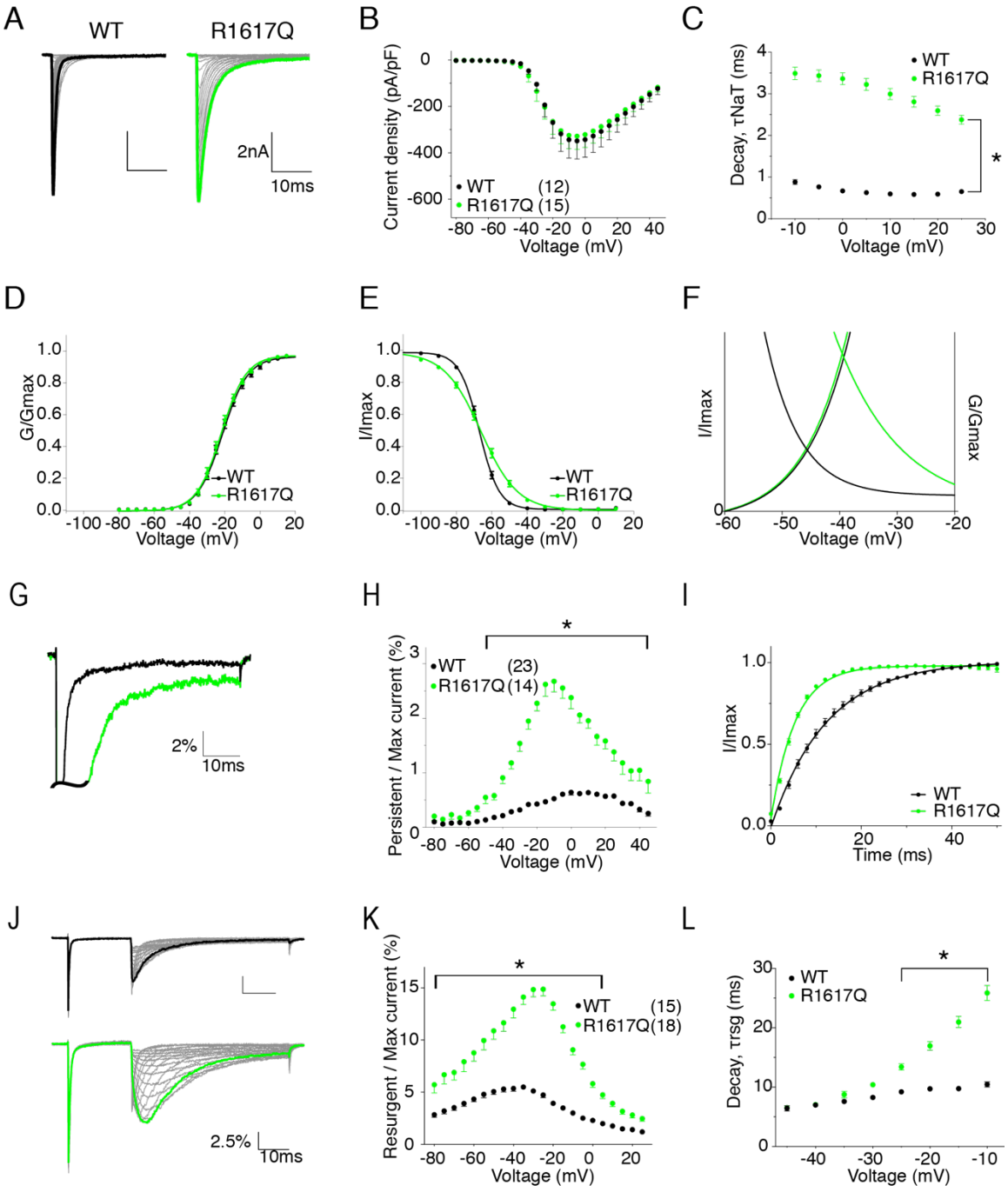

Figure 20. R1617Q has altered voltage-dependence of inactivation and slower rate of decay for transient current, increased persistent current, faster recovery from inactivation, increased resurgent current and altered resurgent current kinetics.

(A) representative current trace families from hNav1.6 WT (left) and R1617Q (right) channels elicited by an activation protocol. Maximum current traces are

highlighted with bolded black and green respectively. (B) Current density-voltage plot of hNav1.6 WT and R1617Q. (C) Rate of decay for transient sodium current (τ_{NaT}) at each depolarization voltages. $P < 0.0001$ at all voltages in two-way ANOVA with Sidak multiple comparison test. (DE) activation and steady-state inactivation curves fitted with Boltzmann functions. (F) window currents shown by Boltzmann fitted curves enlarged from DE combined. (G) representative traces showing persistent current from WT (black) and R1617Q (green) channels. Traces shown are elicited at 0mV and presented as the percentage amplitude normalized to the maximum peak current during the 50ms activation protocol. (H) per cent persistent current-voltage plot with persistent current measured during the last 1ms of the 50ms activation protocol. $P < 0.0001$ from -40mV to 40mV in two-way ANOVA with Sidak multiple comparison test. (I) recovery from inactivation with recovery time duration from 0 to 50ms. (J) representative traces showing resurgent current from WT (top) and R1617Q (bottom) channels. (K) per cent resurgent current plotted against repolarization voltage. $P < 0.0001$ from -75mV to 0mV in two-way ANOVA with Sidak multiple comparison test. (L) Rate of decay for resurgent current (τ_{rsg}) at each repolarization voltages. $P < 0.0001$ from -25mV to -10mV in two-way ANOVA with Sidak multiple comparison test. All values and statistical significance are reported in Table 3.

4. R1872Q increases current amplitude, shifts voltage dependence of activation and inactivation, and slows the decay of transient current.

R1872 locates near the center of the cytoplasmic C-terminal domain (Fig.17). The loss of the positively charged Arg in this region is predicted to interfere with channel inactivation due to its implicated interaction with the channel inactivation gate. Representative traces of hNav1.6 WT and R1872Q are shown in Fig.21A. Fig.21B shows that R1872Q generated larger hNav1.6 current, with a current density of -861.00 ± 97.40 pA/pF compared to -498.10 ± 95.49 pA/pF of WT ($P = 0.016$). Interestingly, the R1872Q transient current decayed slower, particularly at more negative voltages (1.52 ± 0.06 ms in R1872Q vs. 0.89 ± 0.03 ms in WT, $P < 0.0001$) (Fig.21C). This is clearly shown in Fig.21G, where the decay of R1872Q was almost undistinguishable from WT at -10mV, but was dramatically slower at -35mV. This voltage-dependent change of current decay likely contributed to a peculiar pattern of the persistent current-voltage plot (Fig.21H), showing significantly larger percentage of persistent current only at depolarizing voltages ranging from -40mV to -10mV. Important to note, this pattern was not observed when persistent current was measure at 500ms of the prepulse depolarization step in the steady-state inactivation protocol (Fig.21JK). I reasoned that the increased persistent current observed with the 50ms stimulation protocol was due to the slow decay at more negative voltages, instead of a non-inactivating component of the transient current. The voltage-dependence of activation and stead-state inactivation of R1872Q were shifted in opposite directions: a hyperpolarizing shift in activation (V_{50} = -25.5 ± 0.83 mV in R1872Q vs V_{50} = -21.07 ± 0.79 mV in WT, $P = 0.0004$) and a depolarizing shift in steady-state inactivation (V_{50} = -61.69 ± 0.61 mV in R1872Q vs. V_{50} = -67 ± 0.66 mV in WT, $P < 0.0001$) (Fig.21DE) (Table 3). This may suggest that the CTD interacts with different molecular components in the

channel that independently control the voltage-dependence of activation and inactivation. As a result, R1872Q displayed larger window currents (Fig.21F). R1872Q had no significant change in recovery from inactivation (Fig.21I) (Table 3). Fig.21L shows the representative resurgent current traces from WT and R1872Q. The resurgent current of R1872Q had no significant change in amplitude (Fig.21M), but exhibited a substantially slower rate of decay (at -35mV repolarization step, 17.52 ± 1.29 ms in R1872Q vs. 7.25 ± 0.09 ms in WT, $P < 0.0001$) (Fig.21N).

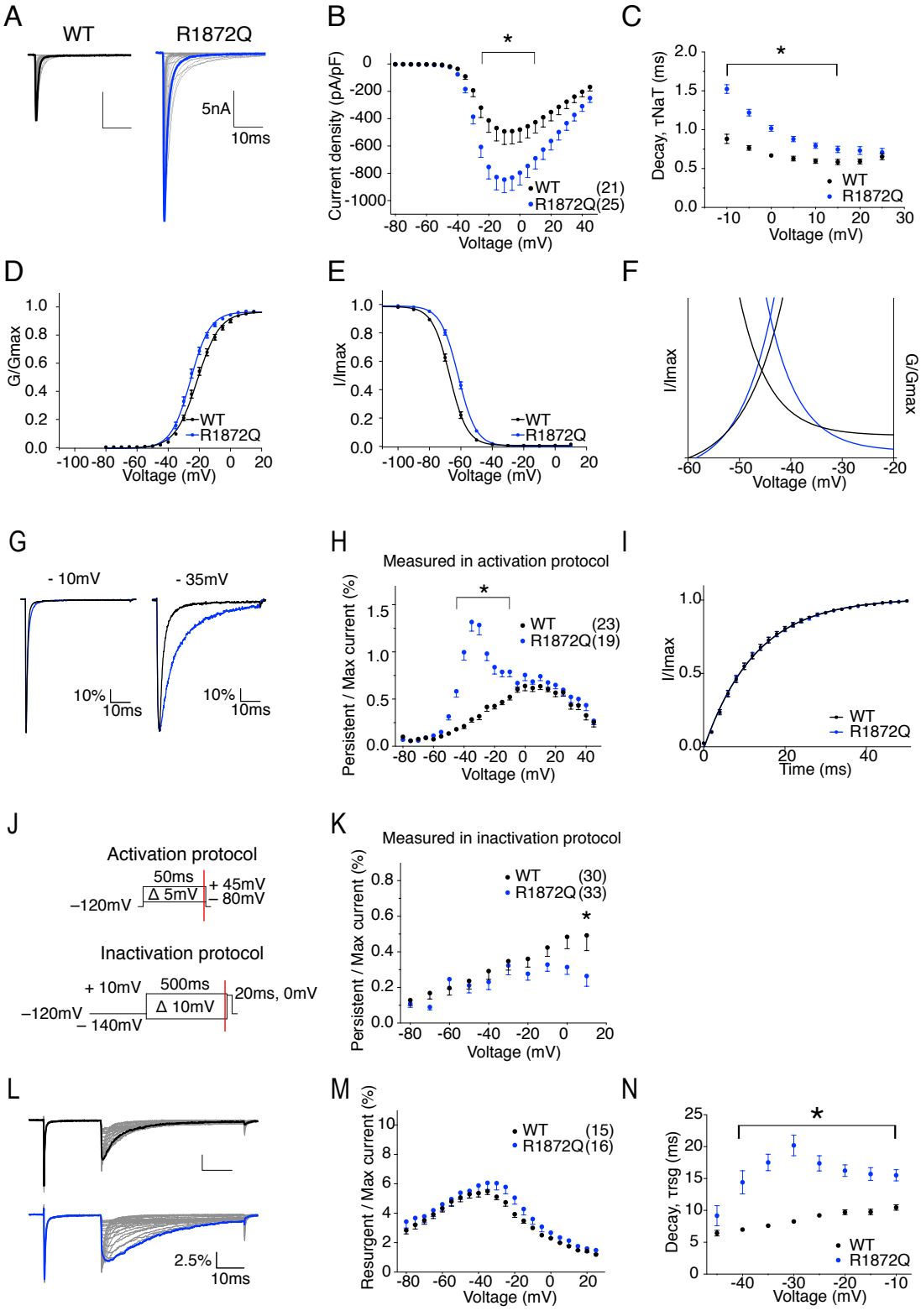
A
WT
R1872Q
5nA
10ms
B
Current density (pA/pF)
Voltage (mV)
WT (21)
R1872Q(25)
C
Decay, τNaT (ms)
Voltage (mV)
WT
R1872Q
D
G/Gmax
Voltage (mV)
WT
R1872Q
E
I/Imax
Voltage (mV)
WT
R1872Q
F
I/Imax
G/Gmax
Voltage (mV)
G
- 10mV
- 35mV
10%
10ms
H
Measured in activation protocol
Persistent / Max current (%)
Voltage (mV)
WT (23)
R1872Q(19)
I
I/Imax
Time (ms)
WT
R1872Q
J
Activation protocol
50ms
+ 45mV
Δ 5mV
– 80mV
–120mV
Inactivation protocol
+ 10mV
500ms
20ms, 0mV
Δ 10mV
–120mV
– 140mV
K
Measured in inactivation protocol
Persistent / Max current (%)
Voltage (mV)
WT (30)
R1872Q(33)
L
2.5%
10ms
M
Resurgent / Max current (%)
Voltage (mV)
WT (15)
R1872Q(16)
N
Decay, τrsg (ms)
Voltage (mV)
WT
R1872Q

Figure 21. R1872Q has increased current amplitude, altered voltage-dependence of both activation and steady-state inactivation, altered pattern of persistent current and enhanced resurgent currents.

(A) representative current trace families from hNav1.6 WT (left) and R1872Q (right) channels elicited by an activation protocol. Maximum current traces are highlighted with bolded black and blue respectively. (B) Current density-voltage plot of hNav1.6 WT and R1872Q. $P < 0.05$ from -25mV to +10mV in two-way ANOVA with Sidak multiple comparison test. (C) Rate of decay for transient sodium current (τ_{NaT}) at each depolarization voltages. $P < 0.0001$ from -10mV to 0mV in two-way ANOVA with Sidak multiple comparison test. (DE) activation and steady-state inactivation curves fitted with Boltzmann functions. (F) window currents shown by Boltzmann fitted curves enlarged from (DE) combined. (G) representative traces showing persistent current from WT (black) and R1872Q (blue) channels elicited at 0mV (left) and -35mV (right). Traces shown are presented as the percentage amplitude normalized to the maximum peak current during the 50ms activation protocol. (H) per cent persistent current-voltage plot with persistent current measured during the last 1ms of the 50ms activation protocol. $P < 0.001$ at -45mV and -10mV in two-way ANOVA with Sidak multiple comparison test. (I) recovery from inactivation with recovery time duration from 0 to 50ms. (J) persistent current measurement at 50ms (red line) of the test pulse in the activation protocol (upper) and at 500ms (red line) of the prepulse of the steady-state inactivation protocol. (K) per cent persistent current-voltage plot with persistent current measured during the last 1ms of the 500ms prepulse in steady-state inactivation protocol. $P < 0.05$ at 10mV in two-way ANOVA with Sidak multiple comparison test. (L) representative traces showing resurgent current from WT (top) and R1872Q (bottom) channels. (M) per cent resurgent current plotted against repolarization voltage. (N) Rate of decay for resurgent current (τ_{rsg}) at each repolarization voltages. $P < 0.0001$ from -40mV to -20mV, $P < 0.001$ at -15mV, $P < 0.01$ at -10mV in two-way ANOVA with Sidak multiple comparison test. All values and statistical significance are reported in Table 3.

Table 3 Biophysical properties of WT and epilepsy mutant *SCN8A* channels

		WT	n	R850Q	n	T767I	n	R1617Q	n	R1872Q	n
Maximal transient I	(pA/pF)	-258.0 ± 38.81	25	-302.1 ± 27.95	37						
		-756.8 ± 147.2	10			-552.7 ± 68.49	20				
		-351.0 ± 78.56	12					-333.2 ± 58.85	15		
		-498.1 ± 95.49	21							-861.00 ± 97.40*	25
Transient I decay (-10mV)	(ms)	0.89 ± 0.03	18	0.97 ± 0.04	28	0.80 ± 0.02*	19	3.49 ± 0.15****	14	1.52 ± 0.06****	24
Activation	$V_{1/2}$ (mV)	-21.07 ± 0.79	21	-25.61 ± 0.67****	31	-31.68 ± 0.81****	21	-21.25 ± 0.73	14	-25.5 ± 0.83***	27
	K	6.89 ± 0.20		9.26 ± 0.13****		6.29 ± 0.15*		6.76 ± 0.16		5.69 ± 0.20***	
Inactivation	$V_{1/2}$ (mV)	-67 ± 0.66	19	-66.95 ± 0.64	36	-68.20 ± 0.60	20	-67.64 ± 0.65	12	-61.69 ± 0.61****	24
	K	5.30 ± 0.38		5.66 ± 0.37**		5.41 ± 0.49		10.07 ± 0.67****		5.39 ± 0.36	
Recovery (τ)	(ms)	13.2 ± 0.72	19	12.48 ± 0.53	29	12.39 ± 0.42	18	5.33 ± 0.20****	15	12.57 ± 0.71	21
Persistent I (-10mV)	(%)	0.52 ± 0.03	23	1.33 ± 0.06****	22	1.21 ± 0.06**	17	2.68 ± 0.20****	14	0.79 ± 0.05	19
Resurgent I (-35mV)	(%)	5.50 ± 0.23	15	7.40 ± 0.53**	17	7.91 ± 0.42****	13	14.13 ± 0.72****	18	6.07 ± 0.45	16
Resurgent I decay (-35mV)	(ms)	7.25 ± 0.09	12	11.35 ± 0.44****	13	11.24 ± 0.29****	12	8.33 ± 0.37*	15	17.52 ± 1.29****	15
Resurgent I decay (-10mV)	(ms)	10.46 ± 0.43	12	11.18 ± 0.44	13	11.98 ± 0.62	10	25.87 ± 1.26****	16	15.51 ± 0.89**	14

**** $P < 0.0001$, *** $P < 0.001$, ** $P < 0.01$, * $P < 0.05$ in upaired t test

C. Computational models of Nav1.6 currents.

The sodium current model was based on a Markov state model described in detail previously (Khaliq, Gouwens et al. 2003) with minor modifications to partially segregate the coupling of voltage dependence of activation and inactivation (Fig.22). A summary of the biophysical properties of modeled channels are reported in Table 3.

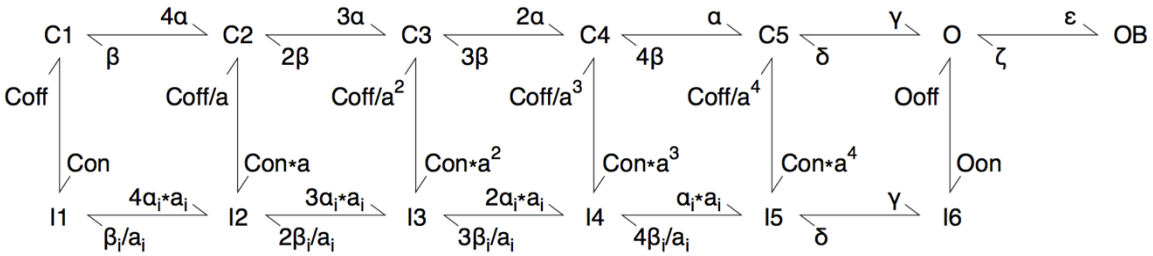

Figure 22. Simple Markov state model of the sodium channel.

Modified based on the model described by Khaliq et al. (2003). States of the channel include closed (C), inactivated (I), open (O), and open-blocked (OB).

1. Modelling WT Nav1.6 current.

To model WT Nav1.6 current, the kinetic parameters remained identical to the original model, except for O_{on}, the rate constant for the $O \rightarrow I_6$ transition (I_{NaT} decay), was modified from 0.75 to 1.132 to match the experimental result. Mutant Nav1.6 currents were modeled as changes relative to this baseline. Quantitative analysis and curve fitting were performed to reconcile experimental and modelled data. ε, the rate constant for O→OB was not altered for experiments with open channel block (resurgent current) implemented, while it was set to 0 otherwise. All modified parameters were reported in Table 4.

2. Modelling Nav1.6-R850Q current.

To model R850Q current, Ooff was modified from 0.005 to 0.018 to induce higher percentage of persistent current (Fig.23A). Parameters α and β were changed from 150 to 90 and 3 to 0.9, respectively, to model voltage dependence alterations observed (Fig.23B). In my experiment data, R850Q had no shift in voltage dependence of steady-state inactivation but hyperpolarized voltage dependence of activation with a shallower slope. However, this was difficult to achieve in the Khaliq et al. model due to the intrinsic coupling of activation and inactivation; shifting voltage dependence of activation unavoidably results in a shift of inactivation in the same direction to similar extend. As a result, the modeled R850Q displayed a slight hyperpolarizing shift in steady-state inactivation. Fig.23C shows the resurgent current traces with ε set to the value in the original model. The impact of the R850Q mutation on the percentage resurgent current were shown in Fig.23D. The increase of resurgent current percentage and altered resurgent current dynamics in simulation was the result of modifications of the forward mentioned parameters without implementing any change for the resurgent current parameters.

3. Modelling Nav1.6-T767I current.

For T767I, Ooff was modified from 0.005 to 0.018 to achieve a higher percentage of persistent current (Fig.23A). α and β were changed from 150 to 450 and 3 to 5 respectively (Fig.23B) to mirror the voltage dependence alterations observed. In my experiment data, T767I displayed a 10mV hyperpolarizing shift in the voltage dependence of activation with no change in its voltage dependence of steady-state inactivation. Again, with activation and inactivation coupling in the original model, I only achieved a 6mV hyperpolarizing shift for activation with minimal alteration, a 2mV hyperpolarizing shift, for inactivation. The impact of the mutations on resurgent current was shown in Fig.23C,D.

4. Modelling Nav1.6-R1617Q current.

For R1617Q, Oon was modified from 1.132 to 0.2866 to mirror a slowed decay of inactivation (Fig.23A); Coff was modified from 0.5 to 0.8 to achieve faster recovery from inactivation (Fig.23E). These alterations were sufficient to achieve a higher percentage of persistent current, as well as a depolarizing shift in steady-state inactivation without changing other parameters. I chose not to modify the voltage dependence parameters to reflect the shallower slope of stead-state inactivation observed in my experimental data, because I were not able to achieve such alteration without excessively modifying the voltage dependence of activation in this model. Fig.23C,D shows the resultant impact on resurgent current dynamics and amplitude, both of which closely aligned with my experimental data without changing the resurgent current parameters. However, the time constant for the rate of recovery from inactivation only displayed a 1.7-fold decrease in the simulation, instead of an observed 2.5-fold decrease. This is due to a faster rate of recovery implemented in the original model. Therefore, my modeled R1617Q channel did not perfectly reflect functional alterations observed

in my experimental data, and thus underrepresents some of the changes incurred by the mutation.

5. Modelling Nav1.6-R1872Q current.

For R1872Q, Oon was modified from 1.132 to 0.656 for a slower inactivation rate (Fig.23A); α and β were changed from 150 to 250 and 3 to 4, respectively (Fig.23B). The impact of the mutations on the resurgent current were shown in Fig.23C,D. Important to note, I did not implement a change in sodium current conductance to match the observed increase of R1872Q current density, considering direct translation of current density change from a model cell line to neuronal data would not be appropriate.

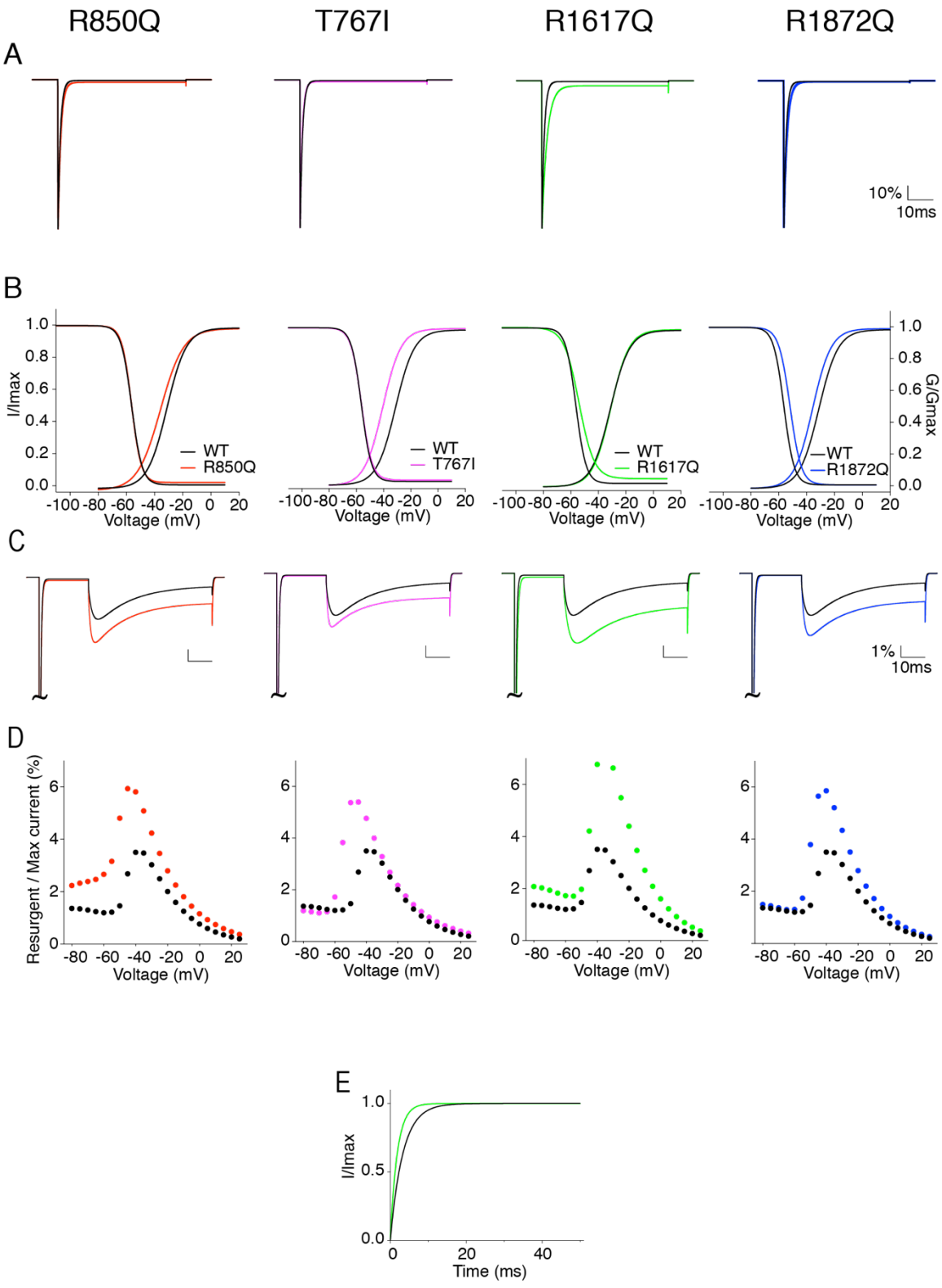

Figure 23. Simulation of sodium current generated by modeled WT and mutant Nav1.6.

(A) example WT (black) and mutant Nav1.6 currents (red: R850Q, pink: T767I, green: R1617Q, blue: R1872Q) generated from modeled neurons without open channel block. (B) I-V/G-V plots showing the voltage dependence of activation and steady-state inactivation of the modeled WT and mutant Nav1.6 channels. (C) example resurgent currents generated by modeled WT and mutant Nav1.6 channels with open channel block. (D) per cent resurgent currents plotted against repolarization voltages from simulated recordings. Peak resurgent currents were measured starting 1.4ms into the repolarization step and normalized to the maximum peak current during a 50ms activation protocol. (E) recovery from inactivation plot with recovery time duration from 0 to 50ms for R1617Q. Values are reported in Table 5.

Table 4 Parameters of modeled sodium channels

	WT	R850Q	T767I	R1617Q	R1872Q
α	150	85	700	150	330
β	3	0.9	5	3	4
αi	150	126	110	650	80
βi	3	3.4	6	3	6
γ	150	137	94	111	103
Coff	0.5	0.4	0.34	5	0.35
Oon	1.132	1.018	1.213	0.2866	0.656
Ooff	0.005	0.018	0.018	0.005	0.005

Table 5 Biophysical properties of modeled WT and mutant *SCN8A* channel

		WT	R850Q	T767I	R1617Q	R1872Q
Transient I	(pA/pF)	-714.6	-713.2	-735.3	-724.5	-716.7
Transient I decay		0.92	1.06	0.85	2.01	1.30
Activation	$V_{1/2}$(mV)	-31.23	-35.78	-40.59	-30.92	-35.59
	K	6.90	8.08	6.73	6.45	6.60
Inactivation	$V_{1/2}$(mV)	-55.85	-56.16	-56.41	-53.86	-51.57
	K	3.84	3.74	4.00	6.15	3.96
Recovery	(ms)	3.30	3.35	3.36	1.68	3.26
Resurgent I	(%)	3.50	5.93	5.40	7.43	5.85

D. Simulations of action potential firing in modeled neurons.

1. Simulation in a single compart model of Purkinje neuron.

To simulate spontaneous and evoked activity of Purkinje neurons, the total sodium conductance of the Khaliq model was replaced by my modeled hNav1.6. To represent heterozygous conditions, 50% of the Nav1.6 sodium conductance was replaced by the modeled mutant channels. Fig.24A shows the spontaneous action potential (AP) firing from WT and mutant Purkinje neurons with open channel block implemented. Modeled neurons incorporated with R850Q, T767I and R1872Q currents demonstrated increased excitability exemplified by a higher frequency of spontaneous (Fig.24AC) as well as evoked APs (Fig.24D) (Table 6). The R1617Q neuron was not more excitable than the WT neuron in response to lower range of stimulation, but its firing frequency continued increasing in the higher stimulation range, showing resistance to depolarization block and reaching a higher maximal AP frequency. This enables the R1617Q neuron to sustain high-frequency, repetitive firing, which is an important characteristic of neurons involved in seizure activity. The simulations demonstrated a differential pattern of excitability outcome caused by functional alterations in activation versus inactivation. Premature opening, as implemented in R850Q, T767I and R1872Q, has prominent effect on enhancing firing, either spontaneous or in response to low intensity stimulation. On the other hand, altered inactivation that led to increased channel availability, as exhibited mainly with R1617Q and R1872Q, boosts the ability of a neuron to sustain high frequency firing.

In addition, simulations without the open channel block mechanism suggested an important role of resurgent current in affecting excitability, especially when mutant channels were involved. As shown in Fig.24B and Table 6, all variants are consistently less excitable without OB, suggesting that

resurgent current is an important contributor to high frequency firing associated with epilepsy mutations. Moreover, the WT neuron demonstrated about 12% reduction of spontaneous AP firing, while the R1617Q, R1872Q, R850Q and T767I mutants showed 9%, 34%, 46% and 40% reduction, respectively. This indicated that the excitability of neurons with mutant channels was generally more sensitive to the existence of the open channel block. As a result, the R1872Q, R850Q and T767I mutant neurons with OB implemented presented larger percentage increase of spontaneous APs (92%, 177%, 219%) compared to those without OB implemented (43%, 70%, 117%). Therefore, resurgent currents can have significant impact on the excitability of neurons with mutant Navs, although resurgent currents did not display as remarkable an influence on the excitability of WT neurons in the simulations. Intriguingly, the effect size of OB inclusion in the model did not correlate with the amplitude of resurgent current (Table 6). For example, the excitability of the R850Q-containing model neuron was most affected by the inclusion of OB, although the modeled R850Q channel did not exhibit the most prominent increase of resurgent current (Fig.24CD). On the contrary, the spontaneous activity of R1617Q was unexpectedly reduced by the inclusion of OB, although it had the largest increase of resurgent current. This emphasizes that neuronal excitability is an integrated outcome of different aspects of channel functions, and such complex integration can potentially be extended to the inter-cellular and network levels.

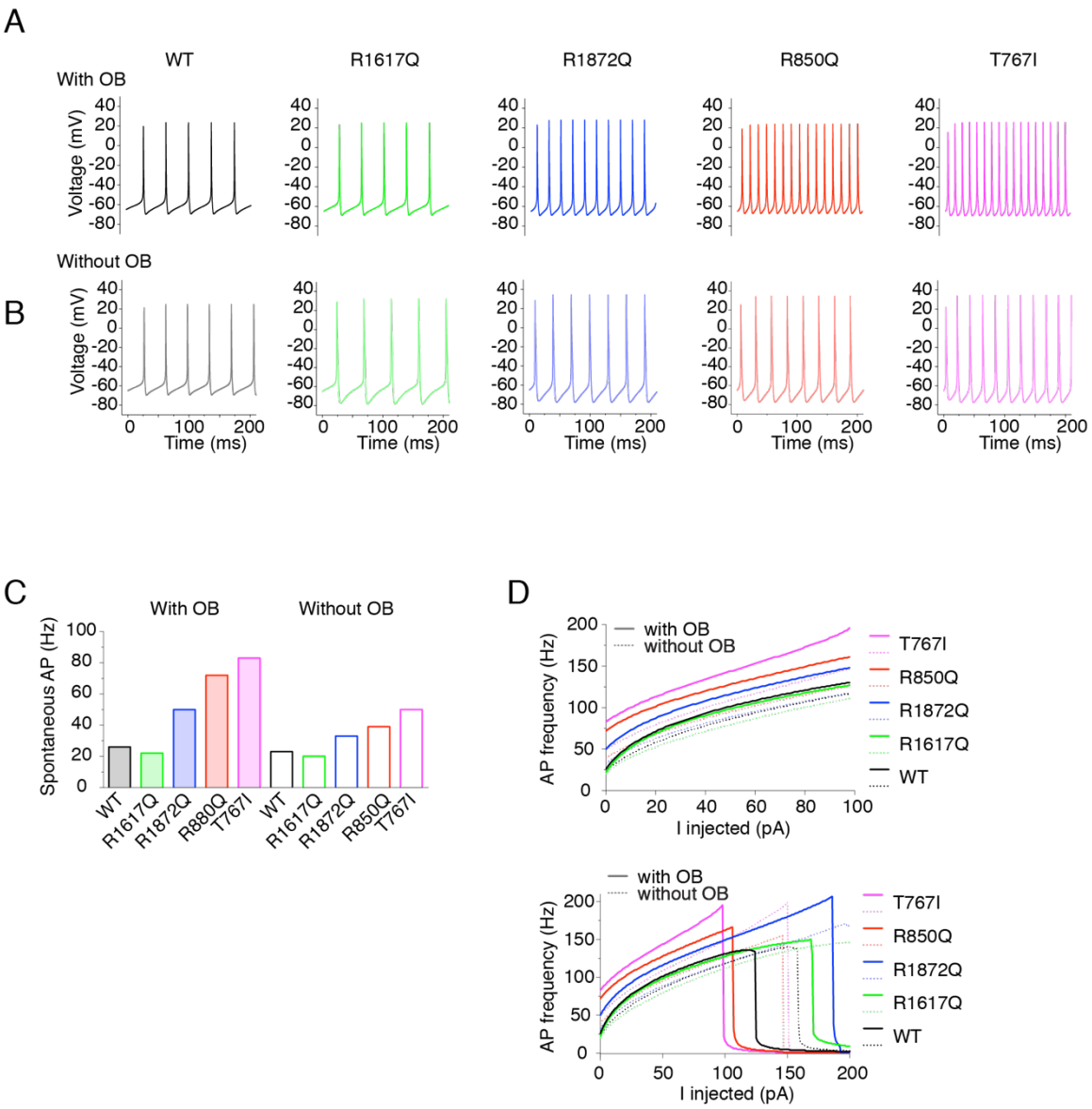

Figure 24. Simulation of action potential firing in Purkinje neuron expressing WT or heterozygous mutant Nav1.6 channels.

(A-B) example traces of spontaneous firing of modeled Purkinje neurons either with 100% WT Nav1.6 current or with 50% WT and 50% mutant Nav1.6 currents (black: WT, green: R1617Q, blue: R1872Q, pink: T767I, red: R850Q) with OB (A) and without OB (B). (C) Quantification of the frequency of spontaneous action potentials. Values are reported in Table 6. (D) Quantification of evoked action potentials.

Table 6 Spontaneous action potential frequency (Hz) of simulated Purkinje neurons

		WT	R1617Q	R1872Q	R850Q	T767I
Spontaneous	With OB	26	22	50	72	83
	Without OB	23	20	33	39	50
Maximum	With OB	136	150	207	166	196
	Without OB	140	146	171	155	199

2. Simulation in a multi-compartmental model of cortical pyramidal neuron.

To further investigate the impact of Nav1.6 mutations on the integrated outcome of neuronal excitability, I incorporated the modeled Nav1.6 in a more sophisticated cortical pyramidal neuron model (Ben-Shalom, Keeshen et al. 2017). This model implemented multiple sodium channel isoforms that were differentially distributed in soma, dendrites, axon initial segment, nodes of Ranvier and along the myelinated axon. The sodium conductance that represents Nav1.6 current in the original model was replaced by the modeled hNav1.6 current. Similar to the Purkinje neuron model, heterozygous mutations of Nav1.6 R1872Q, R850Q and T767I in modeled cortical pyramidal neuron lead to marked increase of excitability with or without OB (Fig.25). However, unlike the Purkinje neuron model, the inclusion of the OB mechanism did not consistently increase action potential firing across all variants. In response to lower range of stimulations, WT and mutant neurons fired more action potentials without OB, while in the higher range of stimulations (up to 4nA) the firing rates were eventually surpassed by those with OB implemented. This supports the notion that resurgent current facilitates but does not guarantee high frequency firing (Lewis and Raman 2014). Therefore, the precise impact of resurgent currents on neuronal excitability also likely depends on cellular background.

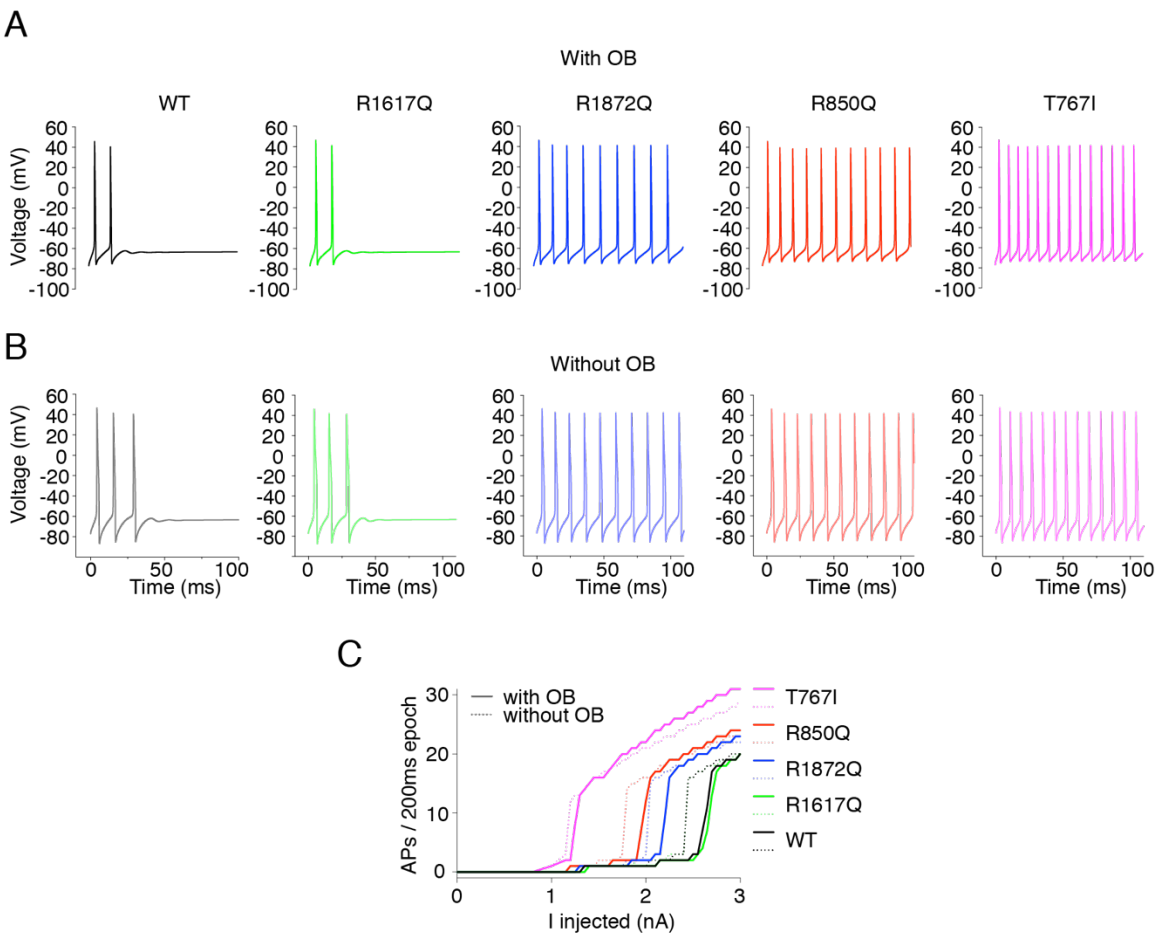

Figure 25. Simulation of action potential firing in cortical pyramidal neuron expressing WT or heterozygous mutant Nav1.6 channels.

(A-B), example traces of action potential firing evoked by 2.3nA current injection in cortical pyramidal neuron models either with 100% WT Nav1.6 current or with 50% WT and 50% mutant Nav1.6 currents (black: WT, green: R1617Q, blue: R1872Q, pink: T767I, red: R850Q) with OB (A) and without OB (B). (C) Quantification of evoked action potentials.

E. Discussion

A growing number of *SCN8A* mutations have been associated with EIEE, but the pathogenic outcomes are hard to predict without functional characterization. Here I report that the novel epilepsy mutation R850Q is gain-of-function, consistent with the hypothesis that a majority of *SCN8A* epilepsy mutations primarily lead to enhanced channel function. R850Q exhibits multiple aberrant properties, including premature opening, impaired inactivation and increased resurgent current. By comparing R850Q with three other *SCN8A* epilepsy mutations that have been previously characterized in mouse Nav1.6 constructs, I show that the mutations affect different aspects of the human Nav1.6 channel properties despite all being gain-of-function. To my surprise, all the evaluated mutations display enhanced resurgent currents, pointing to a potential commonality among gain-of-function *SCN8A* epilepsy mutations. Using computational simulations, I demonstrate that modeled neurons bearing these *SCN8A* epilepsy mutations are hyperexcitable, further supporting the proposed mechanism for *SCN8A* epilepsy being neuronal over-excitation and the hypothesis that altered resurgent currents in hNav1.6 channels likely contribute to increased seizure susceptibility.

EIEE with a *SCN8A* mutation is a devastating condition due to its phenotypic severity and resistance to classic anti-epileptic drugs. Additionally, *SCN8A* cases are highly heterogeneous, displaying variable clinical presentation and treatment response. The disease mechanism is not well understood and requires functional characterization of a wide range of *SCN8A* mutations for more individualized therapeutic development. However, the majority of previous functional analysis of *SCN8A* mutations were conducted with the mouse cDNA construct expressed in heterologous systems. Although these results have provided valuable insights for the molecular underpinnings of the disease, the alterations of channel functions they presented may differ from the same

mutations in human DNA. Moreover, most of the previous studies on *SCN8A* epilepsy mutations did not-test the involvement of resurgent current, the alteration of which can affect neuronal excitability, as it does in many other sodium channelopathies (Jarecki, Piekarz et al. 2010, Hargus, Merrick et al. 2011, Sittl, Lampert et al. 2012, Hargus, Nigam et al. 2013, Tan, Piekarz et al. 2014, Patel, Barbosa et al. 2016, Xiao, Barbosa et al. 2019). In my study, I used a human *SCN8A* cDNA construct (hNav1.6) for functional characterization and systematically compare the outcomes with those from previous studies using the mouse construct. I observed consistent functional changes for the mutation R1872Q, but important functional differences for mutations T767I and R1617Q in the human compared to the mouse channel background. For example, the current amplitude produced by the T767I mutation in hNav1.6 is similar to the amplitude observed with WT hNav1.6, while the T767I mutation was reported to have a 2.5-fold reduction in mouse Nav1.6 (Estacion, O'Brien et al. 2014). On the other hand, the hyperpolarizing shift of voltage dependence of activation and the increase of persistent current are comparable in both backgrounds. As for R1617Q, a similar slowing of current decay and increase of persistent currents are observed with both the human and mouse channel background, but there are differential effects on the voltage dependence of activation and inactivation (Wagnon, Barker et al. 2016). In hNav1.6, the R1617Q mutation altered only the slope of steady-state inactivation, while in the mouse Nav1.6, there is a hyperpolarizing shift of activation and a depolarizing shift of inactivation along with a slope change. Such differences may seem subtle, but they suggest molecular and functional distinctions between the human and mouse channels, which in turn could alter how individual mutations impact intrinsic neuronal excitability and even affect their pharmacological responsiveness, and thus could have important impact when it comes to therapeutic development and testing.

Although it is generally accepted that *SCN8A* epilepsy mutations are primarily gain-of-function, the molecular mechanisms often differ among

individual mutations. The heterogeneity of *SCN8A* epilepsy phenotypes likely stems in part from the various locations and functional consequences of the mutations. Due to the clear functional segregation of channel regions, outcomes of some mutations can be predicted by their location. For example, mutations in DI-DIII voltage sensors are likely to alter channel activation. As shown in this study, missense mutations at R850 and T767, located in DII S4 and S1 respectively, result in premature opening, a functional alteration in activation that is highly predicted to lead to hyperactivity. On the other hand, mutations in DIV voltage sensors usually disrupt channel inactivation. An Arg to Gln substitution at 1617 in DIV S4 exhibits a dramatically slower decay of the transient current, indicating impaired inactivation. This impairment is highlighted by a 2-fold increase of resurgent current, the mechanism of which involves an open channel block (Raman and Bean 2001, Grieco, Malhotra et al. 2005). Since the open channel block competes with the IFM (Ile-Phe-Met motif) inactivation gate for channel binding after activation (Khaliq, Gouwens et al. 2003, Grieco and Raman 2004), the slower inactivation kinetics of R1617Q and many other disease mutations (Jarecki, Piekarz et al. 2010) increase the probability of open channel block, and thus the generation of larger resurgent currents. The same applies to R850Q and R1617Q with impairment of inactivation. Both R850Q and R1617Q neutralize charged residues in S4 segments. While R1617Q may not induce gating pore currents due to its location at the extracellular extreme of the S4 segment, R850Q is predicted to induce gating pore current. However, because gating pore currents are very small and difficult to measure in mammalian expression systems, I were unable to directly determine if either of these mutations induced gating pore currents.

In addition to direct lesion to the molecular components responsible for specific channel function, mutations located in regions involved in intramolecular interactions can also cause predictable functional defects. The C-terminal domain (CTD) has been shown to interact with the IFM inactivation gate via static

interaction between charged residues (Shen, Zhou et al. 2017, Johnson, Potet et al. 2018). Removing any of the charges can disrupt the interaction and affect normal channel inactivation (Lee and Goldin 2008, Nguyen and Goldin 2010, Johnson, Potet et al. 2018). Indeed, I show that an Arg to Gln mutation at 1872, located near the center of CTD, displays abnormal inactivation properties, including shifted voltage dependence of inactivation, slower decay of transient current and higher level of persistent current. Similarly, Wagnon et al. (2016) demonstrated inactivation-related dysfunctions of two other epilepsy mutations at R1872 in mouse Nav1.6, highlighting the functional significance of the IFM-CTD interaction for channel inactivation.

The complicated network of sodium channel regulation is another source of heterogeneity for EIEE13. As shown in this study, the functional consequences of a single residue substitution can impact properties beyond what is predicted based on its location. For example, R850Q and T767I in the domain II voltage-sensor both impair inactivation and R1872Q in the CTD has premature activation. Most interestingly, R850Q, T767I and R1872Q demonstrate slowed resurgent kinetics that are not readily predicted by their location. These alterations may be consequences of the complex nature of subtle intramolecular interactions within the channel as well as intermolecular interactions between the channel and a great variety of regulatory proteins. So far, Nav-β subunits (Hull and Isom 2018), calmodulin, fibroblast growth factor homologous factors (FHFs) (Wang, Chung et al. 2012, Wang, Chung et al. 2014) and ankyrinG (ankG) (Shirahata, Iwasaki et al. 2006, Gasser, Ho et al. 2012) are identified as important interacting partners of Nav channels. They regulate Nav trafficking, expression pattern and gating in isoform- and cell type-specific manners (Deschênes, Neyroud et al. 2002, Herzog, Liu et al. 2003, Chichili, Xiao et al. 2013, Ben-Johny, Yang et al. 2014, Barbosa, Xiao et al. 2017, Yan, Wang et al. 2017). Mutations within or near the interacting interface on either protein can alter the interaction and cause channel dysregulation. Moreover, the wide range

of post-translational modifications of voltage-gated sodium channels (Pei, Pan et al. 2017).

Modifier genes also contribute to the heterogeneity of *SCN8A* epilepsy (Meisler, O'brien et al. 2010). This is implicated by the lack of clear genotype-phenotype correlation with recurrent mutations (Meisler, Helman et al. 2016). R850Q is one of the recurrent mutations that has been identified in at least three unrelated patients. They demonstrate considerable variation in clinical presentations, including age of onset, degree of developmental delay and motor deficit, and treatment response (Kong, Zhang et al. 2015, Wang, Gao et al. 2017). Similarly, Wagnon et al observed tremendous phenotypic heterogeneity in patients carrying the same mutations at 1617 and 1872 (Wagnon, Barker et al. 2016). Such heterogeneity is also common in other monogenic epilepsies (Meisler, Helman et al. 2016), indicating an undeniable role of genetic background in modifying the disease manifestation. Consistently, various monogenic mouse models for epilepsy presented strain-dependent phenotypic severity (Kearney, Buchner et al. 2002, Bergren, Chen et al. 2005, Frank, Mantegazza et al. 2006, Ogiwara, Miyamoto et al. 2007, Papale, Beyer et al. 2009, Mistry, Thompson et al. 2014). Follow-up studies on the genomic composition of these mouse strains identified a number of candidate modifier genes (Sprunger, Escayg et al. 1999, Bergren, Chen et al. 2005, Rusconi, Scalmani et al. 2007, Bergren, Rutter et al. 2009, Singh, Pappas et al. 2009). Interestingly, many of them encode ion channels that contribute to the control of the membrane excitability (Kearney, Yang et al. 2006, Glasscock, Qian et al. 2007, Hawkins, Martin et al. 2011, Calhoun, Hawkins et al. 2016, Hawkins, Zachwieja et al. 2016). This underscores the integrated nature of neuronal and network excitability. As a result, it is not surprising that mouse models combining epilepsy mutations in different ion channel genes can either alleviate (Glasscock, Qian et al. 2007, Martin, Tang et al. 2007, Hawkins, Martin et al. 2011) or aggregate (Kearney, Yang et al. 2006) the phenotypes observed in their

monogenetic counterparts. As pointed out by Klassen et al, it is the combinatorial impact of genetic variants in ion channel genes that determines the potential or the lack of potential for homeostatic compensation of membrane excitability and thus for clinical expression (Klassen, Davis et al. 2011). Therefore, personalized medicine, where genetic background is taken into consideration, is highly desirable in order to achieve accurate diagnosis, prediction and treatment planning for excitability disorders like epilepsy in the clinical setting.

Due to the vast number of epilepsy mutations and the remarkable complexity of sodium channel regulation, it may be impractical to extend functional assays to all combinations of mutations and genetic variants appearing in patients. Computational simulation can be of great value in this matter. In my study, I performed excitability simulations using two neuron models and show predictions of the outcome of allelic epilepsy mutations. To model sodium channel kinetics, I adapted a simple Markov state model that included the open channel block mechanism (Khaliq, Gouwens et al. 2003). This feature enables the simulation of resurgent sodium currents. Extensive evidence has showed that physiological resurgent currents support high-frequency repetitive firing of action potentials by maintaining a relatively constant availability of sodium channels (Raman and Bean 2001). Pathological alterations of resurgent current kinetics are involved in a wide range of excitability disorders (Jarecki, Piekarz et al. 2010, Hargus, Merrick et al. 2011, Sittl, Lampert et al. 2012, Hargus, Nigam et al. 2013, Tan, Piekarz et al. 2014, Patel, Barbosa et al. 2016, Xiao, Barbosa et al. 2019). More importantly, I revealed enhanced resurgent current as a commonality among the four Nav1.6 epilepsy mutations in my study. Therefore, abnormal resurgent currents found in epilepsy mutant Nav1.6 are likely to contribute to neuronal hyperexcitability. Indeed, my simulations demonstrated a cell type- and frequency- dependent role of resurgent current in heightening excitability, which in turn can lead to uncontrolled, synchronized firing involved in seizure activity.

The computational simulations I performed can be expanded to accommodate variants in multiple ion channel genes to predict the integrated effect on neuronal as well as network excitability (Klassen, Davis et al. 2011). However, such simulations are not without limitations. The original sodium channel model (Khaliq, Gouwens et al. 2003) couples the voltage dependence of inactivation with activation, which does not necessarily reflect the complex behaviors of a voltage-gated sodium channel. As illustrated by the R1872Q mutant channel, where the voltage-dependence of activation and inactivation are shifted in opposite directions. Such channel behavior is impossible to be represented by a model constrained by activation-inactivation coupling. Therefore, I partially segregated the coupling to closely mimic channel behaviors observed in my experiments. The modified model allowed us to accurately simulate the opposite direction shifts in R1872Q, and the depolarizing shifts of activation in R850Q and T767I without immensely affecting the voltage dependence of inactivation. Nonetheless, I were not able to satisfactorily achieve all functional alterations observed in R1617Q. The inability to completely mirror R1617Q channel behavior may account for the mild increase of excitability observed in the R1617Q simulation. Therefore, there is a clear need for improved channel models to accurately capture the dynamics of ionic flows in excitable cells in order to produce reliable excitability prediction and assist in individualized medicine.

Taken together, my study demonstrates that while many epilepsy-related *SCN8A* mutations are gain-of-function, they can impact multiple gating properties in distinct combinations. One commonality among them is an alteration in resurgent current, which can play a critical role in determining neuronal excitability and thus seizure activity in patients. I demonstrated that computational simulation is a useful tool to explore the influence of mutations on excitability. Using the human Nav1.6 channel, my data also indicates that the *SCN8A* mutations can exhibit subtle yet potentially important differences in their

biophysical consequences in human versus rodent channels. These important distinctions could influence how specific mutations are targeted therapeutically.

V. S-PALMITOYLATION MODULATES NAV1.6 WITH EPILEPSY MUTATION

A. Overview

In Chapter III, I showed that the S-palmitoylation of the voltage-gated sodium channel isoform Nav1.6 regulates distinct functions of the channel by modifying different residues in the channel. Therefore, I hypothesized that S-palmitoylation can be exploited to modulate Nav1.6 activities in diseased conditions.

A previous study of Nav1.5 suggests that loss of S-palmitoylation due to the mutation C981F in the cardiac sodium channel may be responsible cardiac arrhythmia in human patients (Pei, Xiao et al. 2016). A potentially pathogenic arginine to cysteine mutation (p.Arg662Cys) in Nav1.6 was identified in an epilepsy patient (Carvill, Heavin et al. 2013), but no functional characterization has been reported. Importantly, a cysteine at this position in Nav1.6 was predicted to be a S-palmitoylation site in CSS-Palm. Therefore, I hypothesized that the R662C mutation in Nav1.6 introduced a S-palmitoylation site in the channel and caused Nav1.6 hyperactivity that lead to epilepsy in the patient, and thus can be rescued by blocking S-palmitoylation at this residue.

For disease mutations that do not directly introduce or remove a S-palmitoylation site in the Nav1.6 channel, S-palmitoylation can also be used to modulate Nav1.6 activity to counteract the abnormal channel. After all, disease mutations may indirectly alter channel maturation, trafficking and functional properties even though they do not introduce or remove a S-palmitoylation site in the channel. The S-palmitoylation status of a protein can be influenced by protein secondary structure, protein-protein interaction, interplays between different post-translational interactions (Tian, Jeffries et al. 2008, Ho, Selvakumar et al. 2011, Shipston 2014, Pei, Pan et al. 2017, Summers, Milbrandt et al. 2018, Woolfrey, O'Leary et al. 2018). Conversely, altering S-palmitoylation status of specific sites

offers an opportunity to attenuate abnormal Nav1.6 activity imposed by disease mutations. Additionally, in Chapter IV, I showed that the epilepsy-associated mutation R1872Q introduces multiple gain-of-function abnormality in the Nav1.6 channel, including increased current amplitude, negative shift of voltage dependence of activation, positive shift of voltage dependence of inactivation, and slowed decay of transient current and resurgent current. Among these altered properties, current amplitude and voltage dependence of inactivation can be specifically targeted by altering the S-palmitoylation status of the Nav1.6 channel. Thus, I hypothesized that the aberrant current amplitude and voltage dependence of inactivation in R1872Q can be rescued by S-palmitoylation status manipulation.

B. R660C does not alter Nav1.6 functions or sensitivity to S-palmitoylation manipulation.

As shown in Fig.26, the R660C mutation in Nav1.6 did not display aberrant current density, voltage dependence or recovery from inactivation. Thus, this might be a non-pathogenic variant. Moreover, the response pattern of the R660C mutant channel to 2BP and PA treatments was identical to that of the WT channel, suggesting that it did not have altered sensitivity to S-palmitoylation manipulation. Therefore, the introduction of potential S-palmitoylation might not be S-palmitoylated in our heterologous system.

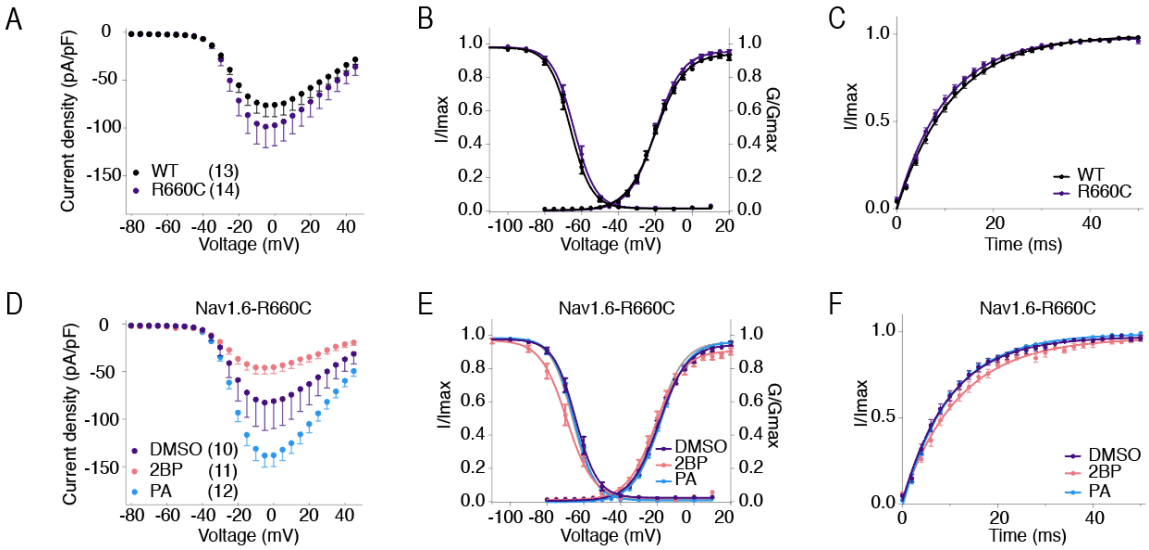

Figure 26. Characterization of Nav1.6 variant R660C and it is sensitivity to 2BP and PA treatment.

(A,D) Current density-voltage plots of WT and R660C. (B,E) Voltage dependence of activation and steady-state inactivation curves fitted with Boltzmann functions. (C,F) Recovery from inactivation with recovery duration from 0 to 50ms.

C. Aberrant R1872Q activity are partially rescued by S-palmitoylation.

Fig.27 shows that blocking S-palmitoylation with 2BP treatment reversed the increased current and depolarized voltage dependence of inactivation caused by the R1872Q mutation. On the other hand, the response pattern of other functional properties, normal or aberrant compared to the WT channel, remained identical to the WT channel. These suggested that S-palmitoylation can be used to rescue disrupted Nav1.6 by targeting specific channel functions.

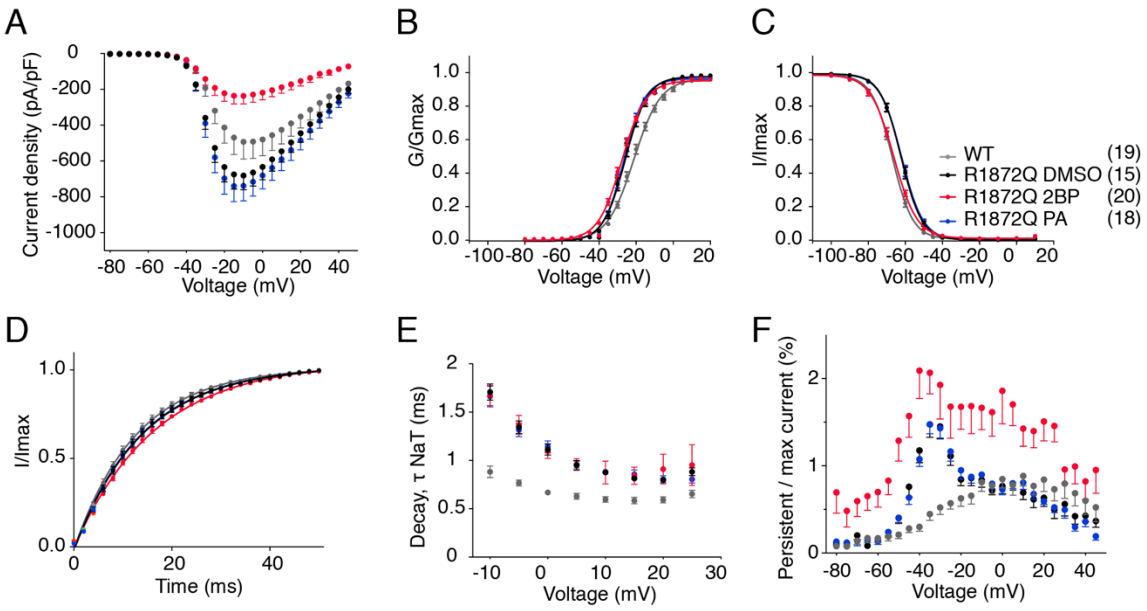

Figure 27. Partial rescue of R1872Q by S-palmitoylation.

(A) Current density-voltage plot of hNav1.6 WT and R1872Q. (B,C) Voltage dependence of activation and steady-state inactivation curves fitted with Boltzmann functions. (D) Recovery from inactivation with recovery time duration from 0 to 50ms. (E) Rate of decay for transient sodium current (τ_{NaT}) at each depolarization voltages. (F) Percent persistent current-voltage plot with persistent current measured during the last 1ms of the 50ms activation protocol.

D. Discussion

Here I characterized the functional properties of an epilepsy-associated mutation R662C in Nav1.6. No appreciable functional alteration has been identified in the mutant channel. There are several possibilities. First of all, the R662C mutation may not be pathogenic. The seizure phenotype observed in the patient can be caused by other pathogenic factors. Secondly, the functional alteration brought by the R662C mutation may not be presented in a cell line. After all, functional characterization in a cell line with very different cellular properties may not faithfully replicate the aberrant behavior of a mutant channel in its original environment. As discussed in Chapter III, S-palmitoylation can not only directly affect ion channel function by shifting conformation, it can also indirectly modulate protein-protein interaction and protein life cycle in a cell-type specific manner. The cell line I used for Nav1.6 expression may lack the functional components that is critical for the presentation of the abnormality caused by the mutation. Additionally, as discusses in Chapter IV, epilepsy is a complex disease and can involve predisposition from modifying genes. The patient carrying the R662C mutation may have unidentified genetic variation that increases seizure susceptibility.

The R662C mutation also does not exhibit any change of sensitivity to S-palmitoylation manipulation. It is possible that the introduced cysteine is not modified by S-palmitoylation. It is also possible that the expression system I used did not have the specific subset of PATs that targets R662C for S-palmitoylation. Therefore, this mutation may result in abnormal S-palmitoylation in particular neuronal cell types with the specific PAT set and cause neuronal over-excitation.

Using the epilepsy-associated mutation R1872Q, I demonstrated that the aberrant increased of Nav1.6 current and positive shift of voltage dependence of inactivation are rescued by blocking S-palmitoylation with 2BP treatment, while

no other channel properties are modified. Therefore, this feature of functional specificity of S-palmitoylation can be advantageous for therapeutic development when targeting a particular property of the channel is desirable.

VI. CONCLUSIONS

A. Summary of findings

1. Nav1.6 S-palmitoylation regulates channel activity and neuronal excitability.

Nav1.6 has powerful control over neuronal excitability in CNS and PNS. Its functions are tightly regulated at multiple levels by an intricate network of molecular mechanisms. In this dissertation, I present the discovery of S-palmitoylation as a novel regulatory mechanism for Nav1.6. S-Palmitoylation is a reversible post-translational lipid modification that dynamically regulates protein functions. Voltage-gated sodium channels subjected to S-palmitoylation can exhibit altered functions in different S-palmitoylation states. I demonstrated that Nav1.6 is chemically modified and functionally regulated by S-palmitoylation. Three S-palmitoylation sites (C1169, C1170, C1978) were identified. They differentially modulate distinct Nav1.6 properties. Interestingly, C1978 is exclusive to Nav1.6 among all Nav isoforms and it is evolutionally conserved in Nav1.6 among most species. It regulates current amplitude uniquely in Nav1.6. Furthermore, I showed that eliminating S-palmitoylation at specific sites altered Nav1.6-mediated excitability in dorsal root ganglion neurons. Therefore, this study reveals S-palmitoylation as a potential isoform-specific mechanism to modulate Nav activity and neuronal excitability in physiological and diseased conditions.

2. Epilepsy-associated mutations in Nav1.6 increase channel activity and are predicted to enhanced neuronal excitability.

SCN8A, the gene that encodes Nav1.6, is a novel causal gene for early infantile epileptic encephalopathy. A rapidly growing number of *SCN8A* mutations have been associated with EIEE since the first discovery in 2012. It is well accepted that gain-of-function mutations in *SCN8A* underlie the disorder, but the

remarkable heterogeneity of its clinical presentation and poor treatment response demand for better understanding of the disease mechanisms. Here, I characterize a new epilepsy-related *SCN8A* mutation, R850Q, in human Nav1.6. I show that it is a gain-of-function mutation, with a hyperpolarizing shift in voltage dependence of activation, a 2-fold increase of persistent current and a slowed decay of resurgent current. I systematically compare its biophysics with three other *SCN8A* epilepsy mutations, T767I, R1617Q and R1872Q, in the human Nav1.6 channel. Although all of these mutations are gain-of-function, the mutations affect different aspects of channel properties. One commonality I discovered is an alteration of resurgent current kinetics, but the mechanisms by which resurgent currents are augmented is not yet clear for all of the mutations. Computational simulations predict increased excitability of neurons carrying these mutations with differential enhancement by open channel block.

3. Aberrant epilepsy-associated mutant Nav1.6 can be partially rescued by S-palmitoylation.

Malfunction of S-palmitoylated neuronal proteins have been shown to be involved in various neurological and psychiatric disorders. Although I did not observe any S-palmitoylation related changes in the epilepsy associated mutation R662C in Nav1.6, the function modulating effect of S-palmitoylation on Nav1.6 can be exploited to alleviate aberrant neuronal activity in diseased conditions. An example is demonstrated by the R1872Q epilepsy mutation, the abnormally increased current and positively shifted voltage dependence of inactivation is rescued by blocking S-palmitoylation. More importantly, S-palmitoylation is controlled by the two enzyme families that catalyze the S-palmitoylation reaction and the reversible process depalmitoylation. Both of them are large enzyme families that display distinct but overlapping substrate preference as well as distribution in different tissue, cell type, and subcellular

compartment. Therefore, these proteins may serve as drugable targets for a wider range of excitability disorders.

B. Benefits and limitations of experimental design

1. Use of the ND7/23 cell line as a model system to study VGSCs

The ND7/23 cell line is used as a non-neuronal model system for all the electrophysiological characterization of VGSCs in this dissertation. Similar to the HEK cell line, the ND7/23 cells are small and have cell morphology that allows for excellent voltage control over the entire cell, minimizing voltage clamp error, and resulting in more precise measurement of sodium currents. Although the HEK cell line is a more commonly used model system for ion channel characterization, Nav1.6 has proven to be one of the most difficult channels to be expressed in the HEK cells. Transient transfection of Nav1.6 in HEK cells results in the majority of the channels stuck in intracellular compartments (ER and / or Golgi), and resultant Nav1.6 current, if any, is too small for accurate measurement and analysis. On the other hand, the use of ND7/23 cell line help boost the surface expression of the Nav1.6 and make electrophysiological characterization possible. Since ND7/23 is a hybrid cell line transformed from rat DRG neuron and mouse neuroblastoma cells and considered a neuronal cell line, it might have preserved some neuronal components that facilitate Nav1.6 folding and trafficking to the surface. However, the use of a neuronal cell line is not without limitation. For one thing, it is unclear what the exact components are responsible for the enhanced expression of the Nav1.6 channel. It is also unknown whether these components have modulating effects on other properties of the channel or whether they directly respond to experimental manipulations. Therefore, the use of ND7/23 cell line may confound the interpretation of experimental results. For another, the ND7/23 cell line express significant TTX-sensitive voltage-gated sodium currents, among which Nav1.7, Nav1.6 and

Nav1.3 are estimated to be responsible for 65%, 20% and 2% of the current, respectively (Rogers, Zidar et al. 2016, Lee, Kim et al. 2019). Therefore, in order to study TTX-sensitive sodium current in the ND7/23 cell line, the channel of interest is rendered TTX-resistant by single amino acid substitution (Nav1.6-Y371S, Nav1.2-F385S) before expression and TTX must be included in the extracellular solution for the isolation of current from the transfected channel. Additionally, although the probability is unknown, it is possible that the endogenous channel would affect the biophysics of the transfected channel by forming dimers (Clatot, Hoshi et al. 2017). Collectively, the use of the ND7/23 cell line provides the benefits of a reduced system for the electrophysiological characterization of the hard-to-express Nav1.6.

2. Use of cultured dorsal root ganglion neuron as a model system to study Nav1.6 and excitability

Cultured dorsal root ganglion (DRG) neurons were used to further validate the findings in ND7/23 cells. The use of DRG neurons was specifically advantageous for addressing the question posed in this dissertation due to the ease of transient transfection and high expression level of Nav1.6. The need for transient transfection of Nav1.6 and its S-palmitoylation deficient variants is imposed by the fact that pharmacological treatments (2BP and PA) affect global S-palmitoylation of a wide range of neuronal proteins, and thus it is impossible to isolate the effect of altering Nav1.6 S-palmitoylation. Moreover, the vast majority of cultured CNS neurons, are either too immature to support sufficient level of Nav1.6 expression (as Nav1.6 is an adult brain isoform that starts its expression relatively late in development) or too difficult to be transfected. However, one limitation of using DRG neurons as the neuronal model system is that they express a combination of endogenous TTX-sensitive (Nav1.6, Nav1.7) and TTX-resistant (mainly Nav1.8) sodium currents (Rush, Cummins et al. 2007). To isolate transfected TTX-resistant Nav1.6 current, the endogenous TTX-resistant

Nav1.8 is knocked down with shRNA. This method results in reduced neuronal excitability: the majority of the DRG neuron only fire one action potential without Nav1.8, because Nav1.8 is the major contributor to action potential upstroke and repetitive firing in DRG neurons (Rush, Cummins et al. 2007). Although Nav1.6 support high frequency, repetitive firing in a wide range of CNS neurons (Maurice, Tkatch et al. 2001, Khaliq, Gouwens et al. 2003, Do and Bean 2004, Van Wart and Matthews 2006, Enomoto, Han et al. 2007, Mercer, Chan et al. 2007, Royeck, Horstmann et al. 2008, Osorio, Cathala et al. 2010), the cellular background of DRG neurons, including the subset of K+ channels, the leaky membrane property, the post-translational modifications and the Nav1.6 interacting proteins, may limit the ability of this channel to generate multiple action potentials. Moreover, although this method provides a clear picture of the role of S-palmitoylation in modulating Nav1.6-mediated neuronal excitability, it does not reflect the firing behavior of DRG neuron *in vivo*. It would be interesting to observe the excitability outcome of Nav1.6 S-palmitoylation with endogenous Nav1.8 intact. Moreover, although Nav1.6 contributes to DRG neuron firing, it has a more prominent role in CNS neurons. The consequence of Nav1.6 S-palmitoylation or the lose of it can be very different in CNS cell types.

3. Use of iCell GlutaNeuron as a model system to study Nav1.6 and excitability

Although Nav1.6 is ubiquitously expressed in both CNS and PNS, it plays a more dominating role in glutamatergic neurons in the central nervous system. It is natural to examine the influence of Nav1.6 modulation in glutamatergic neurons. However, due to the technical difficulty of transient transfection in CNS neurons and the global effect of S-palmitoylation pharmacological treatments (2BP and PA), the iCell GlutaNeuron (Cellular Dynamics International) was used to circumvent these limitations and explore the effects of Nav1.6 S-palmitoylation on neuronal excitability. The iCell GlutaNeuron is a highly pure population of human glutamatergic neurons derived from iPSCs. They can also be particularly

useful for genetic editing experiments as well as for the development of personalized medicine and pharmacological screening for genetic diseases. Unfortunately, the transient transfection of these iCell GlutaNeurons does not result in sufficient Nav1.6 expression for excitability examination: only 40% of the transfected cells are able to fire action potential. The low expression level of Nav1.6 might be due to the lack of appropriate machineries, for example the key PATs for Nav1.6 S-palmitoylation, for optimal Nav1.6 expression in these immature neurons, as with the case of primary embryonic neuronal cultures. It is also possible that the transfection method used is not ideal for ion channel expression in iCell GlutaNeurons.

4. Use of acyl-biotin exchange assay for S-palmitoylation detection

The classic method for S-palmitoylation detection involves metabolic labelling with radioactive [^{3}H]-palmitate followed by fluorography (Schlesinger, Magee et al. 1980, Peseckis, Deichaite et al. 1993). This assay, although being useful, suffers from the hazards of radioactivity, low sensitivity, and lengthy exposure time ranging from days to months. The development of acyl-biotin exchange (ABE) assay enables safe, sensitive and efficient detection of protein S-palmitoylation. More importantly, the ABE assay also detect protein S-palmitoylation in their native environment without the requirement for culture as required by metabolic labelling, although *in vivo* labeling for click chemistry has been demonstrated with reporters for glycan (Baskin, Prescher et al. 2007, Chang, Prescher et al. 2010), the development of *in vivo* labeling methods specifically for protein S-palmitoylation or any other lipid modification still awaits (Gao and Hannoush 2018).

The ABE assay has some limitations. The assay requires complete blockage of free thiols as the first step to avoid false positive S-palmitoylation signal, which depends on the accessibility to the thiols in the denatured protein.

Moreover, the ABE assay cannot differentiate the identity of the lipid modification (chain length and saturation). Additionally, since the ABE assay detect S-palmitoylation through the detection of thioester bond, this assay can result in false positive hits on proteins that use, even just transiently, thioester bonds for biochemistries other than S-palmitoylation (Roth, Wan et al. 2006). The possibility of a false positive signal can be easily eliminated by global S-palmitoylation blockage or enhancement with treatments like 2BP and PA, in response to which the false positive signal would remain unchanged.

5. Use of human channel for electrophysiological characterization

EIEE cases with Nav1.6 mutations are highly heterogeneous, displaying variable clinical presentation and treatment response. The disease mechanism is not well understood and requires functional characterization of a wide range of Nav1.6 mutations for more individualized therapeutic development. However, the majority of previous functional analysis of Nav1.6 mutations were conducted with the mouse cDNA construct. Although these results have provided valuable insights for the molecular underpinnings of the disease, the alterations of channel functions they presented may differ from the same mutations in human DNA. In this dissertation, I used a human Nav1.6 cDNA construct (hNav1.6) for functional characterization and systematically compare the outcomes with those from previous studies using the mouse construct. I observed consistent functional changes for the mutation R1872Q, but important functional differences for mutations T767I and R1617Q in the human compared to the mouse channel background. Such differences may seem subtle, but they suggest molecular and functional distinctions between the human and mouse channels, which in turn could alter how individual mutations impact intrinsic neuronal excitability and even affect their pharmacological responsiveness, and thus could have important impact when it comes to therapeutic development and testing.

6. Use of computational modeling for excitability prediction

Due to the vast number of epilepsy mutations (in Nav1.6 as well as Nav1.1 and Nav1.2) and the remarkable complexity of sodium channel regulation, it may be impractical to extend functional assays to all combinations of mutations and genetic variants appearing in patients. Computational simulation can be of great value in this matter. In my study, I adapted a simple Markov state model (Khaliq, Gouwens et al. 2003) to model sodium current and modified the parameters to reflect biophysical alterations incurred by mutations observed in experimental recordings. The model sodium current was then incorporated into different model neurons for excitability simulations to predict the outcome of allelic mutations. Such computational simulations is well suited for pathogenicity prediction for complex diseases like epilepsy, because the modeling can be expanded to accommodate variants in multiple ion channel genes to predict the integrated effect on neuronal as well as network excitability (Klassen, Davis et al. 2011).

However, such simulations are not without limitations. The original sodium channel model (Khaliq, Gouwens et al. 2003) couples the voltage dependence of inactivation with activation, which does not necessarily reflect the complex behaviors of a voltage-gated sodium channel, and renders some channel behaviors impossible to be represented by a model with an activation-inactivation coupling constrain. Therefore, there is a clear need for improved channel models to accurately capture the dynamics of ionic flows in excitable cells in order to produce reliable excitability prediction and assist in individualized medicine. Additionally, although the multi-compartment model of cortical pyramidal neuron I used implemented differential distribution of Nav1.2 and Nav1.6 in the soma, the AIS, the nodes of Ranvier, and the dendrites, the functional properties of these two channels are uniformed across different compartments. This might not be the case for an actual neuron. An Nav isoform can be differentially regulated by post-

translational modification and protein-protein interaction in distinct neuronal compartments. It is possible that an Nav isoform can demonstrate variation of functional properties and support the generation of action potentials in different ways. Thus, the use of uniformed parameters for an ion channel across multiple compartments can be convenient and useful for simulation, but may not be accurate.

C. Future directions

This dissertation identifies a S-palmitoylation as a novel regulatory mechanism for Nav1.6 with isoform- and site-specificity. This unravels a new research avenue for the modulation of Nav1.6 activity and neuronal excitability, as well as for VGSC targeting with isoform specificity.

I identified a S-palmitoylation site that is unique to and evolutionally conserved in Nav1.6. It would be particularly interesting to elucidate the physiological function of this S-palmitoylation site. For example, the phenotypic consequences of loss of S-palmitoylation at this site can be examined in animal models with knockout strategies.

Although I identified two S-palmitoylation sites that differentially regulate Nav1.6 properties, additional site(s) may exist and contribute to channel modulation. It is worth to note that I observed residual effects of 2BP treatment when all the identified S-palmitoylation sites were removed from the channel (Fig.12FGH), suggesting the existence of additional S-palmitoylation site(s) that participate in channel regulation. It is also possible that the channel regulations involve S-palmitoylation of an Nav1.6 interacting protein. Moreover, the molecular components for channel recovery from inactivation, which has not yet been identified, might also be affected by a S-palmitoylation site, based on my data showing slower recovery time constant when S-palmitoylation is blocked by

2BP treatment. Further experiments are needed to test whether extra S-palmitoylation site(s) exist in the channel. Experimental approaches combining acyl-biotin exchange and mass spectrometry (Collins, Woodley et al. 2017, Edmonds, Geary et al. 2017) might be useful for this purpose.

It is also critical to identify the palmitoylating and depalmitoylating enzymes that are responsible for Nav1.6 modification, because they can be the potential targets for the development of cell type and isoform specific drugs. Moreover, it is possible that the difficulty of heterologous expression of Nav1.6 in the HEK cell line is due to the lack of appropriate zDHHC-PAT that is essential for Nav1.6 correct folding and subsequent targeting to the plasma membrane. A comparison of the PAT repertoire between the HEK and ND7/23 cell lines may reveal the enzymes responsible for Nav1.6 S-palmitoylation. This can be achieved by profiling the endogenous expression of all 23 human zDHHC-PATs at the mRNA level in HEK and ND7/23 cells respectively using quantitative real time PCR (qRT-PCR), and further confirm the expression at protein level by probing the zDHHC-PATs with western blotting or immunocytochemistry if the target zDHHC-PAT antibodies are available. One study has showed that the HEK cell line they use has the highest expression level of zDHHC4, with the other zDHHCs expressed at the level of 5% - 20% of zDHHC4 (Tian, McClafferty et al. 2010). Additionally, Tian et al. demonstrated a systematic though laborious method to identify candidate zDHHC-PATs that are responsible for the S-palmitoylation of the target protein. They combine small interfering RNA (siRNA) knockdown and cDNA overexpression of the 23 zDHHC-PATs individually in the HEK cells and observe subcellular localization of the fluorescent tagged target protein as the experimental output to indicate S-palmitoylation. However, this approach can result in false positive hits due to the nature of over-expression experiments and may only be useful for identifying putative zDHHC-PATs for the reaction.

Regarding the regulation of VGSC S-palmitoylation, further questions include what triggers S-palmitoylation and depalmitoylation at different modification sites in the channel and whether they are constituent or dynamic. This can be achieved by examining the rate of S-palmitoylation turnover on the channel. Kang et al. (Kang, Wan et al. 2008) demonstrated in cultured neurons that proteins that undergo rapid S-palmitoylation cycling, like PSD95, Cdc42, H/N-Ras and Rho-B, display loss of S-palmitoylation signal in the ABE assay after a 5h 2BP blockage. In contrast, S-palmitoylation on Snap25, synaptotagmin 1, Scamp1 and the glutamate transporter EAA1 (Slc1a3), are relatively stable, without showing significant changes of S-palmitoylation signal in the presence of 2BP. However, this method may not be applicable to proteins with multiple S-palmitoylation sites that are differentially regulated. It may also not work in transient expression system due to the tricky timing for target protein expression, S-palmitoylation and the start of 2BP treatment. Understanding S-palmitoylation turnover on the channel can be informing for elucidating the physiological and pathological roles of VGSC S-palmitoylation.

Many neuronal proteins demonstrate activity-dependent shifts of S-palmitoylation status (Hayashi, Rumbaugh et al. 2005, Kang, Wan et al. 2008). It is reasonable to speculate that protein S-palmitoylation level is altered in excitability disorders. Indeed, a broad range of neuronal proteins, including PSD-95, Cyt1, and GlutA1, display enhanced S-palmitoylation in the kainic-acid-induced seizure mouse model (Kang, Wan et al. 2008). Paradoxically, the knock-in mice with S-palmitoylation deficient GluA1 display increased susceptibility to PTZ-induced seizures (Itoh, Yamashita et al. 2018, Itoh, Okuno et al. 2019). Thus, altered S-palmitoylation status of particular proteins can result in abnormal neural excitation, although the cause-and-effect relationship still awaits to be elucidated. Another study finds increased zDHHC8 level in the brains of temporal lobe epilepsy patients (Yang, Zheng et al. 2018), further supporting a role of protein S-palmitoylation in seizure-related conditions. Since Nav1.6 has been

implicated in many neurological diseases and its activity is regulated by S-palmitoylation, it would be interesting to examine whether Nav1.6 S-palmitoylation status is altered in neurological diseases and how this alteration contributes to disease pathologies.

Due to the low expression level of Nav1.6 and insufficient sensitivity of the antibodies that detect the channel, I were not able to directly observe and quantify Nav1.6 on the cell surface and discern quantitative changes in response to S-palmitoylation manipulation. Future experiments are needed to validate my hypothesis that S-palmitoylation of Nav1.6 enhance its membrane targeting. Also, it would be interesting to further dissect the specific role of S-palmitoylation in Nav1.6 trafficking. For one thing, S-palmitoylation can affect multiple stages of ion channel life cycle, from assembly and surface targeting, to internalization and degradation (Shipston 2014). The increased Nav1.6 current in response to PA treatment can result from reduced ER and / or Golgi retention, increased protein stability at the plasma membrane, and / or reduced internalization of the channel. For another, S-palmitoylation of distinct residues of Nav1.6 can serve to differentially target the channel to specialized neuronal compartments like the axon initial segment (AIS), the nodes of Ranvier and dendritic arborization. The AIS organizer AnkG is S-palmitoylated at the C70 residue and this modification is necessary for its localization to the AIS (He, Jenkins et al. 2012). It is not clear whether S-palmitoylation of Nav1.6 affects its interaction with AnkG and further influences its targeting to and stabilization at the AIS. It is tempting speculate that S-palmitoylation is a key regulator of the AIS organization. The post-synaptic density has presented an intriguing case of activity-dependent, rapid (re)organization facilitated by S-palmitoylation, involving the modification of glutamate receptors, AMPA and NMDA (Hayashi, Rumbaugh et al. 2005, Hayashi, Thomas et al. 2009), as well as scaffolding proteins, PSD-95 and AKAP150 (El-Husseini, Schnell et al. 2002, Purkey, Woolfrey et al. 2018). Although the AIS is considered a more stable neuronal structure compared to the

post-synaptic density, AIS is also plastic and changes in length and in position in response to neuronal activity and disease (Grubb and Burrone 2010, Kuba, Oichi et al. 2010, Kaphzan, Buffington et al. 2011, Baalman, Cotton et al. 2013, Hinman, Rasband et al. 2013). However, it is not clear whether such plasticity involves altered S-palmitoylation status of AIS proteins. It is possible that S-palmitoylation can be an important mechanism not only for the initial targeting, and subsequent retention and stabilization of proteins at the AIS, but also for AIS plasticity via dynamic cycling of S-palmitoylation on AIS proteins. In this way, S-palmitoylation can regulate intrinsic neuronal excitability by dynamically modulating AIS proteins. On the other hand, S-palmitoylation at the nodes of Ranvier is predicted to be more static due to the requirement for reliable and regenerative AP propagation down the axon.

VII. REFERENCES

Abriel, H., E. Kamynina, J.-D. Horisberger and O. Staub (2000). "Regulation of the cardiac voltage-gated Na+ channel (H1) by the ubiquitin-protein ligase Nedd4." FEBS letters 466(2-3): 377-380.

Akimzhanov, A. M. and D. Boehning (2015). "Rapid and transient palmitoylation of the tyrosine kinase Lck mediates Fas signaling." Proceedings of the National Academy of Sciences 112(38): 11876-11880.

Allinson, T. M., E. T. Parkin, A. J. Turner and N. M. Hooper (2003). "ADAMs family members as amyloid precursor protein α-secretases." Journal of neuroscience research 74(3): 342-352.

Ashpole, N. M., A. W. Herren, K. S. Ginsburg, J. D. Brogan, D. E. Johnson, T. R. Cummins, D. M. Bers and A. Hudmon (2012). "Ca2+/calmodulin-dependent protein kinase II (CaMKII) regulates cardiac sodium channel NaV1. 5 gating by multiple phosphorylation sites." Journal of Biological Chemistry 287(24): 19856-19869.

Baalman, K. L., R. J. Cotton, S. N. Rasband and M. N. Rasband (2013). "Blast wave exposure impairs memory and decreases axon initial segment length." Journal of neurotrauma 30(9): 741-751.

Bachovchin, D. A., T. Ji, W. Li, G. M. Simon, J. L. Blankman, A. Adibekian, H. Hoover, S. Niessen and B. F. Cravatt (2010). "Superfamily-wide portrait of serine hydrolase inhibition achieved by library-versus-library screening." Proceedings of the National Academy of Sciences 107(49): 20941-20946.

Baek, J.-H., M. Rubinstein, T. Scheuer and J. S. Trimmer (2014). "Reciprocal changes in phosphorylation and methylation of mammalian brain sodium channels in response to seizures." Journal of Biological Chemistry 289(22): 15363-15373.

Bagal, S. K., B. E. Marron, R. M. Owen, R. I. Storer and N. A. Swain (2015). "Voltage gated sodium channels as drug discovery targets." Channels 9(6): 360-366.

Bailey, M. H., C. Tokheim, E. Porta-Pardo, S. Sengupta, D. Bertrand, A. Weerasinghe, A. Colaprico, M. C. Wendl, J. Kim and B. Reardon (2018). "Comprehensive characterization of cancer driver genes and mutations." Cell 173(2): 371-385. e318.

Bant, J. S. and I. M. Raman (2010). "Control of transient, resurgent, and persistent current by open-channel block by Na channel {beta}4 in cultured cerebellar granule neurons." Proc Natl Acad Sci U S A.

Barbosa, C., Z.-Y. Tan, R. Wang, W. Xie, J. A. Strong, R. R. Patel, M. R. Vasko, J.-M. Zhang and T. R. Cummins (2015). "Navβ4 regulates fast resurgent sodium currents and excitability in sensory neurons." Molecular pain 11(1): 60.

Barbosa, C., Z. Y. Tan, R. Wang, W. Xie, J. A. Strong, R. R. Patel, M. R. Vasko, J. M. Zhang and T. R. Cummins (2015). "Navbeta4 regulates fast resurgent sodium currents and excitability in sensory neurons." Mol Pain 11: 60.

Barbosa, C., Y. Xiao, A. J. Johnson, W. Xie, J. A. Strong, J.-M. Zhang and T. R. Cummins (2017). "FHF2 isoforms differentially regulate Nav1. 6-mediated resurgent sodium currents in dorsal root ganglion neurons." Pflügers Archiv-European Journal of Physiology 469(2): 195-212.

Baskin, J. M., J. A. Prescher, S. T. Laughlin, N. J. Agard, P. V. Chang, I. A. Miller, A. Lo, J. A. Codelli and C. R. Bertozzi (2007). "Copper-free click chemistry for dynamic in vivo imaging." Proceedings of the National Academy of Sciences 104(43): 16793-16797.

Beltran-Alvarez, P., A. Espejo, R. Schmauder, C. Beltran, R. Mrowka, T. Linke, M. Batlle, F. Pérez-Villa, G. J. Pérez and F. S. Scornik (2013). "Protein arginine methyl transferases-3 and-5 increase cell surface expression of cardiac sodium channel." FEBS letters 587(19): 3159-3165.

Beltran-Alvarez, P., F. Feixas, S. Osuna, R. Díaz-Hernández, R. Brugada and S. Pagans (2015). "Interplay between R513 methylation and S516 phosphorylation of the cardiac voltage-gated sodium channel." Amino acids 47(2): 429-434.

Beltran-Alvarez, P., S. Pagans and R. Brugada (2011). "The cardiac sodium channel is post-translationally modified by arginine methylation." Journal of proteome research 10(8): 3712-3719.

Beltran-Alvarez, P., A. Tarradas, C. Chiva, A. Pérez-Serra, M. Batlle, F. Pérez-Villa, U. Schulte, E. Sabidó, R. Brugada and S. Pagans (2014). "Identification of N-terminal protein acetylation and arginine methylation of the voltage-gated sodium channel in end-stage heart failure human heart." Journal of molecular and cellular cardiology 76: 126-129.

Ben-Johny, M., P. S. Yang, J. Niu, W. Yang, R. Joshi-Mukherjee and D. T. Yue (2014). "Conservation of Ca2+/calmodulin regulation across Na and Ca2+ channels." Cell 157(7): 1657-1670.

Ben-Shalom, R., C. M. Keeshen, K. N. Berrios, J. Y. An, S. J. Sanders and K. J. Bender (2017). "Opposing effects on NaV1. 2 function underlie differences between SCN2A variants observed in individuals with autism spectrum disorder or infantile seizures." Biological psychiatry 82(3): 224-232.

Bendahhou, S., T. R. Cummins, J. F. Potts, J. Tong and W. S. Agnew (1995). "Serine-1321-independent regulation of the mu 1 adult skeletal muscle Na+ channel by protein kinase C." Proceedings of the National Academy of Sciences 92(26): 12003-12007.

Benjannet, S., A. Elagoz, L. Wickham, M. Mamarbachi, J. S. Munzer, A. Basak, C. Lazure, J. A. Cromlish, S. Sisodia and F. Checler (2001). "Post-translational processing of β-Secretase (β-Amyloid-converting Enzyme) and its ectodomain shedding the pro-and transmembrane/cytosolic domains affect its cellular activity and amyloid-β production." Journal of Biological Chemistry 276(14): 10879-10887.

Berendt, F. J., K.-S. Park and J. S. Trimmer (2010). "Multisite phosphorylation of voltage-gated sodium channel α subunits from rat brain." Journal of proteome research 9(4): 1976-1984.

Bergren, S. K., S. Chen, A. Galecki and J. A. Kearney (2005). "Genetic modifiers affecting severity of epilepsy caused by mutation of sodium channelScn2a." Mammalian Genome 16(9): 683-690.
Bergren, S. K., E. D. Rutter and J. A. Kearney (2009). "Fine mapping of an epilepsy modifier gene on mouse Chromosome 19." Mammalian genome 20(6): 359-366.
Bhattacharyya, R., C. Barren and D. M. Kovacs (2013). "Palmitoylation of amyloid precursor protein regulates amyloidogenic processing in lipid rafts." Journal of Neuroscience 33(27): 11169-11183.
Blanc, M., S. Blaskovic and F. G. van der Goot (2013). Palmitoylation, pathogens and their host, Portland Press Ltd.
Blanc, M., F. David, L. Abrami, D. Migliozzi, F. Armand, J. Bürgi and F. G. van der Goot (2015). "SwissPalm: protein palmitoylation database." F1000Research 4.
Blumenfeld, H., A. Lampert, J. P. Klein, J. Mission, M. C. Chen, M. Rivera, S. Dib-Hajj, A. R. Brennan, B. C. Hains and S. G. Waxman (2009). "Role of hippocampal sodium channel Nav1. 6 in kindling epileptogenesis." Epilepsia 50(1): 44-55.
Boiko, T., M. N. Rasband, S. R. Levinson, J. H. Caldwell, G. Mandel, J. S. Trimmer and G. Matthews (2001). "Compact myelin dictates the differential targeting of two sodium channel isoforms in the same axon." Neuron 30(1): 91-104.
Boiko, T., A. Van Wart, J. H. Caldwell, S. R. Levinson, J. S. Trimmer and G. Matthews (2003). "Functional specialization of the axon initial segment by isoform-specific sodium channel targeting." J Neurosci 23(6): 2306-2313.
Bosmans, F., M. Milescu and K. J. Swartz (2011). "Palmitoylation influences the function and pharmacology of sodium channels." Proceedings of the National Academy of Sciences 108(50): 20213-20218.
Brigidi, G. S., B. Santyr, J. Shimell, B. Jovellar and S. X. Bamji (2015). "Activity-regulated trafficking of the palmitoyl-acyl transferase DHHC5." Nature communications 6: 8200.
Brigidi, G. S., Y. Sun, D. Beccano-Kelly, K. Pitman, M. Mobasser, S. L. Borgland, A. J. Milnerwood and S. X. Bamji (2014). "Palmitoylation of δ-catenin by DHHC5 mediates activity-induced synapse plasticity." Nature neuroscience 17(4): 522.
Bunton-Stasyshyn, R. K., J. L. Wagnon, E. R. Wengert, B. S. Barker, A. Faulkner, P. K. Wagley, K. Bhatia, J. M. Jones, M. R. Maniaci and J. M. Parent (2019). "Prominent role of forebrain excitatory neurons in SCN8A encephalopathy." Brain 142(2): 362-375.
Burel, S., F. C. Coyan, M. Lorenzini, M. R. Meyer, C. F. Lichti, J. H. Brown, G. Loussouarn, F. Charpentier, J. M. Nerbonne and R. R. Townsend (2017). "C-terminal phosphorylation of NaV1. 5 impairs FGF13-dependent regulation of channel inactivation." Journal of Biological Chemistry 292(42): 17431-17448.

Burgess, D. L., D. C. Kohrman, J. Galt, N. W. Plummer, J. M. Jones, B. Spear and M. H. Meisler (1995). "Mutation of a new sodium channel gene, Scn8a, in the mouse mutant 'motor endplate disease'." Nature genetics 10(4): 461.

Buxbaum, J. D., K.-N. Liu, Y. Luo, J. L. Slack, K. L. Stocking, J. J. Peschon, R. S. Johnson, B. J. Castner, D. P. Cerretti and R. A. Black (1998). "Evidence that tumor necrosis factor α converting enzyme is involved in regulated α-secretase cleavage of the Alzheimer amyloid protein precursor." Journal of Biological Chemistry 273(43): 27765-27767.

Cachemaille, M., C. Laedermann, M. Pertin, H. Abriel, R.-D. Gosselin and I. Decosterd (2012). "Neuronal expression of the ubiquitin ligase Nedd4-2 in rat dorsal root ganglia: modulation in the spared nerve injury model of neuropathic pain." Neuroscience 227: 370-380.

Calhoun, J. D., N. A. Hawkins, N. J. Zachwieja and J. A. Kearney (2016). "Cacna1g is a genetic modifier of epilepsy caused by mutation of voltage-gated sodium channel Scn2a." Epilepsia 57(6): e103-e107.

Cantrell, A. R. and W. A. Catterall (2001). "Neuromodulation of Na+ channels: An unexpected form of cellular platicity." Nature Reviews Neuroscience 2(6): 397.

Carvill, G. L., S. B. Heavin, S. C. Yendle, J. M. McMahon, B. J. O'Roak, J. Cook, A. Khan, M. O. Dorschner, M. Weaver and S. Calvert (2013). "Targeted resequencing in epileptic encephalopathies identifies de novo mutations in CHD2 and SYNGAP1." Nature genetics 45(7): 825.

Catterall, W. A. (2010). "Ion channel voltage sensors: structure, function, and pathophysiology." Neuron 67(6): 915-928.

Catterall, W. A. (2012). "Voltage-gated sodium channels at 60: structure, function and pathophysiology." The Journal of physiology 590(11): 2577-2589.

Catterall, W. A., A. L. Goldin and S. G. Waxman (2005). "International Union of Pharmacology. XLVII. Nomenclature and structure-function relationships of voltage-gated sodium channels." Pharmacological reviews 57(4): 397-409.

Catterall, W. A., F. Kalume and J. C. Oakley (2010). "NaV1. 1 channels and epilepsy." The Journal of physiology 588(11): 1849-1859.

Chang, P. V., J. A. Prescher, E. M. Sletten, J. M. Baskin, I. A. Miller, N. J. Agard, A. Lo and C. R. Bertozzi (2010). "Copper-free click chemistry in living animals." Proceedings of the National Academy of Sciences 107(5): 1821-1826.

Cheah, C. S., H. Y. Frank, R. E. Westenbroek, F. K. Kalume, J. C. Oakley, G. B. Potter, J. L. Rubenstein and W. A. Catterall (2012). "Specific deletion of NaV1. 1 sodium channels in inhibitory interneurons causes seizures and premature death in a mouse model of Dravet syndrome." Proceedings of the National Academy of Sciences 109(36): 14646-14651.

Chen, C., V. Bharucha, Y. Chen, R. E. Westenbroek, A. Brown, J. D. Malhotra, D. Jones, C. Avery, P. J. Gillespie and K. A. Kazen-Gillespie (2002).

"Reduced sodium channel density, altered voltage dependence of inactivation, and increased susceptibility to seizures in mice lacking sodium channel β2-subunits." Proceedings of the National Academy of Sciences 99(26): 17072-17077.
Chen, C., R. E. Westenbroek, X. Xu, C. A. Edwards, D. R. Sorenson, Y. Chen, D. P. McEwen, H. A. O'Malley, V. Bharucha and L. S. Meadows (2004). "Mice lacking sodium channel β1 subunits display defects in neuronal excitability, sodium channel expression, and nodal architecture." Journal of Neuroscience 24(16): 4030-4042.
Chen, Y., A. R. Cantrell, R. O. Messing, T. Scheuer and W. A. Catterall (2005). "Specific Modulation of Na+ Channels in Hippocampal Neurons by Protein Kinase Cϵ." Journal of Neuroscience 25(2): 507-513.
Chesarino, N. M., J. C. Hach, J. L. Chen, B. W. Zaro, M. V. Rajaram, J. Turner, L. S. Schlesinger, M. R. Pratt, H. C. Hang and J. S. Yount (2014). "Chemoproteomics reveals Toll-like receptor fatty acylation." BMC biology 12(1): 91.
Chichili, V. P. R., Y. Xiao, J. Seetharaman, T. R. Cummins and J. Sivaraman (2013). "Structural basis for the modulation of the neuronal voltage-gated sodium channel Na V 1.6 by calmodulin." Scientific reports 3: 2435.
Chien, A. J., K. M. Carr, R. E. Shirokov, E. Rios and M. M. Hosey (1996). "Identification of palmitoylation sites within the L-type calcium channel β2a subunit and effects on channel function." Journal of Biological Chemistry 271(43): 26465-26468.
Chlanda, P., E. Mekhedov, H. Waters, A. Sodt, C. Schwartz, V. Nair, P. S. Blank and J. Zimmerberg (2017). "Palmitoylation contributes to membrane curvature in Influenza A virus assembly and hemagglutinin-mediated membrane fusion." Journal of virology 91(21): e00947-00917.
Chow, E. W., M. Watson, D. A. Young and A. S. Bassett (2006). "Neurocognitive profile in 22q11 deletion syndrome and schizophrenia." Schizophrenia research 87(1-3): 270-278.
Ciccone, R., C. Franco, I. Piccialli, F. Boscia, A. Casamassa, V. de Rosa, P. Cepparulo, M. Cataldi, L. Annunziato and A. Pannaccione (2019). "Amyloid β-Induced Upregulation of Na v 1.6 Underlies Neuronal Hyperactivity in Tg2576 Alzheimer's Disease Mouse Model." Scientific reports 9(1): 1-18.
Clatot, J., M. Hoshi, X. Wan, H. Liu, A. Jain, K. Shinlapawittayatorn, C. Marionneau, E. Ficker, T. Ha and I. Deschênes (2017). "Voltage-gated sodium channels assemble and gate as dimers." Nature communications 8(1): 2077.
Cohen, S. A. and L. K. Levitt (1993). "Partial characterization of the rH1 sodium channel protein from rat heart using subtype-specific antibodies." Circulation Research 73(4): 735-742.
Collins, M. O., K. T. Woodley and J. S. Choudhary (2017). "Global, site-specific analysis of neuronal protein S-acylation." Scientific reports 7(1): 4683.

Cordy, J. M., I. Hussain, C. Dingwall, N. M. Hooper and A. J. Turner (2003). "Exclusively targeting β-secretase to lipid rafts by GPI-anchor addition up-regulates β-site processing of the amyloid precursor protein." Proceedings of the National Academy of Sciences 100(20): 11735-11740.

Cox, A. D., C. J. Der and M. R. Philips (2015). Targeting RAS membrane association: back to the future for anti-RAS drug discovery?, AACR.

Deschênes, I., N. Neyroud, D. DiSilvestre, E. Marbán, D. T. Yue and G. F. Tomaselli (2002). "Isoform-specific modulation of voltage-gated Na+ channels by calmodulin." Circulation research 90(4): e49-e57.

Dib-Hajj, S. D., J. S. Choi, L. J. Macala, L. Tyrrell, J. A. Black, T. R. Cummins and S. G. Waxman (2009). "Transfection of rat or mouse neurons by biolistics or electroporation." Nature protocols 4(8): 1118.

Do, M. T. H. and B. P. Bean (2004). "Sodium currents in subthalamic nucleus neurons from Nav1. 6-null mice." Journal of neurophysiology 92(2): 726-733.

Dunphy, J. T., H. Schroeder, R. Leventis, W. K. Greentree, J. K. Knudsen, J. R. Silvius and M. E. Linder (2000). "Differential effects of acyl-CoA binding protein on enzymatic and non-enzymatic thioacylation of protein and peptide substrates." Biochimica et Biophysica Acta (BBA)-Molecular and Cell Biology of Lipids 1485(2-3): 185-198.

Dustrude, E. T., A. Moutal, X. Yang, Y. Wang, M. Khanna and R. Khanna (2016). "Hierarchical CRMP2 posttranslational modifications control NaV1. 7 function." Proceedings of the National Academy of Sciences 113(52): E8443-E8452.

Eaholtz, G., T. Scheuer and W. A. Catterall (1994). "Restoration of inactivation and block of open sodium channels by an inactivation gate peptide." Neuron 12(5): 1041-1048.

Ebersole, B., J. Petko, M. Woll, S. Murakami, K. Sokolina, V. Wong, I. Stagljar, B. Lüscher and R. Levenson (2015). "Effect of C-terminal S-palmitoylation on D2 dopamine receptor trafficking and stability." PLoS One 10(11): e0140661.

Edmonds, M. J., B. Geary, M. K. Doherty and A. Morgan (2017). "Analysis of the brain palmitoyl-proteome using both acyl-biotin exchange and acyl-resin-assisted capture methods." Scientific reports 7(1): 3299.

Ednie, A. R., J. M. Harper and E. S. Bennett (2015). "Sialic acids attached to N- and O-glycans within the Nav1. 4 D1S5–S6 linker contribute to channel gating." Biochimica et Biophysica Acta (BBA)-General Subjects 1850(2): 307-317.

El-Husseini, A. E.-D., E. Schnell, S. Dakoji, N. Sweeney, Q. Zhou, O. Prange, C. Gauthier-Campbell, A. Aguilera-Moreno, R. A. Nicoll and D. S. Bredt (2002). "Synaptic strength regulated by palmitate cycling on PSD-95." Cell 108(6): 849-863.

Enomoto, A., J. M. Han, C.-F. Hsiao and S. H. Chandler (2007). "Sodium currents in mesencephalic trigeminal neurons from Nav1. 6 null mice." Journal of neurophysiology 98(2): 710-719.
Estacion, M., A. Gasser, S. D. Dib-Hajj and S. G. Waxman (2010). "A sodium channel mutation linked to epilepsy increases ramp and persistent current of Nav1. 3 and induces hyperexcitability in hippocampal neurons." Experimental neurology 224(2): 362-368.
Estacion, M., J. E. O'Brien, A. Conravey, M. F. Hammer, S. G. Waxman, S. D. Dib-Hajj and M. H. Meisler (2014). "A novel de novo mutation of SCN8A (Nav1. 6) with enhanced channel activation in a child with epileptic encephalopathy." Neurobiology of disease 69: 117-123.
Fernández-Hernando, C., M. Fukata, P. N. Bernatchez, Y. Fukata, M. I. Lin, D. S. Bredt and W. C. Sessa (2006). "Identification of Golgi-localized acyl transferases that palmitoylate and regulate endothelial nitric oxide synthase." The Journal of cell biology 174(3): 369-377.
Ferriera, H., J. Lilly, P. DiStefano, W. Catterall, T. Scheuer and R. Curtis (2003). "Sodium channel beta4, a new disulfide-linked auxiliary subunit with similarity to beta2." J Neurosci 23: 7577-7585.
Fotia, A. B., J. Ekberg, D. J. Adams, D. I. Cook, P. Poronnik and S. Kumar (2004). "Regulation of neuronal voltage-gated sodium channels by the ubiquitin-protein ligases Nedd4 and Nedd4-2." Journal of Biological Chemistry 279(28): 28930-28935.
Frank, H. Y., M. Mantegazza, R. E. Westenbroek, C. A. Robbins, F. Kalume, K. A. Burton, W. J. Spain, G. S. McKnight, T. Scheuer and W. A. Catterall (2006). "Reduced sodium current in GABAergic interneurons in a mouse model of severe myoclonic epilepsy in infancy." Nature neuroscience 9(9): 1142.
Fredericks, G. J., F. W. Hoffmann, A. H. Rose, H. J. Osterheld, F. M. Hess, F. Mercier and P. R. Hoffmann (2014). "Stable expression and function of the inositol 1, 4, 5-triphosphate receptor requires palmitoylation by a DHHC6/selenoprotein K complex." Proceedings of the National Academy of Sciences 111(46): 16478-16483.
Fröhlich, M., B. Dejanovic, H. Kashkar, G. Schwarz and S. Nussberger (2014). "S-palmitoylation represents a novel mechanism regulating the mitochondrial targeting of BAX and initiation of apoptosis." Cell death & disease 5(2): e1057.
Fukata, M., Y. Fukata, H. Adesnik, R. A. Nicoll and D. S. Bredt (2004). "Identification of PSD-95 palmitoylating enzymes." Neuron 44(6): 987-996.
Fukata, Y. and M. Fukata (2010). "Protein palmitoylation in neuronal development and synaptic plasticity." Nature Reviews Neuroscience 11(3): 161.
Gao, X. and R. N. Hannoush (2018). "A decade of click chemistry in protein palmitoylation: impact on discovery and new biology." Cell chemical biology 25(3): 236-246.

Gardill, B. R., R. E. Rivera-Acevedo, C.-C. Tung, M. Okon, L. P. McIntosh and F. Van Petegem (2018). "The voltage-gated sodium channel EF-hands form an interaction with the III-IV linker that is disturbed by disease-causing mutations." Scientific reports 8(1): 4483.

Gasser, A., X. Cheng, E. S. Gilmore, L. Tyrrell, S. G. Waxman and S. D. Dib-Hajj (2010). "Two Nedd4-binding motifs underlie modulation of sodium channel Nav1. 6 by p38 MAPK." Journal of Biological Chemistry 285(34): 26149-26161.

Gasser, A., T. S.-Y. Ho, X. Cheng, K.-J. Chang, S. G. Waxman, M. N. Rasband and S. D. Dib-Hajj (2012). "An ankyrinG-binding motif is necessary and sufficient for targeting Nav1. 6 sodium channels to axon initial segments and nodes of Ranvier." Journal of Neuroscience 32(21): 7232-7243.

Gauthier-Kemper, A., M. Igaev, F. Sündermann, D. Janning, J. Brühmann, K. Moschner, H.-J. Reyher, W. Junge, K. Glebov and J. Walter (2014). "Interplay between phosphorylation and palmitoylation mediates plasma membrane targeting and sorting of GAP43." Molecular biology of the cell 25(21): 3284-3299.

Gilchrist, J., S. Das, F. Van Petegem and F. Bosmans (2013). "Crystallographic insights into sodium-channel modulation by the β4 subunit." Proceedings of the National Academy of Sciences 110(51): E5016-E5024.

Glasscock, E., J. Qian, J. W. Yoo and J. L. Noebels (2007). "Masking epilepsy by combining two epilepsy genes." Nature neuroscience 10(12): 1554.

Globa, A. K. and S. X. Bamji (2017). "Protein palmitoylation in the development and plasticity of neuronal connections." Current opinion in neurobiology 45: 210-220.

Gorleku, O. A., A.-M. Barns, G. R. Prescott, J. Greaves and L. H. Chamberlain (2011). "Endoplasmic reticulum localization of DHHC palmitoyltransferases mediated by lysine-based sorting signals." Journal of Biological Chemistry 286(45): 39573-39584.

Greaves, J., J. A. Carmichael and L. H. Chamberlain (2011). "The palmitoyl transferase DHHC2 targets a dynamic membrane cycling pathway: regulation by a C-terminal domain." Molecular biology of the cell 22(11): 1887-1895.

Grieco, T. M., J. D. Malhotra, C. Chen, L. L. Isom and I. M. Raman (2005). "Open-channel block by the cytoplasmic tail of sodium channel β4 as a mechanism for resurgent sodium current." Neuron 45(2): 233-244.

Grieco, T. M. and I. M. Raman (2004). "Production of resurgent current in NaV1. 6-null Purkinje neurons by slowing sodium channel inactivation with β-pompilidotoxin." Journal of Neuroscience 24(1): 35-42.

Grubb, M. S. and J. Burrone (2010). "Activity-dependent relocation of the axon initial segment fine-tunes neuronal excitability." Nature 465(7301): 1070.

Gubitosi-Klug, R. A., D. J. Mancuso and R. W. Gross (2005). "The human Kv1. 1 channel is palmitoylated, modulating voltage sensing: Identification of a

palmitoylation consensus sequence." Proceedings of the National Academy of Sciences 102(17): 5964-5968.
Hargus, N. J., E. C. Merrick, A. Nigam, C. L. Kalmar, A. R. Baheti, E. H. Bertram III and M. K. Patel (2011). "Temporal lobe epilepsy induces intrinsic alterations in Na channel gating in layer II medial entorhinal cortex neurons." Neurobiology of disease 41(2): 361-376.
Hargus, N. J., A. Nigam, E. H. Bertram III and M. K. Patel (2013). "Evidence for a role of Nav1. 6 in facilitating increases in neuronal hyperexcitability during epileptogenesis." Journal of neurophysiology 110(5): 1144-1157.
Hawkins, N. A., M. S. Martin, W. N. Frankel, J. A. Kearney and A. Escayg (2011). "Neuronal voltage-gated ion channels are genetic modifiers of generalized epilepsy with febrile seizures plus." Neurobiology of disease 41(3): 655-660.
Hawkins, N. A., N. J. Zachwieja, A. R. Miller, L. L. Anderson and J. A. Kearney (2016). "Fine mapping of a Dravet syndrome modifier locus on mouse chromosome 5 and candidate gene analysis by RNA-seq." PLoS genetics 12(10): e1006398.
Hayashi, T., G. Rumbaugh and R. L. Huganir (2005). "Differential regulation of AMPA receptor subunit trafficking by palmitoylation of two distinct sites." Neuron 47(5): 709-723.
Hayashi, T., G. M. Thomas and R. L. Huganir (2009). "Dual palmitoylation of NR2 subunits regulates NMDA receptor trafficking." Neuron 64(2): 213-226.
He, M., P. Jenkins and V. Bennett (2012). "Cysteine 70 of ankyrin-G is S-palmitoylated and is required for function of ankyrin-G in membrane domain assembly." Journal of Biological Chemistry 287(52): 43995-44005.
Herren, A. W., D. M. Weber, R. R. Rigor, K. B. Margulies, B. S. Phinney and D. M. Bers (2015). "CaMKII phosphorylation of Nav1. 5: novel in vitro sites identified by mass spectrometry and reduced S516 phosphorylation in human heart failure." Journal of proteome research 14(5): 2298-2311.
Herzog, R. I., T. R. Cummins, F. Ghassemi, S. D. Dib-Hajj and S. G. Waxman (2003). "Distinct repriming and closed-state inactivation kinetics of Nav1. 6 and Nav1. 7 sodium channels in mouse spinal sensory neurons." The Journal of physiology 551(3): 741-750.
Herzog, R. I., C. Liu, S. G. Waxman and T. R. Cummins (2003). "Calmodulin binds to the C terminus of sodium channels Nav1. 4 and Nav1. 6 and differentially modulates their functional properties." Journal of Neuroscience 23(23): 8261-8270.
Hines, M. L. and N. T. Carnevale (1997). "The NEURON simulation environment." Neural computation 9(6): 1179-1209.
Hinman, J. D., M. N. Rasband and S. T. Carmichael (2013). "Remodeling of the axon initial segment after focal cortical and white matter stroke." Stroke 44(1): 182-189.

Ho, G. P., B. Selvakumar, J. Mukai, L. D. Hester, Y. Wang, J. A. Gogos and S. H. Snyder (2011). "S-nitrosylation and S-palmitoylation reciprocally regulate synaptic targeting of PSD-95." Neuron 71(1): 131-141.
Hoch, B., R. Meyer, R. Hetzer, E.-G. Krause and P. Karczewski (1999). "Identification and expression of δ-isoforms of the multifunctional Ca2+/calmodulin-dependent protein kinase in failing and nonfailing human myocardium." Circulation research 84(6): 713-721.
Hou, H., A. T. John Peter, C. Meiringer, K. Subramanian and C. Ungermann (2009). "Analysis of DHHC acyltransferases implies overlapping substrate specificity and a two-step reaction mechanism." Traffic 10(8): 1061-1073.
Howie, J., L. Reilly, N. J. Fraser, J. M. V. Walker, K. J. Wypijewski, M. L. Ashford, S. C. Calaghan, H. McClafferty, L. Tian and M. J. Shipston (2014). "Substrate recognition by the cell surface palmitoyl transferase DHHC5." Proceedings of the National Academy of Sciences 111(49): 17534-17539.
Hu, H., S. Haas, J. Chelly, H. Van Esch, M. Raynaud, A. De Brouwer, S. Weinert, G. Froyen, S. Frints and F. Laumonnier (2016). "X-exome sequencing of 405 unresolved families identifies seven novel intellectual disability genes." Molecular psychiatry 21(1): 133-148.
Hu, W., C. Tian, T. Li, M. Yang, H. Hou and Y. Shu (2009). "Distinct contributions of Na v 1.6 and Na v 1.2 in action potential initiation and backpropagation." Nature neuroscience 12(8): 996.
Huang, J., C. Han, M. Estacion, D. Vasylyev, J. G. Hoeijmakers, M. M. Gerrits, L. Tyrrell, G. Lauria, C. G. Faber and S. D. Dib-Hajj (2014). "Gain-of-function mutations in sodium channel NaV1. 9 in painful neuropathy." Brain 137(6): 1627-1642.
Huang, K., S. Sanders, R. Singaraja, P. Orban, T. Cijsouw, P. Arstikaitis, A. Yanai, M. R. Hayden and A. El-Husseini (2009). "Neuronal palmitoyl acyl transferases exhibit distinct substrate specificity." The FASEB Journal 23(8): 2605-2615.
Huang, K., A. Yanai, R. Kang, P. Arstikaitis, R. R. Singaraja, M. Metzler, A. Mullard, B. Haigh, C. Gauthier-Campbell and C.-A. Gutekunst (2004). "Huntingtin-interacting protein HIP14 is a palmitoyl transferase involved in palmitoylation and trafficking of multiple neuronal proteins." Neuron 44(6): 977-986.
Hull, J. M. and L. L. Isom (2018). "Voltage-gated sodium channel β subunits: the power outside the pore in brain development and disease." Neuropharmacology 132: 43-57.
Isom, L. L., K. De Jongh, D. Patton, B. Reber, J. Offord, H. Charbonneau, K. Walsh, A. Goldin and W. Catterall (1992). "Primary structure and functional expression of the beta 1 subunit of the rat brain sodium channel." Science 256(5058): 839-842.
Itoh, M., H. Okuno, D. Yamada, M. Yamashita, M. Abe, R. Natsume, T. Kaizuka, K. Sakimura, M. Hoshino and M. Mishina (2019). "Perturbed expression pattern of the immediate early gene Arc in the dentate gyrus of GluA1 C-

terminal palmitoylation-deficient mice." Neuropsychopharmacology reports 39(1): 61-66.
Itoh, M., M. Yamashita, M. Kaneko, H. Okuno, M. Abe, M. Yamazaki, R. Natsume, D. Yamada, T. Kaizuka and R. Suwa (2018). "Deficiency of AMPAR–Palmitoylation Aggravates Seizure Susceptibility." Journal of Neuroscience 38(47): 10220-10235.
Jarecki, B. W., A. D. Piekarz, J. O. Jackson, 2nd and T. R. Cummins (2010). "Human voltage-gated sodium channel mutations that cause inherited neuronal and muscle channelopathies increase resurgent sodium currents." J Clin Invest 120(1): 369-378.
Jarecki, B. W., A. D. Piekarz, J. O. Jackson and T. R. Cummins (2010). "Human voltage-gated sodium channel mutations that cause inherited neuronal and muscle channelopathies increase resurgent sodium currents." The Journal of clinical investigation 120(1): 369-378.
Jennings, B. C. and M. E. Linder (2012). "DHHC protein S-acyltransferases use similar ping-pong kinetic mechanisms but display different acyl-CoA specificities." Journal of Biological Chemistry 287(10): 7236-7245.
Jensen, M. Ø., V. Jogini, D. W. Borhani, A. E. Leffler, R. O. Dror and D. E. Shaw (2012). "Mechanism of voltage gating in potassium channels." Science 336(6078): 229-233.
Jeyifous, O., E. I. Lin, X. Chen, S. E. Antinone, R. Mastro, R. Drisdel, T. S. Reese and W. N. Green (2016). "Palmitoylation regulates glutamate receptor distributions in postsynaptic densities through control of PSD95 conformation and orientation." Proceedings of the National Academy of Sciences 113(52): E8482-E8491.
Jindal, H. K., E. J. Folco, G. X. Liu and G. Koren (2008). "Posttranslational modification of voltage-dependent potassium channel Kv1. 5: COOH-terminal palmitoylation modulates its biological properties." American Journal of Physiology-Heart and Circulatory Physiology 294(5): H2012-H2021.
Johnson, C. N., F. Potet, M. K. Thompson, B. M. Kroncke, A. M. Glazer, M. W. Voehler, B. C. Knollmann, A. L. George and W. J. Chazin (2018). "A mechanism of calmodulin modulation of the human cardiac sodium channel." Structure 26(5): 683-694. e683.
Johnson, D., M. L. Montpetit, P. J. Stocker and E. S. Bennett (2004). "The sialic acid component of the β1 subunit modulates voltage-gated sodium channel function." Journal of Biological Chemistry 279(43): 44303-44310.
Kalume, F., R. E. Westenbroek, C. S. Cheah, H. Y. Frank, J. C. Oakley, T. Scheuer and W. A. Catterall (2013). "Sudden unexpected death in a mouse model of Dravet syndrome." The Journal of clinical investigation 123(4): 1798-1808.
Kandel, E. R., J. H. Schwartz, T. M. Jessell, D. o. Biochemistry, M. B. T. Jessell, S. Siegelbaum and A. Hudspeth (2000). Principles of neural science, McGraw-hill New York.

Kang, R., J. Wan, P. Arstikaitis, H. Takahashi, K. Huang, A. O. Bailey, J. X. Thompson, A. F. Roth, R. C. Drisdel and R. Mastro (2008). "Neural palmitoyl-proteomics reveals dynamic synaptic palmitoylation." Nature 456(7224): 904.
Kaphzan, H., S. A. Buffington, J. I. Jung, M. N. Rasband and E. Klann (2011). "Alterations in intrinsic membrane properties and the axon initial segment in a mouse model of Angelman syndrome." Journal of Neuroscience 31(48): 17637-17648.
Kearney, J. A., D. A. Buchner, G. De Haan, M. Adamska, S. I. Levin, A. R. Furay, R. L. Albin, J. M. Jones, M. Montal and M. J. Stevens (2002). "Molecular and pathological effects of a modifier gene on deficiency of the sodium channel Scn8a (Nav1. 6)." Human molecular genetics 11(22): 2765-2775.
Kearney, J. A., Y. Yang, B. Beyer, S. K. Bergren, L. Claes, P. DeJonghe and W. N. Frankel (2006). "Severe epilepsy resulting from genetic interaction between Scn2a and Kcnq2." Human molecular genetics 15(6): 1043-1048.
Khaliq, Z. M., N. W. Gouwens and I. M. Raman (2003). "The contribution of resurgent sodium current to high-frequency firing in Purkinje neurons: an experimental and modeling study." J Neurosci 23(12): 4899-4912.
Khaliq, Z. M., N. W. Gouwens and I. M. Raman (2003). "The contribution of resurgent sodium current to high-frequency firing in Purkinje neurons: an experimental and modeling study." Journal of Neuroscience 23(12): 4899-4912.
Klassen, T., C. Davis, A. Goldman, D. Burgess, T. Chen, D. Wheeler, J. McPherson, T. Bourquin, L. Lewis and D. Villasana (2011). "Exome sequencing of ion channel genes reveals complex profiles confounding personal risk assessment in epilepsy." Cell 145(7): 1036-1048.
Ko, P. J. and S. J. Dixon (2018). "Protein palmitoylation and cancer." EMBO reports 19(10).
Kong, E., S. Peng, G. Chandra, C. Sarkar, Z. Zhang, M. B. Bagh and A. B. Mukherjee (2013). "Dynamic palmitoylation links cytosol-membrane shuttling of acyl-protein thioesterase-1 and acyl-protein thioesterase-2 with that of proto-oncogene H-ras product and growth-associated protein-43." Journal of Biological Chemistry 288(13): 9112-9125.
Kong, W., Y. Zhang, Y. Gao, X. Liu, K. Gao, H. Xie, J. Wang, Y. Wu, Y. Zhang and X. Wu (2015). "SCN 8A mutations in Chinese children with early onset epilepsy and intellectual disability." Epilepsia 56(3): 431-438.
Korycka, J., A. Łach, E. Heger, D. M. Bogusławska, M. Wolny, M. Toporkiewicz, K. Augoff, J. Korzeniewski and A. F. Sikorski (2012). "Human DHHC proteins: a spotlight on the hidden player of palmitoylation." European journal of cell biology 91(2): 107-117.
Kuba, H., Y. Oichi and H. Ohmori (2010). "Presynaptic activity regulates Na+ channel distribution at the axon initial segment." Nature 465(7301): 1075.
Laedermann, C. J., M. Cachemaille, G. Kirschmann, M. Pertin, R.-D. Gosselin, I. Chang, M. Albesa, C. Towne, B. L. Schneider and S. Kellenberger (2013).

"Dysregulation of voltage-gated sodium channels by ubiquitin ligase NEDD4-2 in neuropathic pain." The Journal of clinical investigation 123(7): 3002-3013.
Laedermann, C. J., I. Decosterd and H. Abriel (2014). Ubiquitylation of voltage-gated sodium channels. Voltage Gated Sodium Channels, Springer: 231-250.
Laedermann, C. J., M. Pertin, M. R. Suter and I. Decosterd (2014). "Voltage-gated sodium channel expression in mouse DRG after SNI leads to re-evaluation of projections of injured fibers." Molecular pain 10(1): 19.
Lamar, T., C. G. Vanoye, J. Calhoun, J. C. Wong, S. B. Dutton, B. S. Jorge, M. Velinov, A. Escayg and J. A. Kearney (2017). "SCN3A deficiency associated with increased seizure susceptibility." Neurobiology of disease 102: 38-48.
Lee, A. and A. L. Goldin (2008). "Role of the amino and carboxy termini in isoform-specific sodium channel variation." The Journal of physiology 586(16): 3917-3926.
Lee, J., S. Kim, H.-m. Kim, H. J. Kim and F. H. Yu (2019). "NaV1. 6 and NaV1. 7 channels are major endogenous voltage-gated sodium channels in ND7/23 cells." PloS one 14(8).
Lemonidis, K., M. C. Sanchez-Perez and L. H. Chamberlain (2015). "Identification of a novel sequence motif recognized by the ankyrin repeat domain of zDHHC17/13 S-acyltransferases." Journal of Biological Chemistry 290(36): 21939-21950.
Lerche, H., W. Peter, R. Fleischhauer, U. Pika-Hartlaub, T. Malina, N. Mitrovic and F. Lehmann-Horn (1997). "Role in fast inactivation of the IV/S4–S5 loop of the human muscle Na+ channel probed by cysteine mutagenesis." The Journal of Physiology 505(2): 345-352.
Lewis, A. H. and I. M. Raman (2014). "Resurgent current of voltage-gated Na+ channels." The Journal of physiology 592(22): 4825-4838.
Li, M., J. W. West, R. Numann, B. J. Murphy, T. Scheuer and W. A. Catterall (1993). "Convergent regulation of sodium channels by protein kinase C and cAMP-dependent protein kinase." Science 261(5127): 1439-1442.
Li, Y., J. Hu, K. Höfer, A. M. Wong, J. D. Cooper, S. G. Birnbaum, R. E. Hammer and S. L. Hofmann (2010). "DHHC5 interacts with PDZ domain 3 of post-synaptic density-95 (PSD-95) protein and plays a role in learning and memory." Journal of Biological Chemistry 285(17): 13022-13031.
Lievens, P. M.-J., T. Kuznetsova, G. Kochlamazashvili, F. Cesca, N. Gorinski, D. A. Galil, V. Cherkas, N. Ronkina, J. Lafera and M. Gaestel (2016). "ZDHHC3 tyrosine phosphorylation regulates neural cell adhesion molecule palmitoylation." Molecular and cellular biology 36(17): 2208-2225.
Light, P. E., C. H. Wallace and J. R. Dyck (2003). "Constitutively Active Adenosine Monophosphate–Activated Protein Kinase Regulates Voltage-

Gated Sodium Channels in Ventricular Myocytes." Circulation 107(15): 1962-1965.
Lin, D. T. and E. Conibear (2015). Enzymatic protein depalmitoylation by acyl protein thioesterases, Portland Press Ltd.
Lin, D. T. S. and E. Conibear (2015). "ABHD17 proteins are novel protein depalmitoylases that regulate N-Ras palmitate turnover and subcellular localization." Elife 4: e11306.
Linder, M. E. and B. C. Jennings (2013). Mechanism and function of DHHC S-acyltransferases, Portland Press Ltd.
Long, S. B., E. B. Campbell and R. MacKinnon (2005). "Crystal structure of a mammalian voltage-dependent Shaker family K+ channel." Science 309(5736): 897-903.
Lorincz, A. and Z. Nusser (2008). "Cell-type-dependent molecular composition of the axon initial segment." Journal of Neuroscience 28(53): 14329-14340.
Lu, Z., Y.-P. Jiang, C.-Y. C. Wu, L. M. Ballou, S. Liu, E. S. Carpenter, M. R. Rosen, I. S. Cohen and R. Z. Lin (2013). "Increased persistent sodium current due to decreased PI3K signaling contributes to QT prolongation in the diabetic heart." Diabetes 62(12): 4257-4265.
Makinson, C. D., B. S. Tanaka, T. Lamar, A. L. Goldin and A. Escayg (2014). "Role of the hippocampus in Na V 1.6 (Scn8a) mediated seizure resistance." Neurobiology of disease 68: 16-25.
Makinson, C. D., B. S. Tanaka, J. M. Sorokin, J. C. Wong, C. A. Christian, A. L. Goldin, A. Escayg and J. R. Huguenard (2017). "Regulation of thalamic and cortical network synchrony by Scn8a." Neuron 93(5): 1165-1179. e1166.
Maltsev, V. A., V. Reznikov, N. A. Undrovinas, H. N. Sabbah and A. Undrovinas (2008). "Modulation of late sodium current by Ca2+, calmodulin, and CaMKII in normal and failing dog cardiomyocytes: similarities and differences." American Journal of Physiology-Heart and Circulatory Physiology 294(4): H1597-H1608.
Mansouri, M. R., L. Marklund, P. Gustavsson, E. Davey, B. Carlsson, C. Larsson, I. White, K.-H. Gustavson and N. Dahl (2005). "Loss of ZDHHC15 expression in a woman with a balanced translocation t (X; 15)(q13. 3; cen) and severe mental retardation." European journal of human genetics 13(8): 970.
Marionneau, C. and H. Abriel (2015). "Regulation of the cardiac Na+ channel NaV1. 5 by post-translational modifications." Journal of molecular and cellular cardiology 82: 36-47.
Martin, M. S., B. Tang, L. A. Papale, F. H. Yu, W. A. Catterall and A. Escayg (2007). "The voltage-gated sodium channel Scn8a is a genetic modifier of severe myoclonic epilepsy of infancy." Human molecular genetics 16(23): 2892-2899.
Martínez-Hernández, J., C. Ballesteros-Merino, L. Fernández-Alacid, J. C. Nicolau, C. Aguado and R. Luján (2013). "Polarised localisation of the

voltage-gated sodium channel Na v 1.2 in cerebellar granule cells." The Cerebellum 12(1): 16-26.
Maurice, N., T. Tkatch, M. Meisler, L. K. Sprunger and D. J. Surmeier (2001). "D1/D5 dopamine receptor activation differentially modulates rapidly inactivating and persistent sodium currents in prefrontal cortex pyramidal neurons." Journal of Neuroscience 21(7): 2268-2277.
McCormick, K. A., L. L. Isom, D. Ragsdale, D. Smith, T. Scheuer and W. A. Catterall (1998). "Molecular determinants of Na+ channel function in the extracellular domain of the β1 subunit." Journal of Biological Chemistry 273(7): 3954-3962.
McMichael, T. M., L. Zhang, M. Chemudupati, J. C. Hach, A. D. Kenney, H. C. Hang and J. S. Yount (2017). "The palmitoyltransferase ZDHHC20 enhances interferon-induced transmembrane protein 3 (IFITM3) palmitoylation and antiviral activity." Journal of Biological Chemistry 292(52): 21517-21526.
Meadows, L., J. D. Malhotra, A. Stetzer, L. L. Isom and D. S. Ragsdale (2001). "The intracellular segment of the sodium channel β1 subunit is required for its efficient association with the channel α subunit." Journal of neurochemistry 76(6): 1871-1878.
Meisler, M. H., G. Helman, M. F. Hammer, B. E. Fureman, W. D. Gaillard, A. L. Goldin, S. Hirose, A. Ishii, B. L. Kroner and C. Lossin (2016). "SCN8A encephalopathy: Research progress and prospects." Epilepsia 57(7): 1027-1035.
Meisler, M. H., G. Helman, M. F. Hammer, B. E. Fureman, W. D. Gaillard, A. L. Goldin, S. Hirose, A. Ishii, B. L. Kroner, C. Lossin, H. C. Mefford, J. M. Parent, M. Patel, J. Schreiber, R. Stewart, V. Whittemore, K. Wilcox, J. L. Wagnon, P. L. Pearl, A. Vanderver and I. E. Scheffer (2016). "SCN8A encephalopathy: Research progress and prospects." Epilepsia 57(7): 1027-1035.
Meisler, M. H., J. E. O'brien and L. M. Sharkey (2010). "Sodium channel gene family: epilepsy mutations, gene interactions and modifier effects." The Journal of physiology 588(11): 1841-1848.
Meisler, M. H., N. W. Plummer, D. L. Burgess, D. A. Buchner and L. K. Sprunger (2004). "Allelic mutations of the sodium channel SCN8A reveal multiple cellular and physiological functions." Genetica 122(1): 37-45.
Mercer, J. N., C. S. Chan, T. Tkatch, J. Held and D. J. Surmeier (2007). "Nav1. 6 sodium channels are critical to pacemaking and fast spiking in globus pallidus neurons." Journal of Neuroscience 27(49): 13552-13566.
Mercier, A., R. Clément, T. Harnois, N. Bourmeyster, P. Bois and A. Chatelier (2015). "Nav1. 5 channels can reach the plasma membrane through distinct N-glycosylation states." Biochimica et Biophysica Acta (BBA)-General Subjects 1850(6): 1215-1223.
Mikami, M. and J. Yang (2005). "Short hairpin RNA–mediated selective knockdown of NaV1. 8 tetrodotoxin-resistant voltage-gated sodium

channel in dorsal root ganglion neurons." Anesthesiology: The Journal of the American Society of Anesthesiologists 103(4): 828-836.
Mill, P., A. W. Lee, Y. Fukata, R. Tsutsumi, M. Fukata, M. Keighren, R. M. Porter, L. McKie, I. Smyth and I. J. Jackson (2009). "Palmitoylation regulates epidermal homeostasis and hair follicle differentiation." PLoS genetics 5(11): e1000748.
Mistry, A. M., C. H. Thompson, A. R. Miller, C. G. Vanoye, A. L. George and J. A. Kearney (2014). "Strain-and age-dependent hippocampal neuron sodium currents correlate with epilepsy severity in Dravet syndrome mice." Neurobiology of disease 65: 1-11.
Mitchell, D. A., L. D. Hamel, K. D. Reddy, L. Farh, L. M. Rettew, P. R. Sanchez and R. J. Deschenes (2014). "Mutations in the X-linked intellectual disability gene, zDHHC9, alter autopalmitoylation activity by distinct mechanisms." Journal of Biological Chemistry 289(26): 18582-18592.
Mitchell, D. A., G. Mitchell, Y. Ling, C. Budde and R. J. Deschenes (2010). "Mutational analysis of Saccharomyces cerevisiae Erf2 reveals a two-step reaction mechanism for protein palmitoylation by DHHC enzymes." Journal of Biological Chemistry 285(49): 38104-38114.
Mizumaru, C., Y. Saito, T. Ishikawa, T. Yoshida, T. Yamamoto, T. Nakaya and T. Suzuki (2009). "Suppression of APP-containing vesicle trafficking and production of β-amyloid by AID/DHHC-12 protein." Journal of neurochemistry 111(5): 1213-1224.
Morgan, K., E. B. Stevens, B. Shah, P. J. Cox, A. K. Dixon, K. Lee, R. D. Pinnock, J. Hughes, P. J. Richardson and K. Mizuguchi (2000). "β3: an additional auxiliary subunit of the voltage-sensitive sodium channel that modulates channel gating with distinct kinetics." Proceedings of the National Academy of Sciences 97(5): 2308-2313.
Moritz, A. E., D. E. Rastedt, D. J. Stanislowski, M. Shetty, M. A. Smith, R. A. Vaughan and J. D. Foster (2015). "Reciprocal phosphorylation and palmitoylation control dopamine transporter kinetics." Journal of Biological Chemistry 290(48): 29095-29105.
Motoike, H. K., H. Liu, I. W. Glaaser, A.-S. Yang, M. Tateyama and R. S. Kass (2004). "The Na+ channel inactivation gate is a molecular complex: a novel role of the COOH-terminal domain." The Journal of general physiology 123(2): 155-165.
Motoki, K., H. Kume, A. Oda, A. Tamaoka, A. Hosaka, F. Kametani and W. Araki (2012). "Neuronal β-amyloid generation is independent of lipid raft association of β-secretase BACE1: analysis with a palmitoylation-deficient mutant." Brain and behavior 2(3): 270-282.
Mukai, J., A. Dhilla, L. J. Drew, K. L. Stark, L. Cao, A. B. MacDermott, M. Karayiorgou and J. A. Gogos (2008). "Palmitoylation-dependent neurodevelopmental deficits in a mouse model of 22q11 microdeletion." Nature neuroscience 11(11): 1302.

Mukai, J., H. Liu, R. A. Burt, D. E. Swor, W.-S. Lai, M. Karayiorgou and J. A. Gogos (2004). "Evidence that the gene encoding ZDHHC8 contributes to the risk of schizophrenia." Nature genetics 36(7): 725.

Mukai, K., H. Konno, T. Akiba, T. Uemura, S. Waguri, T. Kobayashi, G. N. Barber, H. Arai and T. Taguchi (2016). "Activation of STING requires palmitoylation at the Golgi." Nature communications 7: 11932.

Murray, K. T., S. A. Fahrig, K. K. Deal, S. S. Po, N. N. Hu, D. J. Snyders, M. M. Tamkun and P. B. Bennett (1994). "Modulation of an inactivating human cardiac K+ channel by protein kinase C." Circulation research 75(6): 999-1005.

Murray, K. T., N. Hu, J. R. Daw, H.-G. Shin, M. T. Watson, A. B. Mashburn and A. L. George Jr (1997). "Functional Effects of Protein Kinase C Activation on the Human Cardiac Na sup+ Channel." Circulation research 80(3): 370-376.

Nadolski, M. J. and M. E. Linder (2009). "Molecular recognition of the palmitoylation substrate Vac8 by its palmitoyltransferase Pfa3." Journal of Biological Chemistry 284(26): 17720-17730.

Naumenko, V. S. and E. Ponimaskin (2018). "Palmitoylation as a functional regulator of neurotransmitter receptors." Neural plasticity 2018.

Nguyen, H. M. and A. L. Goldin (2010). "Sodium channel carboxyl-terminal residue regulates fast inactivation." Journal of Biological Chemistry 285(12): 9077-9089.

Noritake, J., Y. Fukata, T. Iwanaga, N. Hosomi, R. Tsutsumi, N. Matsuda, H. Tani, H. Iwanari, Y. Mochizuki and T. Kodama (2009). "Mobile DHHC palmitoylating enzyme mediates activity-sensitive synaptic targeting of PSD-95." The Journal of cell biology 186(1): 147-160.

Numann, R., W. A. Catterall and T. Scheuer (1991). "Functional modulation of brain sodium channels by protein kinase C phosphorylation." Science 254(5028): 115-118.

O'Malley, H. A. and L. L. Isom (2015). "Sodium channel β subunits: emerging targets in channelopathies." Annual review of physiology 77: 481-504.

Ogiwara, I., H. Miyamoto, N. Morita, N. Atapour, E. Mazaki, I. Inoue, T. Takeuchi, S. Itohara, Y. Yanagawa and K. Obata (2007). "Nav1. 1 localizes to axons of parvalbumin-positive inhibitory interneurons: a circuit basis for epileptic seizures in mice carrying an Scn1a gene mutation." Journal of Neuroscience 27(22): 5903-5914.

Ohno, Y., A. Kihara, T. Sano and Y. Igarashi (2006). "Intracellular localization and tissue-specific distribution of human and yeast DHHC cysteine-rich domain-containing proteins." Biochimica et Biophysica Acta (BBA)-Molecular and Cell Biology of Lipids 1761(4): 474-483.

Osorio, N., L. Cathala, M. H. Meisler, M. Crest, J. Magistretti and P. Delmas (2010). "Persistent Nav1. 6 current at axon initial segments tunes spike timing of cerebellar granule cells." The Journal of physiology 588(4): 651-670.

Pan, X., Z. Li, X. Huang, G. Huang, S. Gao, H. Shen, L. Liu, J. Lei and N. Yan (2019). "Molecular basis for pore blockade of human Na+ channel Nav1. 2 by the μ-conotoxin KIIIA." Science 363(6433): 1309-1313.

Pan, X., Z. Li, Q. Zhou, H. Shen, K. Wu, X. Huang, J. Chen, J. Zhang, X. Zhu and J. Lei (2018). "Structure of the human voltage-gated sodium channel Nav1. 4 in complex with β1." Science 362(6412): eaau2486.

Pankow, S., C. Bamberger and J. R. Yates (2019). "A posttranslational modification code for CFTR maturation is altered in cystic fibrosis." Sci. Signal. 12(562): eaan7984.

Papale, L. A., B. Beyer, J. M. Jones, L. M. Sharkey, S. Tufik, M. Epstein, V. A. Letts, M. H. Meisler, W. N. Frankel and A. Escayg (2009). "Heterozygous mutations of the voltage-gated sodium channel SCN8A are associated with spike-wave discharges and absence epilepsy in mice." Human molecular genetics 18(9): 1633-1641.

Parsons, R. and B. Austen (2007). Protein–protein interactions in the assembly and subcellular trafficking of the BACE (β-site amyloid precursor protein-cleaving enzyme) complex of Alzheimer's disease, Portland Press Ltd.

Patel, F. and W. J. Brackenbury (2015). "Dual roles of voltage-gated sodium channels in development and cancer." The International journal of developmental biology 59: 357.

Patel, R. R., C. Barbosa, T. Brustovetsky, N. Brustovetsky and T. R. Cummins (2016). "Aberrant epilepsy-associated mutant Nav1.6 sodium channel activity can be targeted with cannabidiol." Brain 139(Pt 8): 2164-2181.

Patel, R. R., C. Barbosa, T. Brustovetsky, N. Brustovetsky and T. R. Cummins (2016). "Aberrant epilepsy-associated mutant Nav1. 6 sodium channel activity can be targeted with cannabidiol." Brain 139(8): 2164-2181.

Patel, R. R., C. Barbosa, Y. Xiao and T. R. Cummins (2015). "Human Nav1.6 Channels Generate Larger Resurgent Currents than Human Nav1.1 Channels, but the Navbeta4 Peptide Does Not Protect Either Isoform from Use-Dependent Reduction." PLoS One 10(7): e0133485.

Pathak, M. M., V. Yarov-Yarovoy, G. Agarwal, B. Roux, P. Barth, S. Kohout, F. Tombola and E. Y. Isacoff (2007). "Closing in on the resting state of the Shaker K+ channel." Neuron 56(1): 124-140.

Pedro, M. P., A. A. Vilcaes, V. M. Tomatis, R. G. Oliveira, G. A. Gomez and J. L. Daniotti (2013). "2-Bromopalmitate reduces protein deacylation by inhibition of acyl-protein thioesterase enzymatic activities." PloS one 8(10).

Pei, Z., Y. Pan and T. R. Cummins (2017). "Posttranslational modification of sodium channels."

Pei, Z., Y. Xiao, J. Meng, A. Hudmon and T. R. Cummins (2016). "Cardiac sodium channel palmitoylation regulates channel availability and myocyte excitability with implications for arrhythmia generation." Nature communications 7: 12035.

Peseckis, S. M., I. Deichaite and M. Resh (1993). "Iodinated fatty acids as probes for myristate processing and function. Incorporation into pp60v-src." Journal of Biological Chemistry 268(7): 5107-5114.
Plain, F., S. D. Congreve, R. S. Z. Yee, J. Kennedy, J. Howie, C.-W. Kuo, N. J. Fraser and W. Fuller (2017). "An amphipathic α-helix directs palmitoylation of the large intracellular loop of the sodium/calcium exchanger." Journal of Biological Chemistry 292(25): 10745-10752.
Plant, L. D., J. D. Marks and S. A. Goldstein (2016). "SUMOylation of NaV1. 2 channels mediates the early response to acute hypoxia in central neurons." Elife 5: e20054.
Ponimaskin, E., G. Dityateva, M. O. Ruonala, M. Fukata, Y. Fukata, F. Kobe, F. S. Wouters, M. Delling, D. S. Bredt and M. Schachner (2008). "Fibroblast growth factor-regulated palmitoylation of the neural cell adhesion molecule determines neuronal morphogenesis." Journal of Neuroscience 28(36): 8897-8907.
Purkey, A. M., K. M. Woolfrey, K. C. Crosby, D. G. Stich, W. S. Chick, J. Aoto and M. L. Dell'Acqua (2018). "AKAP150 palmitoylation regulates synaptic incorporation of Ca2+-permeable AMPA receptors to control LTP." Cell reports 25(4): 974-987. e974.
Qu, Y., J. C. Rogers, T. N. Tanada, W. A. Catterall and T. Scheuer (1996). "Phosphorylation of S1505 in the cardiac Na+ channel inactivation gate is required for modulation by protein kinase C." The Journal of general physiology 108(5): 375-379.
Raman, I. M. and B. P. Bean (2001). "Inactivation and recovery of sodium currents in cerebellar Purkinje neurons: evidence for two mechanisms." Biophys J 80(2): 729-737.
Raman, I. M., L. K. Sprunger, M. H. Meisler and B. P. Bean (1997). "Altered subthreshold sodium currents and disrupted firing patterns in Purkinje neurons of Scn8a mutant mice." Neuron 19(4): 881-891.
Raymond, F. L., P. S. Tarpey, S. Edkins, C. Tofts, S. O'Meara, J. Teague, A. Butler, C. Stevens, S. Barthorpe and G. Buck (2007). "Mutations in ZDHHC9, which encodes a palmitoyltransferase of NRAS and HRAS, cause X-linked mental retardation associated with a Marfanoid habitus." The American Journal of Human Genetics 80(5): 982-987.
Rocks, O., M. Gerauer, N. Vartak, S. Koch, Z.-P. Huang, M. Pechlivanis, J. Kuhlmann, L. Brunsveld, A. Chandra and B. Ellinger (2010). "The palmitoylation machinery is a spatially organizing system for peripheral membrane proteins." Cell 141(3): 458-471.
Rogers, M., N. Zidar, D. Kikelj and R. W. Kirby (2016). "Characterization of endogenous sodium channels in the ND7-23 neuroblastoma cell line: implications for use as a heterologous ion channel expression system suitable for automated patch clamp screening." Assay and drug development technologies 14(2): 109-130.

Roth, A. F., Y. Feng, L. Chen and N. G. Davis (2002). "The yeast DHHC cysteine-rich domain protein Akr1p is a palmitoyl transferase." The Journal of cell biology 159(1): 23-28.
Roth, A. F., J. Wan, A. O. Bailey, B. Sun, J. A. Kuchar, W. N. Green, B. S. Phinney, J. R. Yates III and N. G. Davis (2006). "Global analysis of protein palmitoylation in yeast." Cell 125(5): 1003-1013.
Roth, A. F., J. Wan, W. N. Green, J. R. Yates and N. G. Davis (2006). "Proteomic identification of palmitoylated proteins." Methods 40(2): 135-142.
Rougier, J.-S., B. Gavillet and H. Abriel (2013). "Proteasome inhibitor (MG132) rescues Nav1. 5 protein content and the cardiac sodium current in dystrophin-deficient mdx5cv mice." Frontiers in physiology 4: 51.
Rougier, J.-S., M. X. van Bemmelen, M. C. Bruce, T. Jespersen, B. Gavillet, F. Apothéloz, S. Cordonier, O. Staub, D. Rotin and H. Abriel (2005). "Molecular determinants of voltage-gated sodium channel regulation by the Nedd4/Nedd4-like proteins." American Journal of Physiology-Cell Physiology 288(3): C692-C701.
Royeck, M., M.-T. Horstmann, S. Remy, M. Reitze, Y. Yaari and H. Beck (2008). "Role of axonal NaV1. 6 sodium channels in action potential initiation of CA1 pyramidal neurons." Journal of neurophysiology 100(4): 2361-2380.
Rubinstein, M., S. Han, C. Tai, R. E. Westenbroek, A. Hunker, T. Scheuer and W. A. Catterall (2015). "Dissecting the phenotypes of Dravet syndrome by gene deletion." Brain 138(8): 2219-2233.
Rusconi, R., P. Scalmani, R. R. Cassulini, G. Giunti, A. Gambardella, S. Franceschetti, G. Annesi, E. Wanke and M. Mantegazza (2007). "Modulatory proteins can rescue a trafficking defective epileptogenic Nav1. 1 Na+ channel mutant." Journal of Neuroscience 27(41): 11037-11046.
Rush, A. M., T. R. Cummins and S. G. Waxman (2007). "Multiple sodium channels and their roles in electrogenesis within dorsal root ganglion neurons." The Journal of physiology 579(1): 1-14.
Rush, A. M., S. D. Dib-Hajj and S. G. Waxman (2005). "Electrophysiological properties of two axonal sodium channels, Nav1. 2 and Nav1. 6, expressed in mouse spinal sensory neurones." The Journal of physiology 564(3): 803-815.
Sanders, S. J., A. J. Campbell, J. R. Cottrell, R. S. Moller, F. F. Wagner, A. L. Auldridge, R. A. Bernier, W. A. Catterall, W. K. Chung and J. R. Empfield (2018). "Progress in understanding and treating SCN2A-mediated disorders." Trends in neurosciences 41(7): 442-456.
Scala, F., M. N. Nenov, E. J. Crofton, A. K. Singh, O. Folorunso, Y. Zhang, B. C. Chesson, N. C. Wildburger, T. F. James and M. A. Alshammari (2018). "Environmental enrichment and social isolation mediate neuroplasticity of medium spiny neurons through the GSK3 pathway." Cell reports 23(2): 555-567.

Schlesinger, M., A. Magee and M. Schmidt (1980). "Fatty acid acylation of proteins in cultured cells." Journal of Biological Chemistry 255(21): 10021-10024.
Schmidt, J. and W. Catterall (1987). "Palmitylation, sulfation, and glycosylation of the alpha subunit of the sodium channel. Role of post-translational modifications in channel assembly." Journal of Biological Chemistry 262(28): 13713-13723.
Schmidt, M. F. and M. J. Schlesinger (1979). "Fatty acid binding to vesicular stomatitis virus glycoprotein: a new type of post-translational modification of the viral glycoprotein." Cell 17(4): 813-819.
Schubert, B., A. Vandongen, G. E. Kirsch and A. M. Brown (1990). "Inhibition of cardiac Na+ currents by isoproterenol." American Journal of Physiology-Heart and Circulatory Physiology 258(4): H977-H982.
Schwiening, C. J. (2012). "A brief historical perspective: Hodgkin and Huxley." The Journal of physiology 590(11): 2571-2575.
Sharkey, L. M., X. Cheng, V. Drews, D. A. Buchner, J. M. Jones, M. J. Justice, S. G. Waxman, S. D. Dib-Hajj and M. H. Meisler (2009). "The ataxia3 mutation in the N-terminal cytoplasmic domain of sodium channel Nav1. 6 disrupts intracellular trafficking." Journal of Neuroscience 29(9): 2733-2741.
Shen, H., D. Liu, K. Wu, J. Lei and N. Yan (2019). "Structures of human Nav1. 7 channel in complex with auxiliary subunits and animal toxins." Science 363(6433): 1303-1308.
Shen, H., Q. Zhou, X. Pan, Z. Li, J. Wu and N. Yan (2017). "Structure of a eukaryotic voltage-gated sodium channel at near-atomic resolution." Science 355(6328): eaal4326.
Shin, H.-G. and K. T. Murray (2001). "Conventional protein kinase C isoforms and cross-activation of protein kinase A regulate cardiac Na+ current." FEBS letters 495(3): 154-158.
Shipston, M. J. (2011). "Ion channel regulation by protein palmitoylation." Journal of Biological Chemistry 286(11): 8709-8716.
Shipston, M. J. (2014). "Ion channel regulation by protein S-acylation." The Journal of general physiology 143(6): 659-678.
Shirahata, E., H. Iwasaki, M. Takagi, C. Lin, V. Bennett, Y. Okamura and K. Hayasaka (2006). "Ankyrin-G regulates inactivation gating of the neuronal sodium channel, Nav1. 6." Journal of neurophysiology 96(3): 1347-1357.
Sidera, C., R. Parsons and B. Austen (2004). Proteolytic cascade in the amyloidogenesis of Alzheimer's disease, Portland Press Limited.
Singh, N. A., C. Pappas, E. J. Dahle, L. R. Claes, T. H. Pruess, P. De Jonghe, J. Thompson, M. Dixon, C. Gurnett and A. Peiffer (2009). "A role of SCN9A in human epilepsies, as a cause of febrile seizures and as a potential modifier of Dravet syndrome." PLoS genetics 5(9): e1000649.
Sittl, R., A. Lampert, T. Huth, E. T. Schuy, A. S. Link, J. Fleckenstein, C. Alzheimer, P. Grafe and R. W. Carr (2012). "Anticancer drug oxaliplatin

induces acute cooling-aggravated neuropathy via sodium channel subtype NaV1. 6-resurgent and persistent current." Proceedings of the National Academy of Sciences 109(17): 6704-6709.
Smith, M. R. and A. L. Goldin (1997). "Interaction between the sodium channel inactivation linker and domain III S4-S5." Biophysical Journal 73(4): 1885-1895.
Smith, M. R., R. D. Smith, N. W. Plummer, M. H. Meisler and A. L. Goldin (1998). "Functional analysis of the mouse Scn8a sodium channel." Journal of Neuroscience 18(16): 6093-6102.
Smith, R. S., C. J. Kenny, V. Ganesh, A. Jang, R. Borges-Monroy, J. N. Partlow, R. S. Hill, T. Shin, A. Y. Chen and R. N. Doan (2018). "Sodium channel SCN3A (NaV1. 3) regulation of human cerebral cortical folding and oral motor development." Neuron 99(5): 905-913. e907.
Smotrys, J. E., M. J. Schoenfish, M. A. Stutz and M. E. Linder (2005). "The vacuolar DHHC-CRD protein Pfa3p is a protein acyltransferase for Vac8p." J Cell Biol 170(7): 1091-1099.
Spampanato, J., A. Escayg, M. H. Meisler and A. L. Goldin (2001). "Functional effects of two voltage-gated sodium channel mutations that cause generalized epilepsy with febrile seizures plus type 2." Journal of neuroscience 21(19): 7481-7490.
Spampanato, J., J. Kearney, G. De Haan, D. McEwen, A. Escayg, I. Aradi, B. MacDonald, S. Levin, I. Soltesz and P. Benna (2004). "A novel epilepsy mutation in the sodium channel SCN1A identifies a cytoplasmic domain for β subunit interaction." Journal of Neuroscience 24(44): 10022-10034.
Spratt, P. W., R. Ben-Shalom, C. M. Keeshen, K. J. Burke Jr, R. L. Clarkson, S. J. Sanders and K. J. Bender (2019). "The Autism-Associated Gene Scn2a Contributes to Dendritic Excitability and Synaptic Function in the Prefrontal Cortex." Neuron.
Sprunger, L. K., A. Escayg, S. Tallaksen-Greene, R. L. Albin and M. H. Meisler (1999). "Dystonia associated with mutation of the neuronal sodium channel Scn8a and identification of the modifier locus Scnm1 on mouse chromosome 3." Human molecular genetics 8(3): 471-479.
Summers, D. W., J. Milbrandt and A. DiAntonio (2018). "Palmitoylation enables MAPK-dependent proteostasis of axon survival factors." Proceedings of the National Academy of Sciences 115(37): E8746-E8754.
Sun, W., J. L. Wagnon, C. L. Mahaffey, M. Briese, J. Ule and W. N. Frankel (2013). "Aberrant sodium channel activity in the complex seizure disorder of Celf4 mutant mice." The Journal of physiology 591(1): 241-255.
Symonds, J. D. and S. M. Zuberi (2018). "Genetics update: Monogenetics, polygene disorders and the quest for modifying genes." Neuropharmacology 132: 3-19.
Tan, Z.-Y., A. D. Piekarz, B. T. Priest, K. L. Knopp, J. L. Krajewski, J. S. McDermott, E. S. Nisenbaum and T. R. Cummins (2014). "Tetrodotoxin-resistant sodium channels in sensory neurons generate slow resurgent

currents that are enhanced by inflammatory mediators." Journal of Neuroscience 34(21): 7190-7197.
Tan, Z.-Y., B. T. Priest, J. L. Krajewski, K. L. Knopp, E. S. Nisenbaum and T. R. Cummins (2014). "Protein kinase C enhances human sodium channel hNav1. 7 resurgent currents via a serine residue in the domain III–IV linker." FEBS letters 588(21): 3964-3969.
Tao, X., A. Lee, W. Limapichat, D. A. Dougherty and R. MacKinnon (2010). "A gating charge transfer center in voltage sensors." Science 328(5974): 67-73.
Tarpey, P. S., R. Smith, E. Pleasance, A. Whibley, S. Edkins, C. Hardy, S. O'meara, C. Latimer, E. Dicks and A. Menzies (2009). "A systematic, large-scale resequencing screen of X-chromosome coding exons in mental retardation." Nature genetics 41(5): 535.
Teener, J. W. and M. M. Rich (2006). "Dysregulation of sodium channel gating in critical illness myopathy." Journal of Muscle Research & Cell Motility 27(5-7): 291-296.
Thomas, G. M., T. Hayashi, S.-L. Chiu, C.-M. Chen and R. L. Huganir (2012). "Palmitoylation by DHHC5/8 targets GRIP1 to dendritic endosomes to regulate AMPA-R trafficking." Neuron 73(3): 482-496.
Thompson, C. H., N. A. Hawkins, J. A. Kearney and A. L. George (2017). "CaMKII modulates sodium current in neurons from epileptic Scn2a mutant mice." Proceedings of the National Academy of Sciences 114(7): 1696-1701.
Tian, L., O. Jeffries, H. McClafferty, A. Molyvdas, I. C. Rowe, F. Saleem, L. Chen, J. Greaves, L. H. Chamberlain and H.-G. Knaus (2008). "Palmitoylation gates phosphorylation-dependent regulation of BK potassium channels." Proceedings of the National Academy of Sciences 105(52): 21006-21011.
Tian, L., H. McClafferty, O. Jeffries and M. J. Shipston (2010). "Multiple palmitoyltransferases are required for palmitoylation-dependent regulation of large conductance calcium-and voltage-activated potassium channels." Journal of Biological Chemistry 285(31): 23954-23962.
Topinka, J. R. and D. S. Bredt (1998). "N-terminal palmitoylation of PSD-95 regulates association with cell membranes and interaction with K+ channel Kv1. 4." Neuron 20(1): 125-134.
Trudeau, M. M., J. C. Dalton, J. W. Day, L. P. Ranum and M. H. Meisler (2006). "Heterozygosity for a protein truncation mutation of sodium channel SCN8A in a patient with cerebellar atrophy, ataxia, and mental retardation." Journal of medical genetics 43(6): 527-530.
Tyrrell, L., M. Renganathan, S. D. Dib-Hajj and S. G. Waxman (2001). "Glycosylation alters steady-state inactivation of sodium channel Nav1. 9/NaN in dorsal root ganglion neurons and is developmentally regulated." Journal of Neuroscience 21(24): 9629-9637.

Ushiro, H. and S. Cohen (1980). "Identification of phosphotyrosine as a product of epidermal growth factor-activated protein kinase in A-431 cell membranes." Journal of Biological Chemistry 255(18): 8363-8365.
Valdez-Taubas, J. and H. Pelham (2005). "Swf1-dependent palmitoylation of the SNARE Tlg1 prevents its ubiquitination and degradation." The EMBO journal 24(14): 2524-2532.
van Bemmelen, M. X., J.-S. b. Rougier, B. Gavillet, F. Apothéloz, D. e. Daidié, M. Tateyama, I. Rivolta, M. A. Thomas, R. S. Kass and O. Staub (2004). "Cardiac voltage-gated sodium channel Nav1. 5 is regulated by Nedd4-2 mediated ubiquitination." Circulation research 95(3): 284-291.
Van Wart, A. and G. Matthews (2006). "Expression of sodium channels Nav1.2 and Nav1.6 during postnatal development of the retina." Neurosci Lett 403(3): 315-317.
Van Wart, A. and G. Matthews (2006). "Impaired firing and cell-specific compensation in neurons lacking nav1. 6 sodium channels." Journal of Neuroscience 26(27): 7172-7180.
Veeramah, K. R., J. E. O'Brien, M. H. Meisler, X. Cheng, S. D. Dib-Hajj, S. G. Waxman, D. Talwar, S. Girirajan, E. E. Eichler, L. L. Restifo, R. P. Erickson and M. F. Hammer (2012). "De novo pathogenic SCN8A mutation identified by whole-genome sequencing of a family quartet affected by infantile epileptic encephalopathy and SUDEP." Am J Hum Genet 90(3): 502-510.
Vetrivel, K. S., X. Meckler, Y. Chen, P. D. Nguyen, N. G. Seidah, R. Vassar, P. C. Wong, M. Fukata, M. Z. Kounnas and G. Thinakaran (2009). "Alzheimer disease Aβ production in the absence of S-palmitoylation-dependent targeting of BACE1 to lipid rafts." Journal of Biological Chemistry 284(6): 3793-3803.
Vijayaragavan, K., M. Boutjdir and M. Chahine (2004). "Modulation of Nav1. 7 and Nav1. 8 peripheral nerve sodium channels by protein kinase A and protein kinase C." Journal of neurophysiology 91(4): 1556-1569.
Waechter, C., J. Schmidt and W. Catterall (1983). "Glycosylation is required for maintenance of functional sodium channels in neuroblastoma cells." Journal of Biological Chemistry 258(8): 5117-5123.
Wagner, S., L. S. Maier and D. M. Bers (2015). "Role of sodium and calcium dysregulation in tachyarrhythmias in sudden cardiac death." Circulation research 116(12): 1956-1970.
Wagnon, J. L., B. S. Barker, J. A. Hounshell, C. A. Haaxma, A. Shealy, T. Moss, S. Parikh, R. D. Messer, M. K. Patel and M. H. Meisler (2016). "Pathogenic mechanism of recurrent mutations of SCN8A in epileptic encephalopathy." Annals of clinical and translational neurology 3(2): 114-123.
Wagnon, J. L., M. J. Korn, R. Parent, T. A. Tarpey, J. M. Jones, M. F. Hammer, G. G. Murphy, J. M. Parent and M. H. Meisler (2014). "Convulsive

seizures and SUDEP in a mouse model of SCN8A epileptic encephalopathy." Human molecular genetics 24(2): 506-515.
Wagnon, J. L. and M. H. Meisler (2015). "Recurrent and non-recurrent mutations of SCN8A in epileptic encephalopathy." Frontiers in neurology 6: 104.
Wang, C., B. C. Chung, H. Yan, S.-Y. Lee and G. S. Pitt (2012). "Crystal structure of the ternary complex of a NaV C-terminal domain, a fibroblast growth factor homologous factor, and calmodulin." Structure 20(7): 1167-1176.
Wang, C., B. C. Chung, H. Yan, H.-G. Wang, S.-Y. Lee and G. S. Pitt (2014). "Structural analyses of Ca 2+/CaM interaction with Na V channel C-termini reveal mechanisms of calcium-dependent regulation." Nature communications 5: 4896.
Wang, J., H. Gao, X. Bao, Q. Zhang, J. Li, L. Wei, X. Wu, Y. Chen and S. Yu (2017). "SCN8A mutations in Chinese patients with early onset epileptic encephalopathy and benign infantile seizures." BMC medical genetics 18(1): 104.
West, J. W., R. Numann, B. J. Murphy, T. Scheuer and W. A. Catterall (1991). "A phosphorylation site in the Na+ channel required for modulation by protein kinase C." Science 254(5033): 866-868.
West, J. W., D. E. Patton, T. Scheuer, Y. Wang, A. L. Goldin and W. A. Catterall (1992). "A cluster of hydrophobic amino acid residues required for fast Na (+)-channel inactivation." Proceedings of the National Academy of Sciences 89(22): 10910-10914.
Wittmack, E. K., A. M. Rush, A. Hudmon, S. G. Waxman and S. D. Dib-Hajj (2005). "Voltage-gated sodium channel Nav1. 6 is modulated by p38 mitogen-activated protein kinase." Journal of Neuroscience 25(28): 6621-6630.
Wong, J. C., C. D. Makinson, T. Lamar, Q. Cheng, J. C. Wingard, E. F. Terwilliger and A. Escayg (2018). "Selective targeting of Scn8a prevents seizure development in a mouse model of mesial temporal lobe epilepsy." Scientific reports 8(1): 126.
Woolfrey, K. M., H. O'Leary, D. J. Goodell, H. R. Robertson, E. A. Horne, S. J. Coultrap, M. L. Dell'Acqua and K. U. Bayer (2018). "CaMKII regulates the depalmitoylation and synaptic removal of the scaffold protein AKAP79/150 to mediate structural long-term depression." Journal of Biological Chemistry 293(5): 1551-1567.
Wu, X.-B., D.-L. Cao, X. Zhang, B.-C. Jiang, L.-X. Zhao, B. Qian and Y.-J. Gao (2016). "CXCL13/CXCR5 enhances sodium channel Nav1. 8 current density via p38 MAP kinase in primary sensory neurons following inflammatory pain." Scientific reports 6: 34836.
Xiao, Y., C. Barbosa, Z. Pei, W. Xie, J. A. Strong, J.-M. Zhang and T. R. Cummins (2019). "Increased resurgent sodium currents in Nav1. 8 contribute to nociceptive sensory neuron hyperexcitability associated with peripheral neuropathies." Journal of Neuroscience 39(8): 1539-1550.

Xie, W., Z. Y. Tan, C. Barbosa, J. A. Strong, T. R. Cummins and J. M. Zhang (2016). "Upregulation of the sodium channel NaVbeta4 subunit and its contributions to mechanical hypersensitivity and neuronal hyperexcitability in a rat model of radicular pain induced by local dorsal root ganglion inflammation." Pain 157(4): 879-891.

Xu, B., J. L. Roos, S. Levy, E. Van Rensburg, J. A. Gogos and M. Karayiorgou (2008). "Strong association of de novo copy number mutations with sporadic schizophrenia." Nature genetics 40(7): 880.

Xue, Y., Z. Liu, J. Cao and J. Ren (2011). "Computational prediction of post-translational modification sites in proteins." Yang NS, Ed: 105-124.

Yan, H., C. Wang, S. O. Marx and G. S. Pitt (2017). "Calmodulin limits pathogenic Na+ channel persistent current." The Journal of general physiology: jgp. 201611721.

Yanai, A., K. Huang, R. Kang, R. R. Singaraja, P. Arstikaitis, L. Gan, P. C. Orban, A. Mullard, C. M. Cowan and L. A. Raymond (2006). "Palmitoylation of huntingtin by HIP14is essential for its trafficking and function." Nature neuroscience 9(6): 824.

Yang, G., W. Xiong, L. Kojic and M. S. Cynader (2009). "Subunit-selective palmitoylation regulates the intracellular trafficking of AMPA receptor." European Journal of Neuroscience 30(1): 35-46.

Yang, Q., F. Zheng, Y. Hu, Y. Yang, Y. Li, G. Chen, W. Wang, M. He, R. Zhou and Y. Ma (2018). "ZDHHC8 critically regulates seizure susceptibility in epilepsy." Cell death & disease 9(8): 795.

Yang, W., D. Di Vizio, M. Kirchner, H. Steen and M. R. Freeman (2010). "Proteome scale characterization of human S-acylated proteins in lipid raft-enriched and non-raft membranes." Molecular & Cellular Proteomics 9(1): 54-70.

Yokoi, N., Y. Fukata, A. Sekiya, T. Murakami, K. Kobayashi and M. Fukata (2016). "Identification of PSD-95 depalmitoylating enzymes." Journal of Neuroscience 36(24): 6431-6444.

Zaman, T., I. Helbig, I. B. Božović, S. D. DeBrosse, A. C. Bergqvist, K. Wallis, L. Medne, A. Maver, B. Peterlin and K. L. Helbig (2018). "Mutations in SCN3A cause early infantile epileptic encephalopathy." Annals of neurology 83(4): 703-717.

Zhang, T., L. S. Maier, N. D. Dalton, S. Miyamoto, J. Ross Jr, D. M. Bers and J. H. Brown (2003). "The δC isoform of CaMKII is activated in cardiac hypertrophy and induces dilated cardiomyopathy and heart failure." Circulation research 92(8): 912-919.

CURRICULUM VITAE

Yanling Pan

EDUCATION

Indiana University, Indianapolis, IN 2020
Ph.D. in Medical Neuroscience

The University of Hong Kong, Hong Kong, China 2014
M.Phil. in Neuroscience

Southern Medical University, Guangzhou, China 2012
B.Sc. in Basic Medical Science

PUBLICATIONS

Pan, Y., Xiao, Y., Pei, Z., & Cummins, T. R. (2020). S-palmitoylation of the sodium channel Nav1. 6 regulates its activity and neuronal excitability. *Journal of Biological Chemistry*, jbc-RA119.

Pan, Y., & Cummins, T. R. (2020). Distinct functional alterations in SCN8A epilepsy mutant channels. *The Journal of physiology, 598(2), 381-401*.

Hamilton, J., Brustovetsky, T., Sridhar, A., Pan, Y., Cummins, T. R., Meyer, J. S., & Brustovetsky, N. (2019). Energy Metabolism and Mitochondrial Superoxide Anion Production in Pre-symptomatic Striatal Neurons Derived from Human-Induced Pluripotent Stem Cells Expressing Mutant Huntingtin. *Molecular neurobiology*, 1-17.

VanderWall, K. B., Huang, K. C., Pan, Y., Lavekar, S. S., Fligor, C. M., Allsop, A., ... & Cummins, T. R. (2019). Retinal ganglion cells harboring the OPTN (E50K) mutation exhibit neurodegenerative phenotypes when derived from hPSC-derived three dimensional retinal organoids. *bioRxiv*, 820159.

Pei, Z., Pan, Y., & Cummins, T. R. (2017). Posttranslational modification of sodium channels. In *Voltage-gated Sodium Channels: Structure, Function and Channelopathies* (pp. 101-124). Springer, Cham.

POSTER PRESENTATIONS

Pan Y., Cummins T. R. Palmitoylation distinctively modulates Nav1.6 and Nav1.2. [abstract]. In: Society for Neuroscience; Oct 19-23, 2019; Chicago, IL; Abstract # 6835.

Pan Y., Cummins T. R. Distinct functional alterations in SCN8A epilepsy mutant channels [abstract]. In: Society for Neuroscience; Nov 3-7, 2018; San Diego, CA; Abstract # 2018-S-2076-SfN.

Pan, Y., & Cummins, T. R. Palmitoylation distinctively modulates Nav1.6 and Nav1.2. [abstract]. In: FASEB Ion Channel Regulation Conference; Jul 9-14, 2017; Steamboat Springs, CO.

Pan Y., Xiao Y., Cummins T. R. Palmitoylation Modifies Biophysical Properties of Voltage-gated Sodium Channel 1.6 [abstract]. In: Society for Neuroscience; Nov 12-16, 2016; San Diego, CA; Abstract # 2016-S-2603-SfN.

Pan Y., Dai Y., Cheung M. P. L., Yip H. K. The inhibition of GSK3β promotes oligodendroglial progenitor cell differentiation in spinal cord injury [abstract]. In: 9th Federation of European Neuroscience Societies (FENS) Forum of Neuroscience; July 5-9, 2014; Milan, Italy; Abstract # FENS-1353.

Pan Y., Dai Y., Cheung M. P. L., Yip H. K. The Role of GSK3β Pathway in Oligodendroglial Progenitor Cell Differentiation and Remyelination after Spinal Cord Injury [abstract]. In: Ninth International Symposium on Healthy Aging “Aging with Confidence”; Mar 8-9, 2014; Hong Kong, China; Abstract # P13.

Dai Y., Pan Y., Yip H. K. Inhibition of Stat/Smad co-transcription factor p300 regulates differentiation of adult spinal cord neural progenitors and ameliorates functional recovery in chronic spinal cord injury [abstract]. In: Ninth International Symposium on Healthy Aging “Aging with Confidence”; Mar 8-9, 2014; Hong Kong, China; Abstract # P5.

AWARDS AND HONORS

2018	Graduate and Professional Educational Grants (GPEG)	IUPUI
2017	Medical Neuroscience Travel Award	Indiana University
2016	IUSM Graduate Student Travel Grant	Indiana University
2013	Postgraduate Scholarship	The University of Hong Kong
2012	Postgraduate Scholarship	The University of Hong Kong